



High-Performance Indoor VHF-UHF Antennas:

Technology Update Report

15 May 2010

(Revised 16 August, 2010)

M. W. Cross, P.E. (Principal Investigator)

Emanuel Merulla, M.S.E.E.

Richard Formato, Ph.D.

Prepared for:

National Association of Broadcasters

Science and Technology Department

1771 N Street NW

Washington, DC 20036

Mr. Kelly Williams, Senior Director

Prepared by:

MegaWave Corporation

100 Jackson Road

Devens, MA 01434

Contents:

<u>Section</u>	<u>Title</u>	<u>Page</u>
1.	Introduction and Summary of Findings.....	3
2.	Specific Design Methods and Technologies Investigated.....	7
2.1	Advanced Computational Methods.....	7
2.2	Fragmented Antennas.....	22
2.3	Non-Foster Impedance Matching.....	26
2.4	Active RF Noise Cancelling.....	35
2.5	Automatic Antenna Matching Systems.....	37
2.6	Physically Reconfigurable Antenna Elements.....	58
2.7	Use of Metamaterials in Antenna Systems.....	75
2.8	Electronic Band-Gap and High Impedance Surfaces.....	98
2.9	Fractal and Self-Similar Antennas.....	104
2.10	Retrodirective Arrays.....	112
3.	Conclusions and Design Recommendations.....	128

1.0 Introduction and Summary of Findings

In 1995 MegaWave Corporation, under an NAB sponsored project, developed a broadband VHF/UHF set-top antenna using the continuously resistively loaded printed thin-film bow-tie shown in Figure 1-1. It featured a low VSWR ($< 3:1$) and a constant dipole-like azimuthal pattern across both the VHF and UHF television bands.



Figure 1-1: MegaWave 54-806 MHz Set Top TV Antenna, 1995

In the 15 years since then much technical progress has been made in the area of broadband and low-profile antenna design methods and actual designs. These improvements have been published in: technical textbooks, peer-reviewed articles, patents, government research and development reports, and seminar proceedings. As a developer of advanced antenna systems, primarily for the U.S. government, MegaWave constantly reviews these sources and acquires the latest computer based EM simulation tools in order to preserve its competitive advantage. In this project, this knowledge was used to identify ten candidate design methods and technologies that have the potential to materially improve the performance of indoor VHF-UHF TV antennas. This report describes each candidate and its potential to improve indoor "set-top" reception of DTV signals between 54 and 698 MHz.

Of course, it must be kept in mind that, while advanced design methods and actual physical designs exist, so do the laws of electromagnetics. Maxwell's equations have resulted both in practical as well as, what Dr. R. C. Hansen humorously calls, "Pathological Antennas". These pathological designs are described in his most recent textbook [1], especially in the area of electrically-small and broadband designs. It is instructive to apply these fundamental limitations to the problem at hand, the set-top TV antenna.

[1] Hansen, R.C., "Electrically Small, Superdirective, and Superconducting Antennas," Wiley, 2006

Consider that a half-wavelength in the low VHF TV band varies between 9.2 and 5.6 feet; between 34 and 27 inches in the high VHF band and between 12.6 and 8.5 inches in the UHF (470-698 MHz) band. A dipole antenna whose physical length is less than its wavelength divided by pi (λ/π) is considered to be an electrically “small” antenna (ESA). ESAs unfortunately are characterized by narrow bandwidths and low gains. Assuming 2 to 3 feet as a maximum acceptable length for an indoor or set-top antenna, it definitely falls into the ESA category in the low VHF band. But, in addition to size constraints and the resulting difficulty in obtaining acceptable performance from a single antenna over the 54 to 698 MHz spectrum, there are other concerns. Indoor and set-top antennas are fundamentally disadvantaged due to building penetration losses and by proximity to sources of manmade radio noise. The former effect is more pronounced at UHF and the latter at low VHF channels. Both can have a significant deleterious effect on antenna performance. This brief discussion highlights the difficult problems inherent in designing efficient, high performance antennas for the indoor/set-op TV environment. Fortunately, emerging technologies may effectively address these concerns.

This report is organized as follows. Sections 2.1 through 2.10 contain summaries of each advanced method and hardware technology identified as a potential candidate for high-performance indoor VHF-UHF DTV antennas. Each section includes a list of references and, in many cases, photographs and performance data for multiple implementations of the technology that is described. Section 3 includes conclusions and a conceptual design for a practical indoor/set top VHF-UHF antenna system.

The authors evaluated each technology and arrived at the conclusions and design concept after sorting the nine hardware candidates into three categories as follows:

- Mature technologies that **do not** require any CE-909-A channel designator or signal quality information from the DTV receiver:
 - Fragmented Antennas (Section 2.2)
 - Non-Foster Impedance Matching (Section 2.3)
- Mature technologies that **do** require channel and quality data from the receiver:
 - Active RF Noise Cancelling (Section 2.4)
 - Automatic Antenna Matching Systems (Section 2.5)
 - Physically Reconfigurable Antenna Elements (Section 2.6)
- Emerging technologies that show promise, but are not sufficiently mature or practical at this time:
 - Metamaterials (Section 2.7)
 - Electromagnetic Band Gap (EBG) Materials (Section 2.8)
 - Fractal/Self Similar Antennas (Section 2.9)
 - Retrodirective Arrays (Section 2.10)

A common thread connects each of these technology areas: **advanced computational methods**. Whether a particular technology is mature and immediately applicable or emerging and highly speculative, various schemes for antenna design optimization are universally applicable and described in Section 2.1. These methodologies apply to all of the candidate technologies discussed in Sections 2.2 through 2.10, and accordingly was placed at the beginning of Section 2. If even one of the optimization algorithms described had been available during the development of MegaWave’s 1995 broadband set top antenna, it is likely that markedly better gain performance would have resulted, especially in the low and high VHF bands. Another attractive and potentially very significant capability offered by optimization algorithms is the possibility of discovering entirely new antenna geometries, rather than simply optimizing a pre-existing geometry.

Table 1-1 **subjectively** ranks the nine identified candidate hardware technologies (2.2 - 2.10). A score of 10 represents perfection. By maturity we mean how close to off-the-shelf a particular technology’s hardware is and how well its basic principle of operation has been vetted in the literature. The term SWAP refers to size/weight and power.

	Method/ Technology	Active/ Passive	Requires CE-909-A Interface	Maturity	Vetted	Risk	Design Complexity	SWAP	Comments
2.1	Adv. Comp. Methods	N/A	N/A	9	9	Very Low	N/A	N/A	Applies to all Technologies
2.2	Fragmented	Passive	No	7	7	Low	Low	9	Planar
2.3	Non-Foster	Active	No	6	7	Low	Moderate	7	Limited Bandwidth
2.4	Active Noise Cancelling	Active	Yes	7	6	Low	High	3	Requires I&Q
2.5	Automated Antenna Matching	Active	Yes	7	7	Moderate	High	7	Requires complex TV interface
2.6	Reconfigurable Antennas	Active	Yes	6	7	Moderate	High	6	Control of MEMS w/DC
2.7	Metamaterials	Passive	No	3	4	High	High	8	Emerging/ Availability an issue
2.8	EBG	Passive	No	5	6	High	High	5	Inherently Narrow Band Maybe useful for shielding
2.9	Fractal/Self Similar	Passive	No	6	4	Moderate	Moderate	8	Controversial Performance Gain
2.10	Retrodirective	Active	Yes	4	5	Very High	Very High	2	Narrow - Band, Large

Table 1-1: Candidate Technologies Considered and Their Ranking

As an example of how advanced computational methods could be combined with an advanced hardware technique, that does not require a CE-909-A interface, is described at the end of Section 3 and summarized here.

Using the genetic algorithm described in Section 2.1.5 a fragmented antenna was designed and combined with a non-Foster-matching circuit to provide a planar 54-698 MHz dipole approximately 13 by 13 inches with significantly better gain, especially in the 54-88 and 174-216 MHz bands, than the 1995 MegaWave/NAB set top antenna. Figure 1 shows the broadband fragmented planar element's design obtained after approximately 24 hours of computational time on a PC. Details of the specific method used are in Section 2.2 of this report. It is well matched across the UHF DTV band, but requires some passive matching in the high VHF band (which would also serve as the band combiner) and the more robust matching capability of the active Non-Foster-Matching technique, described in Section 2.3, for the low-VHF band.

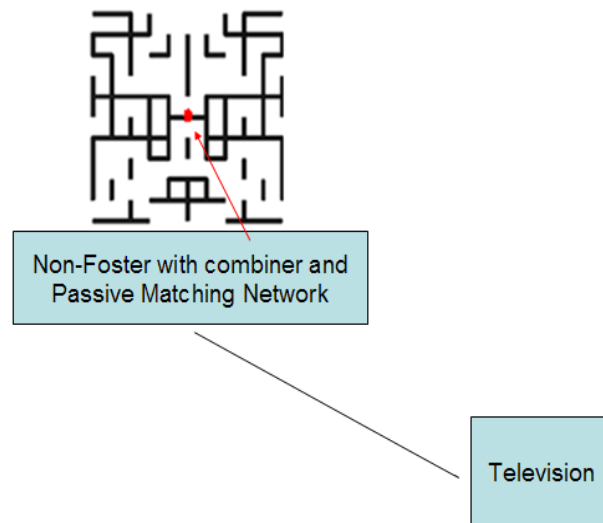


Figure 1. 13 x 13 Inch Planar Fragmented Non-Foster Matched VHF-UHF Antenna

An omni-directional version could also be designed. It should be stressed that the above is included here only to illustrate the notion of combining advanced computational broadband antenna element designs with emerging electronic antenna matching capabilities and that other antenna element geometries are also possible, depending on the starting conditions, trade space dimensions and performance goals provided to the optimizer.

The authors want to make clear that 90 percent of the techniques and ideas contained in this study are the work of others, as published in the open literature and referenced herein.

2.0 Specific Design Methods and Hardware Technologies Investigated

2.1 Advanced Computational Methods

2.1.1 Summary

Optimization methodologies abound, and they are extensively used in every aspect of engineering design, in particular antenna design. Optimization algorithms are useful in two ways. They can be used to optimize the design parameters for a user-specified antenna geometry (for example, element spacing, length and diameter in a Yagi-Uda array). They also can *generate designs* that are impossible to achieve otherwise. In both cases, optimization involves meeting specific performance objectives (typically, VSWR, gain, bandwidth, and so on).

Optimization algorithms have become progressively more important as the limitations of classic analytical techniques have become progressively more apparent. While the equations underlying electromagnetic theory are well understood and accurately describe all electromagnetic phenomena, in most practical cases they cannot be solved analytically or, oftentimes, even numerically. Designing better antennas requires improved methodologies, and state-of-the-art optimization algorithms have proven very effective. There is no question that these techniques are applicable to the set-top antenna design problem, and that they should receive considerable attention in future design activities.

There are many different optimization methodologies that fall into two broad categories: analytical methods and heuristic methods. Analytical methods are based on precise mathematical formulations of the optimization problem. Even though they may be fundamentally numerical in nature, they involve standard mathematical operations such as computing derivatives or evaluating integrals. Heuristic methods may involve equations, but the equations are not the result of an analysis. Instead, they are offered without “proof” based on the fact that they “work.”

Many optimization heuristics are Nature inspired. The steps an algorithm performs to optimize an *antenna* are based, for example, on how *bacteria* forage for food. As disparate as these entities may seem, there is a connection, at least in the sense that bacteria finding a good food source is similar to finding an antenna with a good gain-bandwidth product. Optimization algorithms of this type are usually referred to as “metaheuristics,” a term intended to emphasize that the method is both *empirical* and *conceptual* in nature. Thus, an effective bacteria foraging algorithm can be implemented in many different ways because the bacteria foraging metaheuristic simply suggests an analogy to Nature that is implemented in a computer algorithm working on

an antenna problem. The metaheuristic thus is an *algorithmic framework* instead of a list of steps or instructions.

Several Nature inspired metaheuristics are described. A brief summary of each algorithm is provided, and several example antenna problems solved by a variety of algorithms are discussed. The algorithms include Ant Colony Optimization (ACO), Particle Swarm Optimization (PSO), Genetic Algorithm (GA), Simulated Annealing (SA), Central Force Optimization (CFO), Invasive Weed Optimization (IWO), Intelligent Water Drop (IWD) algorithm, and Bacteria Foraging Optimization (BFO). There are many other optimization algorithms [for example, Space Gravitation Optimization (SGO), Integrated Radiation Optimization (IRO)], but they have not been applied to antennas or antenna related problems.

Each of these algorithms, except one, is inherently *stochastic* because its Nature inspired algorithmic model relies on randomness in its functioning. The underlying equations contain true *random variables* whose values are computed from a probability distribution and consequently cannot be known in advance. As a result, every time a stochastic optimizer run is made, its results are different than the previous run even when exactly the same run setup parameters are used. The performance of stochastic optimizers is necessarily characterized statistically (for example, average values, standard deviations). This may be a limitation in the utility of optimization algorithms if they are used in a set-top antenna on a real time basis. For example, a self-structuring antenna (SSA) must reconfigure itself in real time in response, for example, to a changing environment.

The one algorithm that is not inherently stochastic is Central Force Optimization (CFO) whose Nature inspiring metaphor is gravitational kinematics, the branch of physics that deals with the motion of masses moving under the influence of gravity. The underlying equations are Newton's equations of motion, which are completely *deterministic*. CFO analogizes these equations in "CFO space" by flying "probes" that are similar to small satellites to search a decision space "landscape" for the maximum (optimal) values of a function (for example, antenna gain as a function of element length and polar angle). CFO has been applied to antenna design and network synthesis, and tested against many recognized benchmark functions used to evaluate optimization algorithms. It therefore may be especially useful for the set-top antenna problem.

2.1.2 Introduction

This section describes developments in antenna design optimization over the past fifteen years or so that have been driven largely by the availability of progressively more powerful computers. A plethora of new optimization algorithms have been

introduced and tested and are now in widespread use. The new antenna designs often are non-intuitive, occasionally even counter-intuitive, but all share the common feature of not being accessible in any other way. State-of-the-art optimization algorithms can effectively solve intractable problems that have no analytical solutions or are too complex to apply traditional analytical techniques. These approaches are useful right now in designing set-top television antennas, and they will continue to be useful whatever form future set-stop systems take. Some of the more important and interesting optimization algorithms are described here.

Optimization Methodologies. The problem of locating the maximum values of a function is generally referred to as “multidimensional search and optimization.” As pointed out above, any problem involving three or more design parameters (“decision variables”) is a multidimensional problem, and simple methods such as plotting the function to be maximized cannot be used. Methods for solving these problems fall into two broad categories: analytical methods and heuristic methods. Analytical methods, which involve computing derivatives and gradients, are of limited use, especially in the complex landscapes associated with antenna design. Stringent performance requirements in terms of bandwidth, radiation pattern, and standing wave ratio (SWR) make antenna optimization problems particularly difficult because the landscape is usually extremely multimodal with narrow resonances and often high sensitivity to slight parameter variations. Heuristic optimization methodologies, which are inherently numerical in nature, are effective in dealing with these issues, and consequently they are considered here while analytical approaches are not.

An entire class of heuristic optimization algorithms are “Nature inspired”, and these appear to be the most effective. A Nature inspired algorithm is a computer search and optimization program whose function mimics some natural process. These programs are described as being “metaphorical” because they analogize some natural process without precisely modeling it. For example, “Ant Colony Optimization” (ACO) is an algorithm that simulates (to some degree) the behavior of ants seeking food. Thus, ACO is *inspired* by the *metaphor* of ant foraging. All such algorithms *evolve* a solution to the optimization problem over a series of steps or iterations, and almost all such algorithms are *stochastic population*-based methodologies. An initial population (of ants, for example) randomly (stochastically) moves through the decision space (landscape) step-by-step (iterating) in such a way that it converges on the largest food supply (maximum function value). The ants’ progress is controlled by a set of equations that mimic real ant behavior in Nature. There are many Nature inspired algorithms, ACO being one of the earliest ones. The more important algorithms are discussed below with examples of their application to antenna optimization.

2.1.3 Ant Colony Optimization

Figure 1 illustrates the basic idea behind Ant Colony Optimization (ACO) [1]. The irregular objects represent the ants' nest (bottom) and a desirable source of food (top). It has been observed that ants seeking food eventually traverse the shortest path between the nest and food by marking that trail with a chemical pheromone that each ant can sense (probably by smell). If the path is unobstructed [(a) in the figure], then the ants simply walk a more-or-less straight line between home and the food supply. But, if an obstruction is imposed [(b) and (c) in the figure], then more ants eventually end up on the shorter trail between the food and the nest, which in turn results in a greater pheromone concentration along that "optimal" trail. By depositing progressively more pheromone on the shortest path, almost all of the ants eventually end up on that path, and the "best" solution has been found. The red lines in the bottom part of the diagram illustrate the path evolution with the eventual result that the shortest path is identified.

The ACO algorithm mimics the ants' behavior using equations that represent the *random* motion of individual ants subject to their pheromone environment. Instead of searching for food, the metaphorical ACO ants search the landscape of a decision space for the maximum value of the function to be maximized. But the process they follow is a simplified model of ant behavior as observed in Nature. And, just as real ants eventually discover the best food source, ACO's "ants" eventually converge on the function's global maximum value.

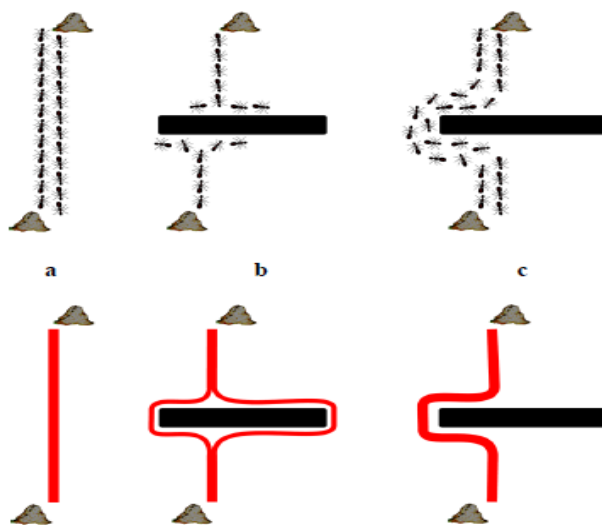


Fig. 1 Ant Colony Optimization: ants searching the shortest route using a pheromone trail.

Figure 1. Ant Colony Optimization Metaheuristic (reproduced from [1]).

2.1.4 Particle Swarm Optimization

Particle Swarm Optimization (PSO) [2] is another stochastic population-based Nature inspired evolutionary algorithm. PSO analogies the swarming behavior of fish or bees seeking food. Unlike ACO in which each “ant” creates a pheromone trail for other ants to follow, PSO’s population of “agents” collectively communicate two pieces of information: each individual agent’s “best” solution (greatest food concentration) and the population’s overall (global) best solution. Equations that mimic bee and fish swarming then control each agent’s subsequent motion in the decision space based on the competing tendencies of moving toward the global best and randomly exploring the vicinity of its best solution. As shown in Figure 2 for bees swarming around a flower concentration, after many steps PSO agents converge on the global best solution (highest flower concentration) because the local search fails to reveal any better solutions.

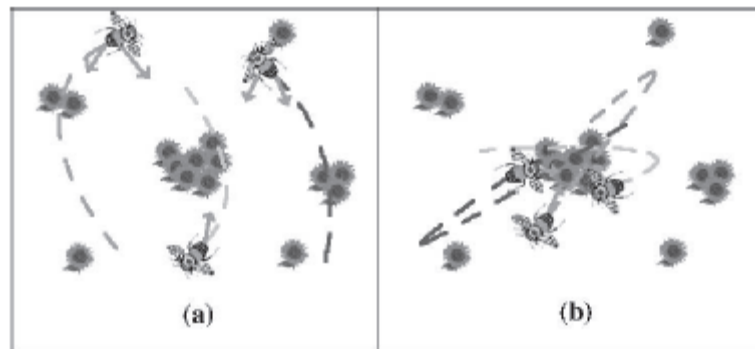


Figure 2. Particle Swarm Optimization metaheuristic (reproduced from [2]).

2.1.5 Genetic Algorithms

A Genetic Algorithm (GA) [3] analogizes the process of natural evolution or “survival of the fittest.” When biological parents “mate,” they exchange DNA to create a new individual (“child”) whose characteristics are drawn from both parents by combining the parents’ DNA. A GA creates successive generations of children who then serve as parents for the next generation whose children, in turn, will exhibit better “fitness” than the previous generation. In the context of search and optimization, the fitness is the value of the function to be maximized, so that the “best” fitness corresponds to the function’s global maximum. As the GA progresses generation after generation, the best discovered fitness improves and eventually converges on the function’s global maximum.

Figure 3 shows a typical GSA flowchart for an antenna optimization algorithm. It starts with a definition of the decision space (parameters to be optimized) and the “fitness function” to be maximized (for example, antenna directivity, or some specified combination of performance parameters such as gain, bandwidth, and so on). An initial population of “individuals” is randomly created, and each individual is defined by a *chromosome* that may be a binary sequence or a real number. Each chromosome comprises a set of *genes*, and each gene is one of the design parameters. For example, if the three design parameters were element length, inter-element spacing, and element diameter in a four element Yagi-Uda array, then there is a total of eleven design parameters, and each one is a gene. Thus, the optimization problem is defined on an 11-dimensional decision space, and the objective is to determine each of the eleven parameters so as to maximize some specific *fitness* function, say, the array’s gain-bandwidth product. A separate computer program is used compute the fitness at each step for each chromosome (the “evaluate fitness” box in Figure 3).

After the initial population’s fitnesses are evaluated, the “selection” process chooses two parent chromosomes that will mate (“crossover”) to produce two children chromosomes in the next generation. The selection and crossover processes take many varied forms. For example, the selection of parents may be random, or “best mates worst,” or best pairs pair wise through the population, and so on. The crossover operation likewise can take many forms. For example, the parents’ chromosomes may be split at the midpoint with first and second parts being swapped, or a random break point might be used, or some other combinatorial approach taken. Finally, the children thus created are subject to some level of *mutation*, a random perturbation of the chromosome structure just as real chromosomes are mutated in Nature. The steps described thus far are essentially common to all Gas, but the next step in the flowchart (“elitist model”) is not. In this GA, the worst individual in the new generation is replaced by the best individual from the previous generation, thus preserving the best solution from generation to generation as the algorithm progresses. As a final step, the best fitness is tested for convergence, and the process repeated until convergence is achieved.

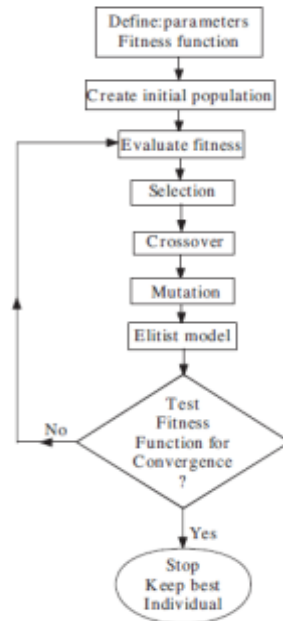


Figure 2. Flow chart diagram of real-coded GA.

Figure 3. GA flow chart (reproduced from [3]).

2.1.6 Simulated Annealing

Simulated Annealing (SA) [4] is a stochastic algorithm based on a metaphor drawn from physics instead of biology, as ACO, PSO, and GA are. SA analogizes the statistical mechanics of physical systems in thermal equilibrium with many degrees of freedom. In particular, the physical processes involved in annealing a solid as it cools forms the basis of the SA optimization algorithm, which has proven effective in optimizing problems with large numbers of decision variables. Because of SA's complexity, the algorithm is not described in detail. Instead its performance against a classic test problem is discussed.

The Traveling Salesman Problem (TSP) is a recognized example of combinatorial optimization that SA was used to solve because it constitutes a good test of an algorithm's effectiveness. The salesman must visit N different cities once each and return to his starting point. The problem is to determine the least costly route using a "cost" or "objective" function that is specified beforehand. Minimizing the cost is the same as maximizing its negative (note that minimization and maximization problems are exactly the same except for multiplying the objective function by -1). The TSP is a multidimensional search and optimization problem in the same vein as an antenna optimization problem, so that an algorithm suitable for one very likely is applicable to the other.

For the SA test, the TSP cost function is simply the total distance travelled by the salesman (to be minimized). Two different distance metric can be used, the standard Euclidean distance (“square root of the sum of the squares”), or the “Manhattan” metric (sum of the separations along the two coordinate axes), the latter being used in this case because it is simpler (less computationally intensive). Evolved solutions for TSP appear in Figure 6 and show a clear tendency towards removing redundancy in the travelled route, with the final solution (d) being close to optimal as discussed in [4].



Figure 4. Evolution of SA solutions to TSP (reproduced from [4]).

2.1.7 Central Force Optimization

Central Force Optimization (CFO) [5] is a new algorithm that departs significantly from all other Nature inspired metaheuristics. ACO, PSO, SA, and the other algorithms described below are all inherently *stochastic*. Every run with the same setup parameters in general produces a different set of solutions. No two runs yield the same results because these algorithms rely on true randomness in their functioning. The values of certain key variables in the algorithm are, by definition, random variables that are computed from a probability distribution. The values of these variables must vary from one calculation to the next, and their values are completely unknown and unknowable until the probabilistic calculation is performed.

CFO is quite different. It is based on an analogy drawn from gravitational kinematics, which in turn is based on Newton’s laws of gravity and motion. Newton’s laws are mathematically precise (completely *deterministic*) and, as a result, so too is CFO. CFO searches the decision space by “flying” probes through it whose trajectories are computed by deterministic equations that analogize Newton’s laws of motion.

Figure 5 shows how CFO's probes move through a 3D decision space at each time step sampling the decision space by computing the fitness of the function to be maximized (shown by the darkened circles). CFO thus provides some major advantages over stochastic algorithms, *viz*, every run with the same setup returns exactly the same answers, and because of that characteristic only one run is necessary (stochastic algorithms usually are run many times and the results averaged). CFO has been effectively used for antenna optimization, and it holds considerable promise for use in set-top antenna design.

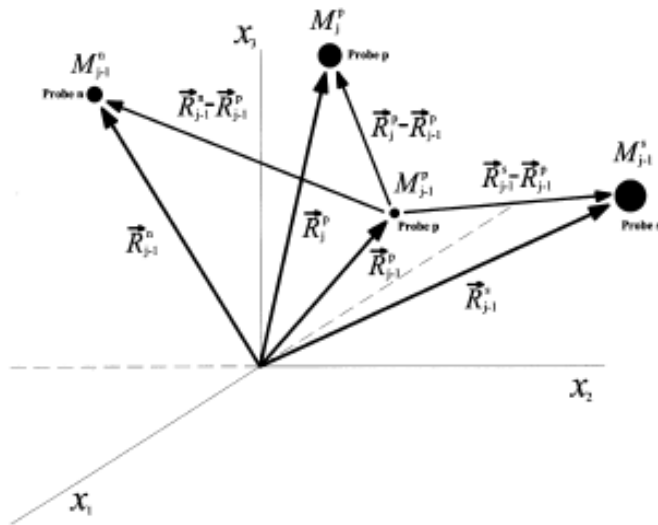


Figure 5. Central Force Optimization metaheuristic (reproduced from [5]).

2.1.8 Invasive Weed Optimization

Invasive Weed Optimization (IWO) [6] draws its inspiration from the colonization characteristics of invasive flora as understood from weed biology and ecology. Like ACO, PSO, GA, and SA, IWO is a population-based stochastic algorithm. Weeds exhibit a very strong tendency to opportunistically occupy (colonize) the interstitial spaces in a cropping field. Spaces not occupied by crops, which usually do not spread, become weed-filled, and the weed then grows and propagates by consuming unutilized resources in the field. The weed that uses these resources most effectively becomes the dominant (fittest) weed. When a weed flowers, it produces seeds that are randomly dispersed throughout the field until all interstitial space is occupied and all resources utilized.

Figure 6 shows a flow chart the IWO implementation used to solve electromagnetic problems in [6]. This flowchart starts out much the same as the GA flowchart with a randomly generated population whose fitness is evaluated in the initial step. Each weed then produces a number of seeds (reproduction) based on its fitness, with weeds having better fitnesses being allowed to produce more seeds. The seeds are

then randomly dispersed through the decision space using a normal (Gaussian) distribution of random numbers with mean value equal to the weed’s location. After the new seeds have been dispersed, they are allowed to grow into new flowering weeds, and the process is repeated until a convergent solution is generated. Because the number of weeds grows constantly, a maximum weed population serves as a ceiling on weed count. Whenever it is exceeded, the bottom worst plants are “weeded out” by being discarded.

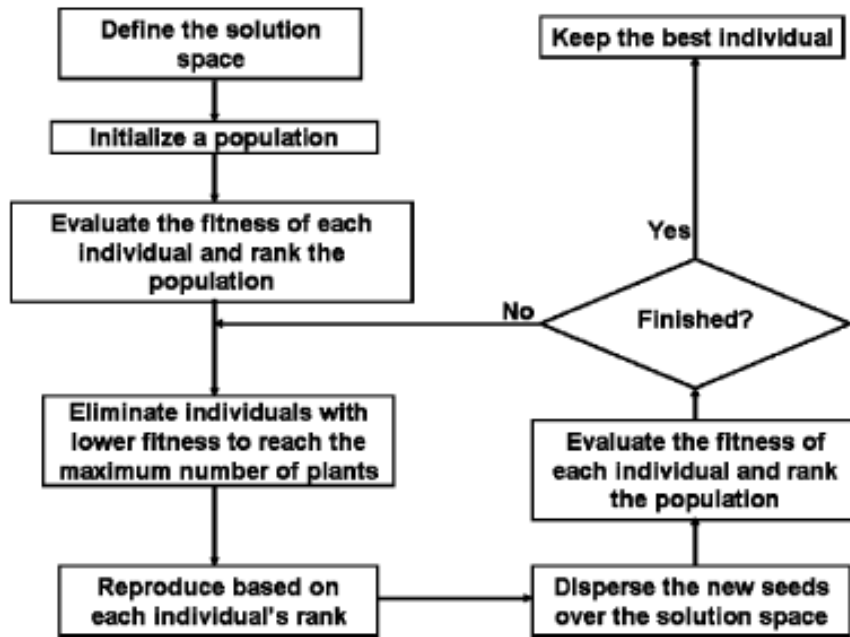


Figure 6. Invasive Weed Optimization flow chart (reproduced from [6]).

2.1.9 Intelligent Water Drop Algorithm

The Intelligent Water Drop algorithm (IWD) [7], like SA and CFO, analogizes a physical process. But, like SA and unlike CFO, it is stochastic in nature instead of deterministic. IWD is inspired by the notion that the seemingly random meanders in a river or stream bed are, in fact, based on mechanisms that can be applied to effectively solve optimization problems. Two principal factors are considered in IWD: water velocity and soil characteristics. Each IWD flows from a source to a destination, initially with non-zero velocity and zero soil. Along its route, velocity and soil both may be gained and lost. Soil inhibits drop velocity, so that between points the IWD’s velocity increases inversely with soil (in a non-linear manner). Figure 7 shows typical IWD results for the Travelling Salesman Problem (see also discussion above on SA and TSP).

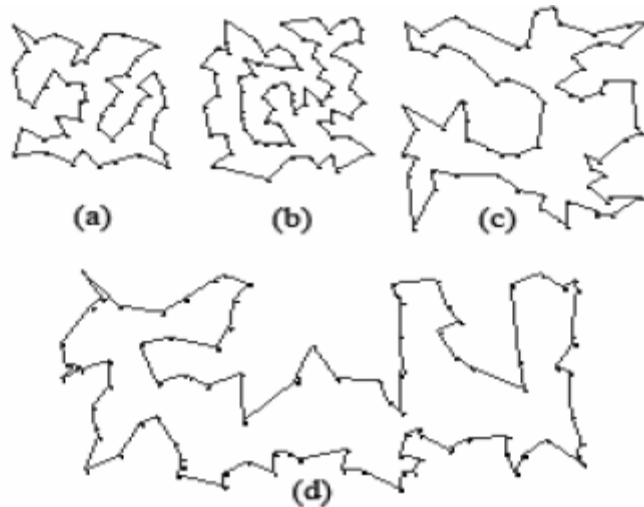


Figure 7. IWD results for the Traveling Salesman Problem (reproduced from [7]).

2.1.10 Bacteria Foraging Optimization

Bacteria Foraging Optimization (BFO) [8] mimics the natural behavior of bacterial seeking food. The motion of individual bacteria is driven by avoiding noxious elements in the environment while “swimming” upward along the food concentration gradient hopefully locating a denser source of food. *Chemotaxis* is the process by which a bacterium tumbles to orient itself, swims a fixed distance, and samples the food concentration at its new location. If the concentration is greater than at the previous location, then the bacterium continues in the same direction for another step. But if the concentration is lower, then the bacterium tumbles into a new direction and explores it instead. Each bacterium has a finite lifetime that limits the number of steps it can take. At the end their lifetime bacteria that are in the highest food concentration regions are allowed to “reproduce” by splitting into two new bacteria, while those in other regions die. Because the bacteria are dispersed, after the reproduction step, only the best half are retained, while the others die, thus preserving the total number of bacteria. The user specifies the maximum number of chemotactic and reproductive steps, maximum swim length, and maximum swims in a given direction.

2.1.11 An Antenna Optimization Example

This section presents a specific example of an optimized antenna design, a Self-structuring antenna (SSA) that can alter its electrical shape in near-real time in response to factors such as a changing environment or a change in mission. Typically these structures comprise wire segments that can be interconnected using control signals from a micro-controller device. An example of a SSA that was optimized using three different optimization algorithms appears in Figure 8 [9]. The antenna in this case is an asymmetric wire array containing 39 switches resulting in 549 *billion* possible antenna configurations.

The specific problem addressed in [9] was whether or not the optimization algorithms would provide better performance than a simple random search for a configuration that met specific performance criteria.

The wire structure was modeled with the Numerical Electromagnetics Code (NEC) following all modeling guidelines with respect to wire segmentation and segment length to diameter and wavelength ratios. The objective was to obtain low VSWR (< 2) values at frequencies of 40, 100 and 400 MHz. The antenna grid measured 0.6 meter square (0.08λ on a side at 40 MHz), which electrically is quite small. Figures 8, 9 and 10 compare the results of a random search to those produced by the three optimization algorithms. Random search performed very poorly at the lowest frequency, while each of the optimization algorithms performed relatively well. The GA produced the “tightest” results at 40 MHz (minimum standard deviation), and achieved the design objective in 60% of the trials. This example shows that real-time-optimized SSAs are within reach for the set-top antenna application at this time, and that fairly economical designs may be possible.

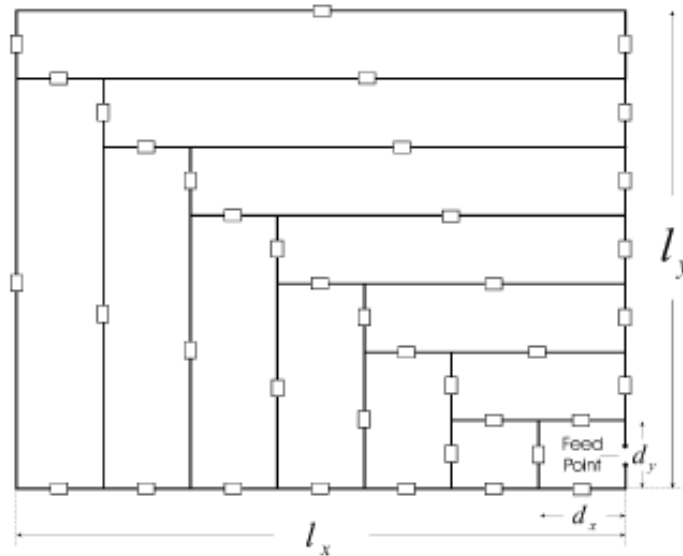


Figure 8. SSA geometry (reproduced from [9]).

TABLE IV
 LOWEST SWR FOR A RANDOM SEARCH OF 1500 EVALUATIONS

	400 MHz	100 MHz	40 MHz
Trial 1	1.1157	2.5939	365.4
Trial 2	1.0509	2.5277	958.7
Trial 3	1.0847	1.3926	281.0
Trial 4	1.0251	1.4578	2274.8
Trial 5	1.1516	2.9019	1267.7
Trial 6	1.0936	1.3708	222.7
Trial 7	1.1020	1.5983	28.34
Trial 8	1.0649	1.3312	98.042
Trial 9	1.1206	2.6590	1306.8
Trial 10	1.0816	1.9016	133.4
mean	1.0891	1.9765	694.6
σ	0.0365	0.6317	737.66

TABLE V
 LOWEST SWR FOR AN ACO SEARCH OF 1500 EVALUATIONS

	400 MHz	100 MHz	40 MHz
Trial 1	1.0471	1.0246	2.1052
Trial 2	1.0123	1.0371	2.6384
Trial 3	1.0173	1.0418	1.2983
Trial 4	1.0049	1.0363	2.6466
Trial 5	1.0316	1.1012	12.392
Trial 6	1.0075	1.1692	2.6620
Trial 7	1.0314	1.1049	1.7787
Trial 8	1.0366	1.2319	1.3721
Trial 9	1.0046	1.1065	9.9923
Trial 10	1.0106	1.1854	6.9844
mean	1.0204	1.1039	4.3870
σ	0.0151	0.0719	3.9714

Figure 9. SSA VSWR, random search [left], ACO [right] (reproduced from [9]).

TABLE VI
 LOWEST SWR FOR AN SA SEARCH OF 1500 EVALUATIONS

	400 MHz	100 MHz	40 MHz
Trial 1	1.1687	1.1516	3.0731
Trial 2	1.0203	1.0225	1.4967
Trial 3	1.0108	1.0644	18.143
Trial 4	1.0028	1.1539	3.2275
Trial 5	1.0019	1.2632	1.6679
Trial 6	1.0071	1.1619	1.6165
Trial 7	1.0014	1.0465	1.1154
Trial 8	1.0105	1.1120	8.3711
Trial 9	1.0029	1.1734	4.2047
Trial 10	1.0246	1.0263	4.5326
mean	1.0251	1.1176	4.7449
σ	0.0511	0.0775	5.1755

TABLE VII
 LOWEST SWR FOR A GA SEARCH OF 1500 EVALUATIONS

	400 MHz	100 MHz	40 MHz
Trial 1	1.0096	1.1212	1.0864
Trial 2	1.0092	1.0909	2.8490
Trial 3	1.0096	1.0778	2.2738
Trial 4	1.0057	1.0414	1.4017
Trial 5	1.0086	1.0482	2.3839
Trial 6	1.0180	1.0764	1.9164
Trial 7	1.0041	1.0694	1.2298
Trial 8	1.0126	1.0873	1.7648
Trial 9	1.0056	1.0942	1.7939
Trial 10	1.0032	1.0735	4.9056
mean	1.0086	1.0780	2.1605
σ	0.0044	0.0229	1.1065

Figure 10. SSA VSWR, SA [left], GA [right] (reproduced from [9]).

2.1.12 References

- [1] Pechac, P., "Electromagnetic Wave Propagation Modeling Using the Ant Colony Optimization Algorithm," *Radioengineering*, **11**, No. 3, September 2002, p. 1.
- [2] Robinson, J., and Rahmat-Samii, Y., "Particle Swarm Optimization in Electromagnetics," *IEEE Trans. Antennas and Propagation*, **52**, no. 2, Feb. 2004, p. 397.

- [3] Mahanti, G. K., Pathak, N., and Mahanti, P., "Synthesis of Thinned Linear Antenna Arrays with Fixed Sidelobe Level Using Real-Coded Genetic Algorithm," *Prog. in Electromagnetics Research*, **PIER 75**, 319-329, 2007.
- [4] Kirkpatrick, S., Gelatt, C. D., and Vecchi, M. P., "Optimization by Simulated Annealing," *Science*, **220**, no. 4598, 13 May 1983, p. 671.
- [5] Formato, R. A., "Central Force Optimization: A New Metaheuristic with Applications in Applied Electromagnetics," *Prog. in Electromagnetics Research*, **PIER 77**, 425-491, 2007.
- [6] Karimkashi, S., and Kishk, A. A., Invasive Weed Optimization and its Features iElectromagnetics," *IEEE Trans. Antennas and Propagation*, **58**, no. 4., April 2010, p. 1269.
- [7] Shah-Hosseini, H., "The Intelligent Water Drops Algorithm: A Nature-Inspired Swarm- Based Optimization Algorithm," *Int. J. Bio-Inspired Computation*, **1**, nos.1/2, p. 71, 2009.
- [8] Datta, T., and Misra, I. S., "Adaptive antenna Array Processing: The Bacteria-Foraging Algorithm and Particle-Swarm Optimization," *IEEE Antennas and Propagation Magazine*, **51**, no. 6, December 2009, p. 69.
- [9] Coleman, C. M., Rothwell, E. J., and Ross, J. e., "Investigation of Simulated Annealing, Ant-Colony Optimization, and Genetic Algorithms for Self-Structuring Antennas," *IEEE Trans. Antennas and Propagation*, **52**, 4, p. 1007, April 2004.

2.2 Fragmented Antennas

As an additional illustration of the power of an electro-magnetic (EM) optimization algorithm, this section describes the computer program **FAopt** that begins with a grid of wires as shown in Figures 1 and 2 and optimizes the placement of these wires using a Binary Genetic Algorithm (BGA) and the NEC-4 [1] Method of Moments (MoM) FORTRAN code. Each bit in the BGA chromosome is either a 1 or a 0, representing the presence or absence of a wire, respectively. Quadrant 1 and 3 are a mirror image of each other as well as quadrant 2 and 4, so that the antenna is symmetrical about its diagonal. The resulting antenna is comprised of a series of plated conductors, some of which are connected to one another. Some are capacitively/inductively coupled and act as parasitic elements to increase the element impedance and radiation pattern bandwidth. These types of radiating elements, when implemented as pixels rather than wires, (see Maloney et al of GTRI [2]) are generally called “fragmented” antennas [3]. **FAopt** allows the user to choose the polarization as either vertical or horizontal, and the antenna can be either directional or omni-directional. The user also can choose the dimensions for the desired antenna, as well as the frequency range. This program was used to design a set-top antenna to operate in the VHF and UHF bands. (See Section 3.0). During optimization a window is shown that updates the progress of the optimizer with the best “figure of merit” (FoM) displayed along with the standing wave ratio.

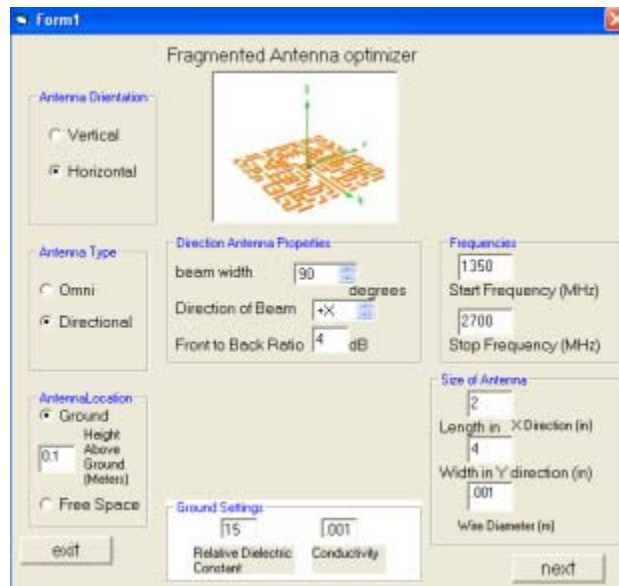


Figure 1: FAopt Code’s GUI

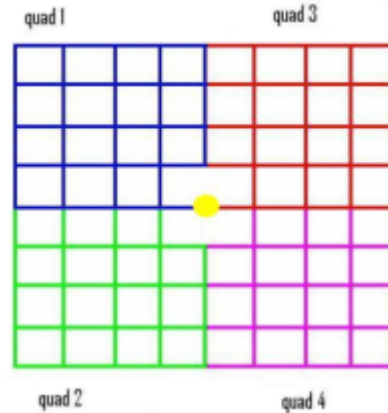


Figure 2: Wire Grid

As an example, a thin planar directional antenna was optimized using **FAopt** as a horizontally polarized antenna from 2400-2480MHz with 8 blocks per row/column per quadrant. The orientation appears in Figure 1, and the antenna model is shown in Figure 3. The dimensions for this antenna are 2" by 2". A prototype was built as shown in Figure 4.



Figure 3. Fragmented Directional WiFi Antenna

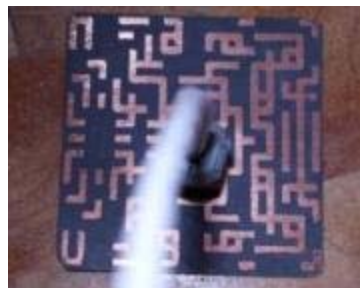


Figure 4. Fragmented Directional WiFi Antenna

The simulation results, which were confirmed by measurements, shows the average gain of this antenna to be better than 1.9 dBi. This antenna is a directional WiFi antenna optimized to have a F/B ratio of about 6 dBi. Its radiation pattern is very consistent

across the band as shown in Figure 6, and its measured VSWR is better than 2:1 across the band. Further work, such as changing the grid template or the optimization routine, could be undertaken to make this approach more efficient for designing set-top VHF/UHF antennas.

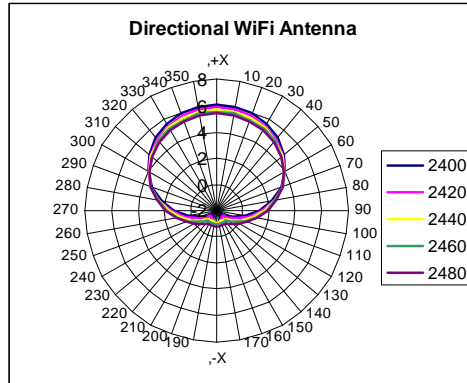


Figure 5. Pattern of Directional WiFi Antenna

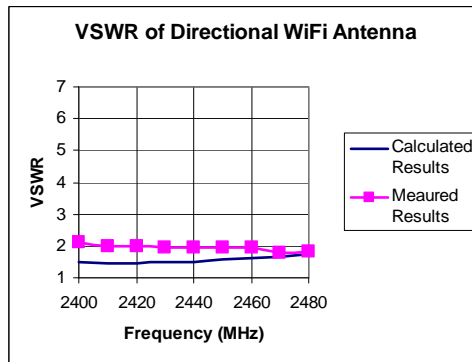


Figure 6. VSWR of Directional WiFi Antenna

The F/B ratio of simulated and measured are in fair agreement as shown in Figure 7.

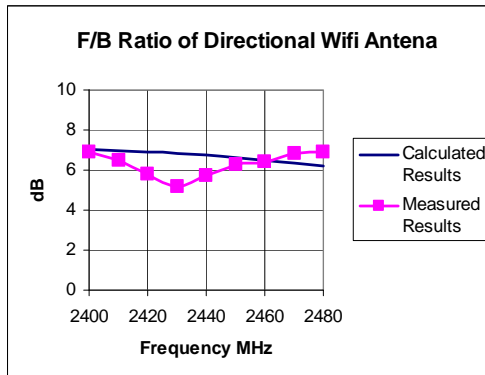


Figure 7. F/B Ratio of Directional WiFi Antenna

References

- [1] G. J. Burke, "Numerical Electromagnetics Code-NEC-4 Method of Moments", Lawrence Livermore National Laboratory, 1996
- [2] J. G. Maloney, M. P. Kesler, P. H. Harms, G. S. Smith, United States Patent No. US 6323809 B1, Nov 27,2001
- [3] B. Thors, H. Steyskal and H. Holter, "Broad-Band Fragmented Aperture Phased Array element Design Using Genetic Algorithms", IEEE Trans. *Antennas Propag.*, Vol 53, no. 10, pp. 3280-3287

2.3 Non-Foster Impedance Matching

Foster's reactance theorem, which dates to 1924, states that a lossless reactance must have a positive slope with frequency. Any lossless matching network presumably satisfies the theorem, but a great deal of research that has been done on "non-Foster matching" in the past 15 years suggests otherwise. This section examines how non-Foster networks may be useful in set-top antennas to match an electrically small element (characterized by a low real and high negative imaginary complex impedance) within, for example, the low-VHF band.

Until recently no one has created a practical antenna system using this method that showed much of an improvement in performance. This was due to limitations in the semiconductor technology at the time that permitted only narrow band solutions. Semiconductor technology has improved considerably in recent years resulting in increased bandwidth, lowered noise, and decreased losses in the devices. Electrically small antennas present high Q impedances characterized by large reactances and small radiation resistances. For such antennas, the effectiveness of passive matching circuits is severely limited by gain bandwidth theory, which predicts narrow bandwidths and/or poor gain. The result inevitably is a poor signal to noise ratio compared with a larger antenna.

Non-Foster matching uses negative impedance converters (NIC) to create "negative" capacitors and "negative" inductors [1-2]. It is possible, for example, to use negative capacitance to cancel out the reactance in a short dipole or monopole. This leaves only a small real impedance which could then be matched to, say, 75Ω using a transformer. One disadvantage of this approach is that transformers add to the antenna size which could be undesirable. An alternative to matching could be achieved by placing the non-Foster matching circuit away from the feed to control both the real impedance as well as the reactance of the antenna [3]. The potential improvement in antenna performance is very significant. Theoretical bandwidth improvements have been shown for a small loop (increasing bandwidth from 50 MHz to 300MHz at a center frequency of 700MHz), as well as a small broadband dipole (increasing bandwidth from 250MHz to 1000MHz, lowering the lower operating frequency from 250 MHz to 190 MHz).

It should be noted that the Figures and Tables in this section were taken from references 2 through 5, listed at the end of this section.

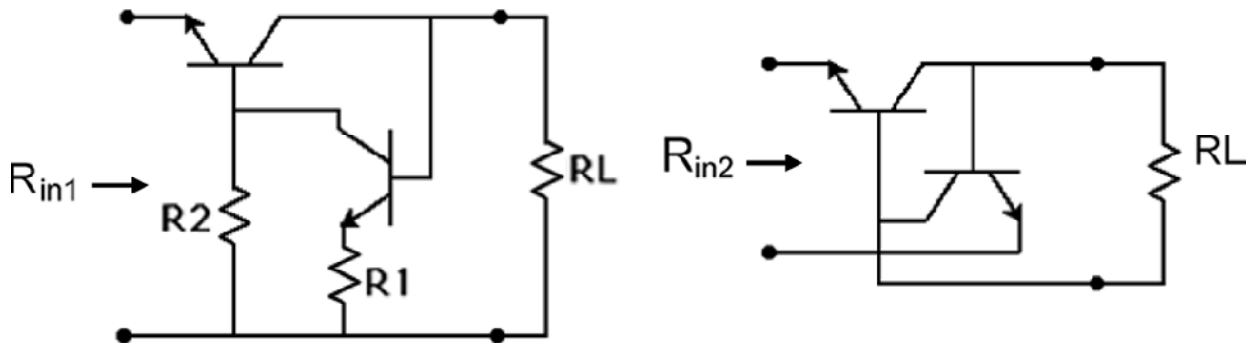


Figure 1. Linvill's ideal OCS NICs terminated in a resistance.

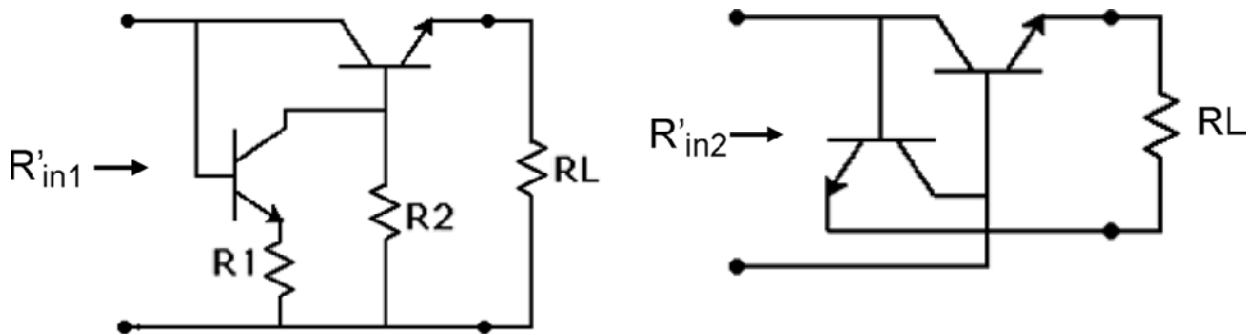


Figure 2. Linvill's ideal SCS NICs terminated in a resistance.

With an ideal transistor, a pure negative resistance is achievable. In Linvill's actual realizations (Figures 1 and 2), a substantial reactive component of the input impedance Z accompanies the negative resistance, resulting in a low Q , where the "resistive" Q is defined as: $Q = \text{Re}(Z) / \text{Im}(Z)$. The circuits shown are "open-circuit stable" (OCS), meaning, practically, that if a very large resistance terminates the negative-resistance one-ports on the left, then the overall network will be stable. The networks of Figure 1 can be turned around as shown in Figure 2, where negative resistances of the "short-circuit stable" (SCS) variety are obtained. Again, practically speaking, this means these networks will be stable if a very large conductance is placed across the input. An initial step in improving the power efficiency of non-Foster matching is simply to use a single-transistor version of the NIC [4].

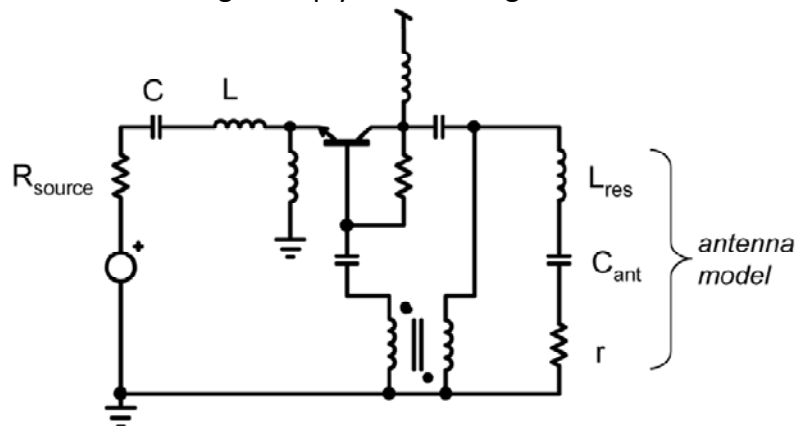


Figure 3. Non Foster Matching

An example of a non-Foster matching circuit is shown in Figure 3. Although not shown in the schematic, a transformer would be used at the input to make the effective value of R_{source} , as seen by the matching circuit, to be 18.75Ω (4:1 impedance ratio). The circuit negates antenna's Capacitance C_{ant} and the voltage-managing resonating inductor L_{res} , as well as the radiation resistance r . The idea is to cancel the negated L_{res} and C_{ant} with C and L on the left, respectively. The negated r is absorbed by the much larger source resistance and does not affect operation of the circuit. The source resistance would be 75 ohms in this case.

An example of non-Foster matching for a 12 inch dipole is shown in Figure 4. It is shown in Figure 5 that this non-Foster matching network creates a negative capacitance that is used to cancel out the reactance of the 12" dipole. This is used along with a transformer to help match the radiation resistance of the antenna to the source impedance of 50Ω . The non-Foster matching network is compared to a similar dipole with a lossy passive network for improvements in signal to noise as shown in Figures 6 and 7. The improvement in SNR is quite remarkable, as much as 25 dB around 44 MHz.

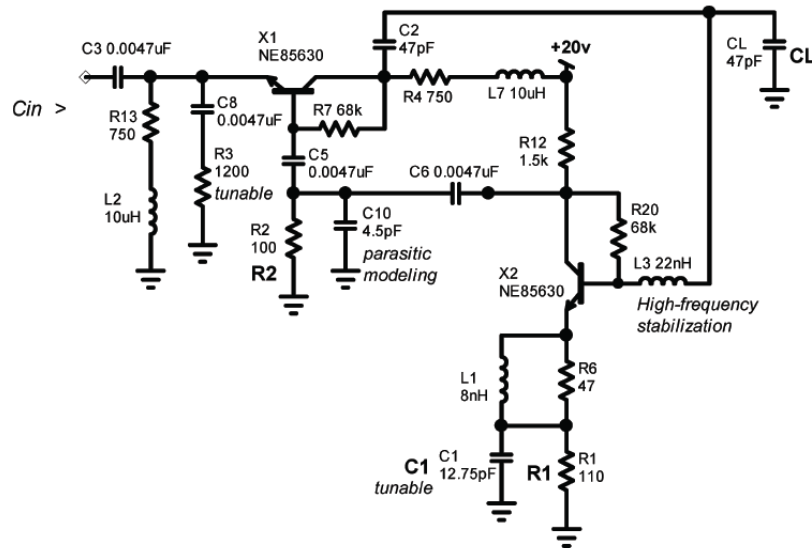


Figure 4. Non-Foster Matching Network for a 12" Dipole.

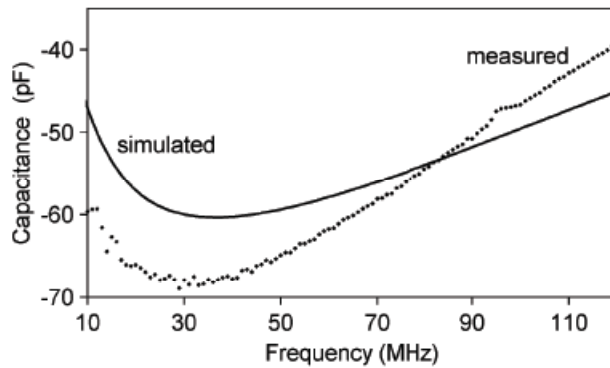


Figure 5. Measured and simulated results for capacitance of non-Foster matching network.

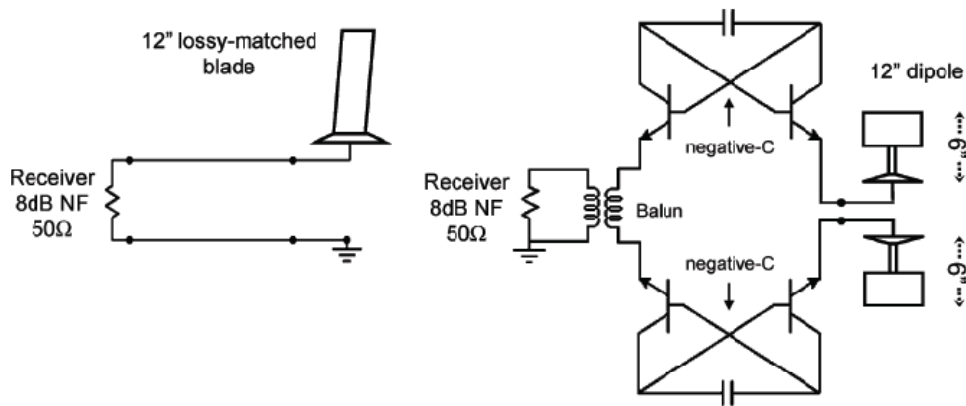


Figure 6. Setup for Signal to Noise improvement measurement.

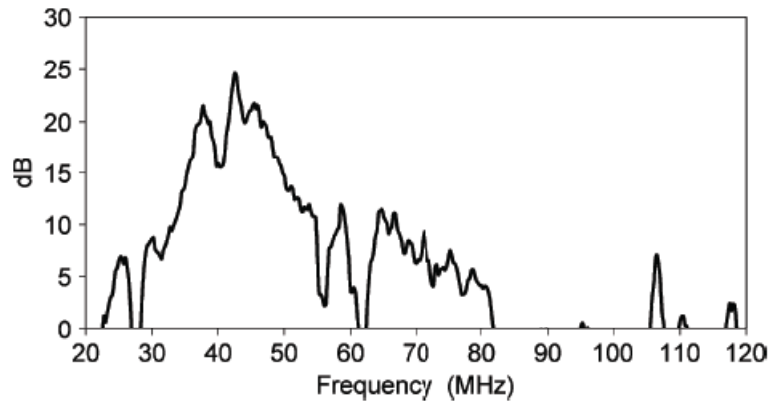


Figure 7. Measured Improvement of Signal to Noise

Non-Foster matching may be particularly useful for the set-top application because it works best with electrically small antennas. Therefore, this type of match could be useful when designing a small VHF/UHF DTV set-top antenna. Improvements in signal to noise measurements have been shown from 20MHz to 400 MHz [5]. In particular, the use of non-Foster techniques to impedance match a lossy electrically-small dipole antenna has been quite effective. On an antenna range, there was a measured 30 dB gain improvement over 60 – 200 MHz, with several dB of improvement as high as 400 MHz. Again, the comparison was to the same antenna with no matching at all. Although no S/N measurements were made, the circuits used were based upon the same low-noise designs developed earlier for lower-frequency circuits. Because of the lossiness of the antenna, passive matching can do a little better than no matching at all, and these results are illustrated in simulation. This computer simulation designed a number of “best-effort” passive matching networks and calculated the transducer gain (S_{21}) between a 50 ohm source and the complex impedance of a 6-inch monopole. S_{21} for no matching and S_{21} for a single, ideal negative capacitance whose value (-5.54pF) exactly cancels the antenna reactance at 30 MHz, were calculated. Plots of the real and imaginary parts of the antenna impedance are shown in Figure 8. The various matching networks are illustrated in Figure 9; each of these would appear in place of the NIC in Figure 10b.

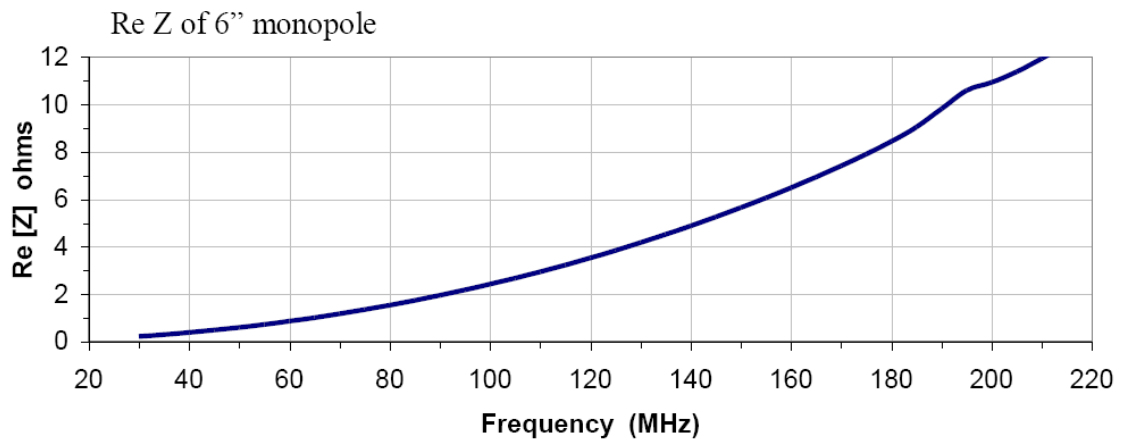


Figure 9-A. Real Part of Antenna Impedance for a six inch monopole

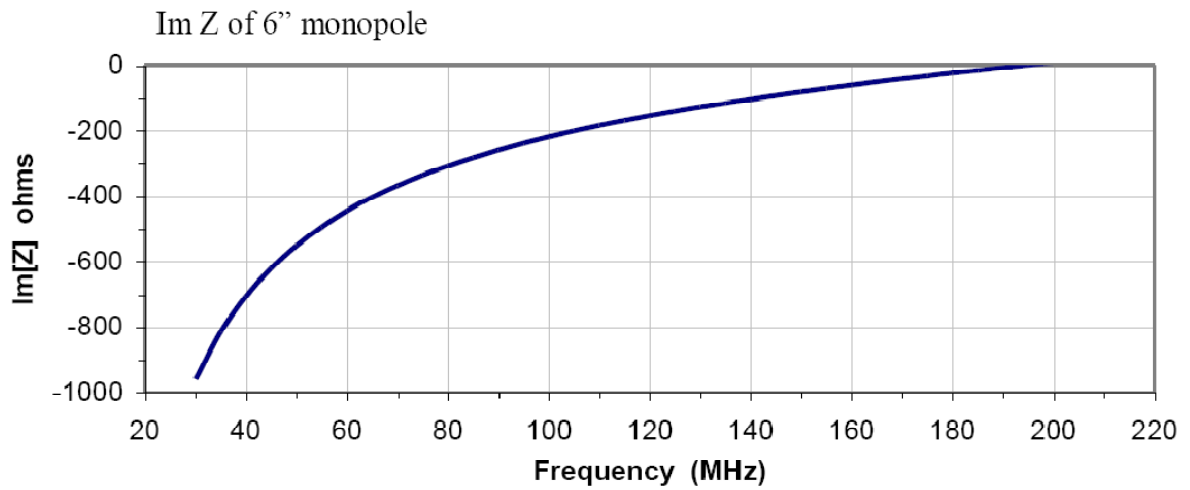


Figure 9-B. Imaginary Part of Antenna Impedance for a six inch monopole

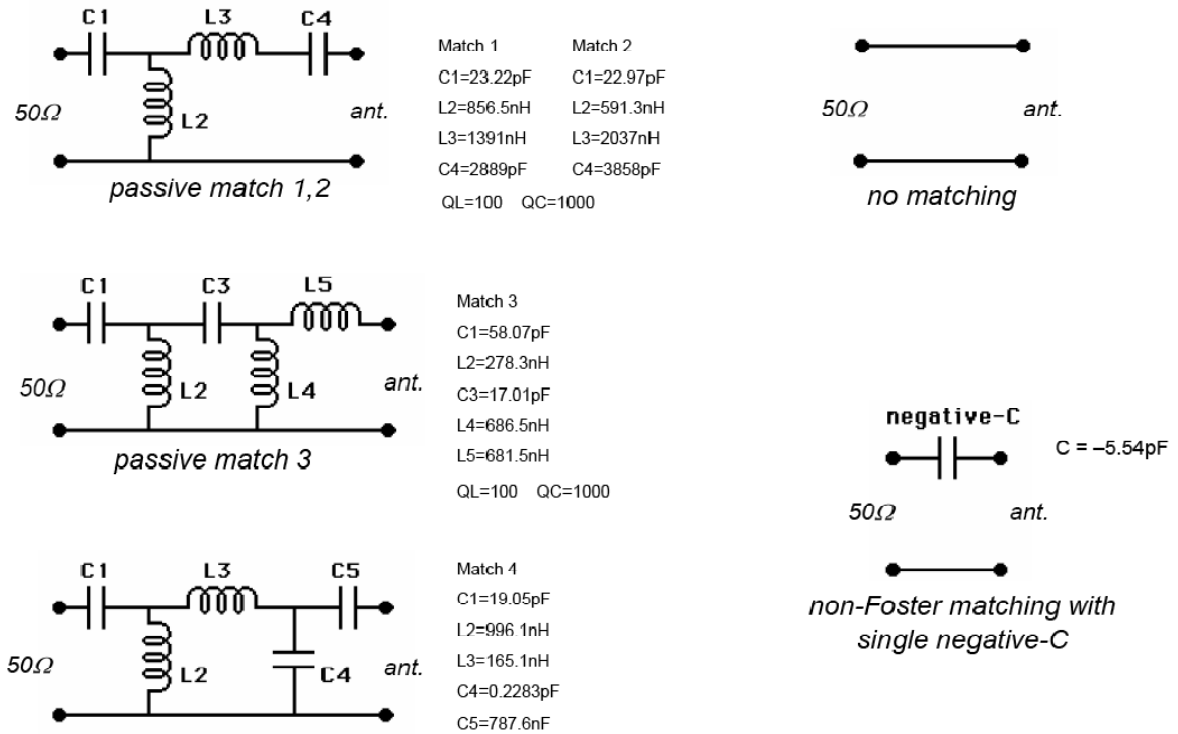


Figure 10. Various Matching Techniques for six inch monopole

<i>Average gain 30-220 MHz</i>	
Non-Foster neg-C:	-13.2 dB
Passive match 4:	-21.9 dB
Passive match 3:	-23.1 dB
No matching:	-23.9 dB
Passive match 1:	-26.7 dB
Passive match 2:	-28.4 dB

Table 1. Computed Average Gain of all matching techniques.

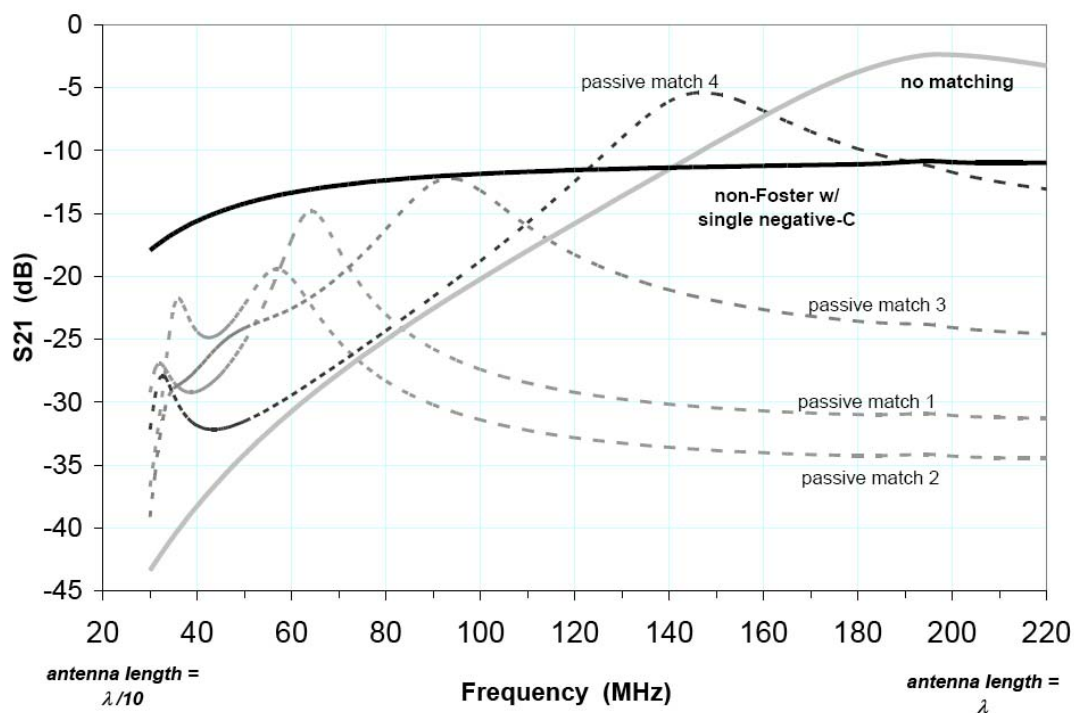


Figure 11. Plots of Computed Gains of all matching techniques for a six inch monopole

The six inch monopole was then built using both the non-Foster matching network and an unmatched antenna. They were both measured with the results shown in Figure 12. In the design, NE68019 BJTs were used in the NICs because these devices provided good overall performance over the entire frequency band. Again, the results are quite remarkable, with the non-Foster antenna showing average gain improvements between about 2 and 28 dB. It is noteworthy that the greatest improvements are at lower frequencies, between about 60 and 210 MHz, approximately the low and high VHF bands.

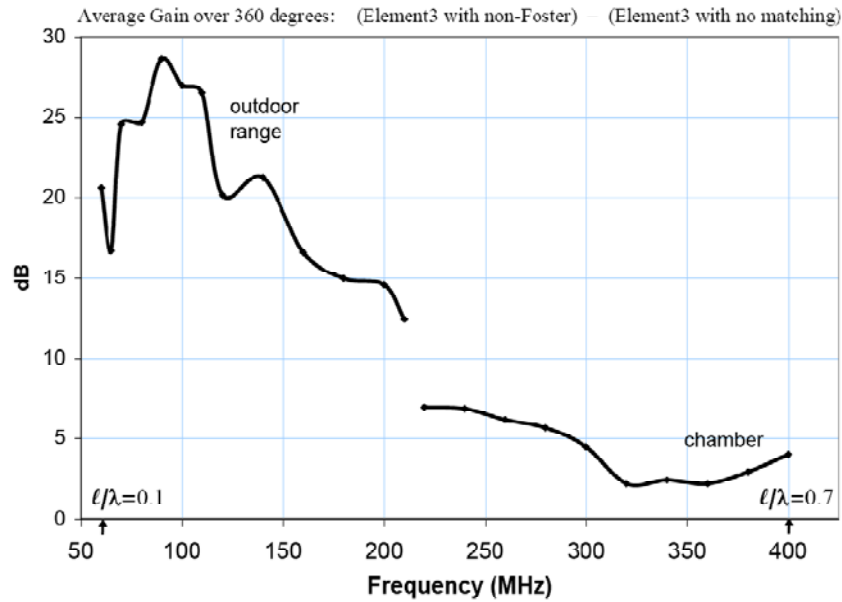


Figure 12. Gain of a non-Foster matching network over the same antenna with no matching.

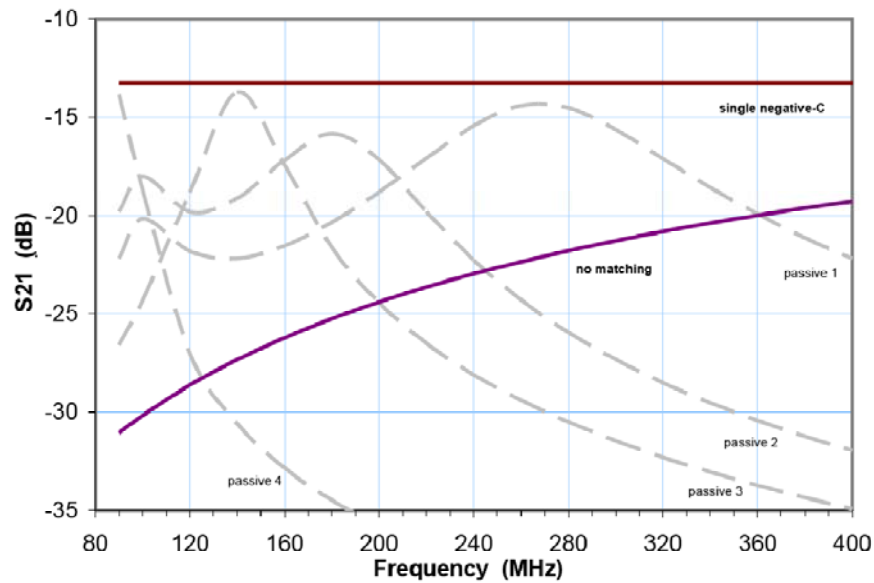


Figure 13. Plots of Computed Gains of all matching techniques for a six inch dipole

Results for an electrically small lossy dipole are shown in Figure 13 (this antenna was simulated, not measured). The actual gain may be less due to noise of the device if this were to be built and tested. Thus, realization of non-Foster technology is still limited by the analog circuitry performance. With respect to the set-top application, it is very reasonable to expect that as better silicon devices are developed covering the entire television frequency range will be possible with substantially better antenna performance in terms of gain and signal-to-noise ratio.

References

- [1] R.C Hansen, "Electrically Small Super directive and Super conducting Antennas", John Wiley & Sons Inc. 2006
- [2] J. T Aberle, R. Leopsinger-Romak, C. A Balanis, "Antennas with Non-Foster Matching Networks", Morgan & Claypool Publishers, 2007
- [3] S. Koulouridis and J.L. Volakis, "Non-Foster circuits for small broadband antennas",
- [4] S. E. Sussman-Fort and R. M. Rudish "Non-Foster Impedance Matching of Electrically-Small Antennas", IEEE Transactions on Antennas and Prop., Vol 57, NO. 8, August 2009
- [5] S. E. Sussman-Fort and R. M. Rudish, "Non-Foster impedance matching of a lossy, electrically-small antenna over an extended frequency range" presented at the Antenna Applicat. Symp., Allerton Park, IL, Sep. 2007

2.4 Active RF Noise Cancelling

Considerable work has been done to mitigate noise from devices near receiving antennas, as is particularly useful in set-top antennas. An antenna placed on top of a television is especially vulnerable because it may pick up noise from internal circuitry. But this noise can be reduced, which in turn reduces the noise floor, or, equivalently, increases the signal-to-noise ratio (SNR). Intersil [1] has created the QHx220 chip that accomplishes this e.g. at UHF frequencies, or more precisely from 300 MHz up to >3GHz. MegaWave has evaluated the Intersil noise cancellation chip QHx220 shown in Figure 1. The chip was tested for signal to noise improvements at 535MHz as shown in Figure 2. Measured results showed an improvement of about 12dB in SNR as shown in Figures 3 and 4. This technology has been extended down to FM covering the VHF III band [2], which is necessary for this approach to be viable in the set-top environment.

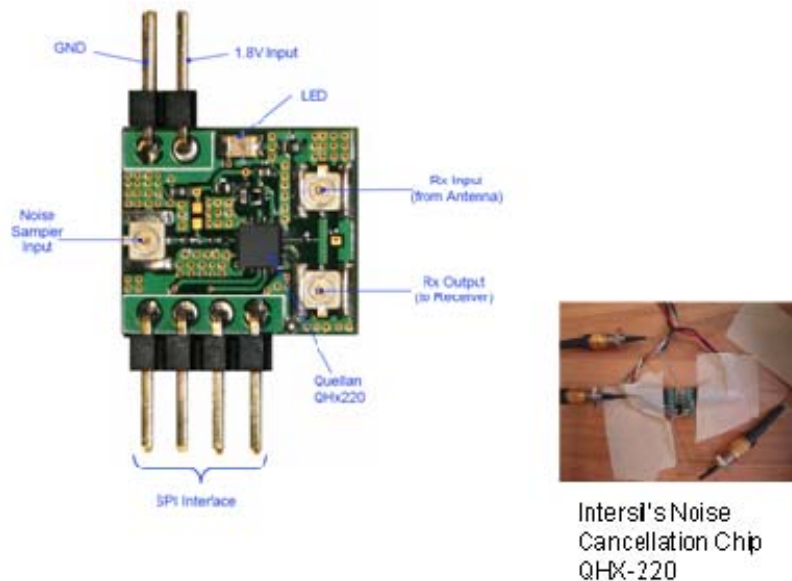


Figure 1: Intersil's Noise Cancellation Chip QHx220

This system works on a principle similar to Bose and Sony noise cancelling headsets, but at a ~1,000,000 times higher frequency. It requires an I and Q setting obtained from the DTV receiver's channel setting and the system's link quality parameter (BER, SNR, RSSI, etc.). This is done on either a micro-processor or in the baseband processor, which run a set of small algorithms. As a result the noise minimum is centered in the desired TV channel and signals - formerly buried in the noise floor - are being restored (Figure 4, e.g. at 549MHz).

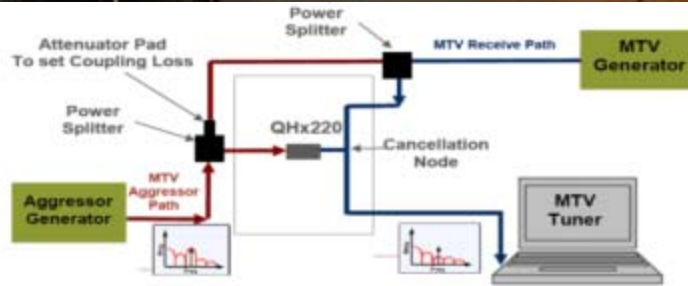
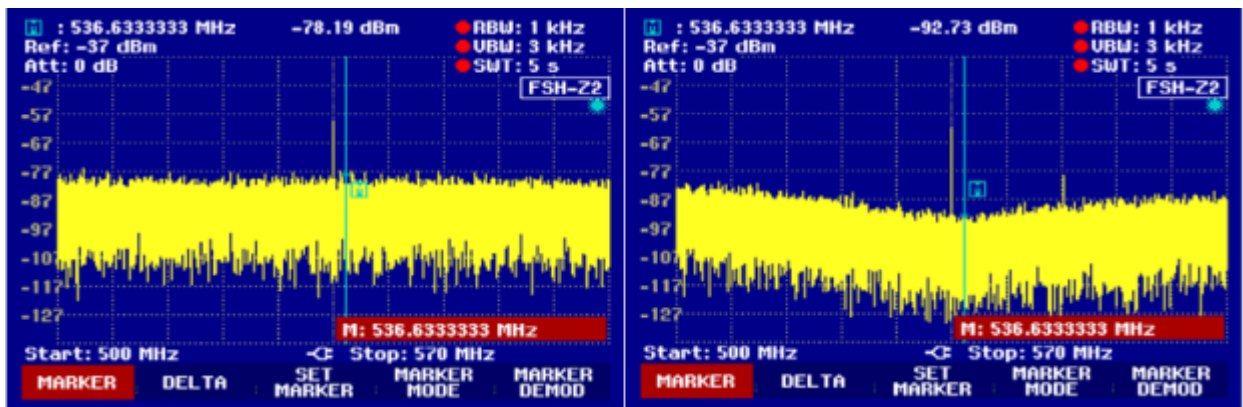


Figure 2 Noise Cancellation Test and Evaluation Setup



Figures 3-4: Measured results before and after noise cancellation

References

[1] Intersil Corporation, 1001 Murphy Ranch Rd, Milpitas, Ca 95035, www.Intersil.com

[2] QHx120 (development) works from 75MHz up to 225MHz.

2.5 Automatic Antenna Matching Systems

2.5.1 Summary

From an impedance matching point of view, the ideal antenna has a perfectly flat, purely resistive input impedance across its entire operating frequency range. The value of that impedance should be $70\ \Omega$ because this is the nominal industry standard characteristic impedances of the coaxial cable used in television receivers. Of course, no antenna is perfect. Quite to the contrary, most antennas' impedance variations with frequency are usually quite dramatic. This is particularly true for electrically small antennas, which tend to exhibit low radiation resistances and very high reactances in a narrow frequency range. Set-top DTV television antennas are not necessarily electrically small in the high VHF and UHF bands, but are at low VHF. Due to their required bandwidth (54-698 MHz) they invariably exhibit wide impedance fluctuations.

An impedance mismatch leads to losses and reflected energy that is not transferred to the receiver. These inefficiencies can be mitigated to a great degree by precise impedance matching that is provided by an "antenna tuner" (AT) connected between the antenna output terminals and the receiver input port. The AT may comprise a network of discrete components, or it may be a distributed, continuously varying structure (a tapered transmission line, for example), or some combination of both.

Lumped element matching networks go back to the earliest days of radio, and they often require manual adjustment of the matching elements (usually variable capacitors or roller inductors). In the early 1960s the military developed "ALE" (automatic link establishment) systems that employed remotely controlled automatic antenna tuners. These networks are usually located at the antenna feed and remotely tuned automatically based on VSWR (voltage standing wave ratio) measurements made at the transmitter. Essentially the same approach is taken with the built-in automatic ATs that are common in modern transmitters (most amateur radios contain built-in auto ATs, for example).

Modern low-power ATs use relays to switch lumped elements (inductors, capacitors) in and out of the matching network until the desired match is achieved. This technology is highly developed and readily available for use in set-top TV receive antennas. It therefore is not reviewed in this report. Instead, the emphasis here is on new, developing technologies that may be useful for antenna impedance matching. Four broad categories have been identified.

(a) *Voltage controlled reactive elements* are capacitors and inductors whose values are controlled by an applied voltage. Instead of switching discrete components

in and out of a matching network using relays, the same operation is accomplished by varying the voltage applied to the reactive element. This type of non-mechanical system provides faster response time and more continuous control in a less noisy and probably smaller space than a relay-based AT.

(b) *Integrated ATs* are “antenna tuners on a chip,” a complete device that is fabricated on a single chip or in a very small module with only a few external components. Integrated ATs have received considerable attention for cellular applications, and they work quite well. Chip-level devices successfully match up to 10:1 VSWRs in the highly fluctuating cellular antenna environment with rapid response times and high efficiency. These devices are constantly improving, and it is likely that existing technology can meet set-top AT requirements.

(c) *Tunable tracking filters* are already used across the VHF/UHF TV bands for wideband DTV (digital television) tuners, and they work quite well, providing very flat passbands, steep skirts, and harmonic suppression from the tuner’s local oscillator. Extremely small devices have been designed and computer-simulated, and some measured data are available confirming achievement of design objectives. This is an evolving technology that may be transferrable to set-top AT requirements.

(d) *Software defined radio (SDR)* is a new concept in wireless communications that seeks to move system properties from the hardware layer to a high-level software layer by developing hardware modules that are fully software-controllable and configurable. SDR radios are gaining wide acceptance in many applications, and it is a developing technology. SDR “smart antenna” technology, which may be applicable to the set-top environment, consequently is a candidate technology for a television AT.

2.5.1.1 Voltage Controlled Reactive Elements

(a) *BZN (pyrochlore bismuth zinc niobate)* is a non-ferroelectric dielectric material that shows great promise for a new class of voltage tunable thin film capacitors [1]. When it was introduced in 2006, BZN exhibited the lowest loss of any room temperature complex oxide film with a very high dielectric constant and high tunability of (loss tangent ~ 0.0005 , dielectric constant ~ 180 , $\sim 55\%$ tuning range @ 1 MHz). Losses increase in the microwave range, but are controllable by modifying the electrode structure.

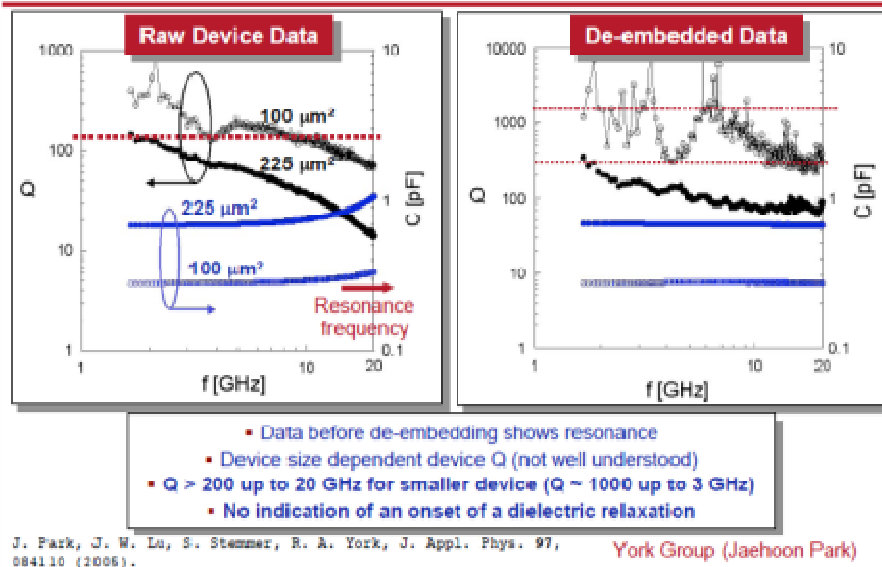


Figure 1. BZN capacitor high-frequency measurements (reproduced from [1])

Measured data for different size BZN thin film capacitors at higher frequencies appear in Figure 1. For small devices ($100 \mu\text{m}^2$) the Q -factor exceeds 200 up to 20 GHz (de-embedded data, right plot). Through about 3 GHz $Q \sim 1000$. In addition, self-resonance in the BZN thin film structure is well above 20 GHz. By comparison, the best state-of-the-art thin-film BST (barium strontium titanate) devices in 2006 exhibited Q s that decreased monotonically from about 100 at 1 GHz to around 20 at 20 GHz. BZN is a far superior tunable dielectric. BZN and similar materials (see below) hold considerable promise for the development of completely solid-state ATs that can be used to tune set-top TV broadcast band antennas.

(b) *PZN (lead zinc niobate)* thin film interdigital capacitors (IDC) have been fabricated to increase tunability and reduce bias voltage compared to BZN IDC implementations. Cubic pyrochlore PZN thin film dielectrics provide superior performance through the microwave range. Figure 2 shows a typical configuration. The IDC is fabricated on a silicon substrate in the usual coplanar waveguide (CPW) configuration. Figure 3 plots the measured low-frequency dielectric constant (blue) which increases from just over 200 to about 230 at 10 MHz. The tunability as a function of applied bias voltage decreases from unity to about 0.75 with an applied electric field of 2 mV/cm (bias voltage of 5.5 volts). At 1 GHz the device Q falls to about 10 at all bias voltages, but the tunability remains at 26% (compared to 25% at 1 MHz) for 5.5 volts applied bias. The PZN tunable capacitor thus is a strong candidate for voltage-tunable

set-top television antenna ATs, and its performance is comparable or better than that of BZN devices.

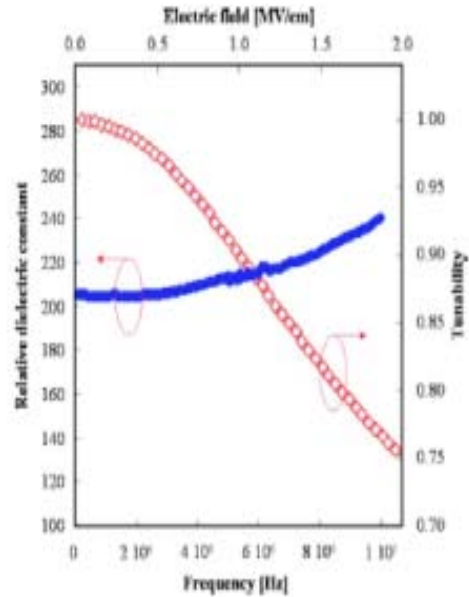
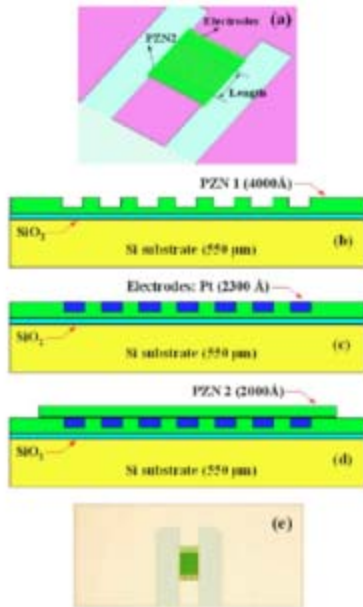


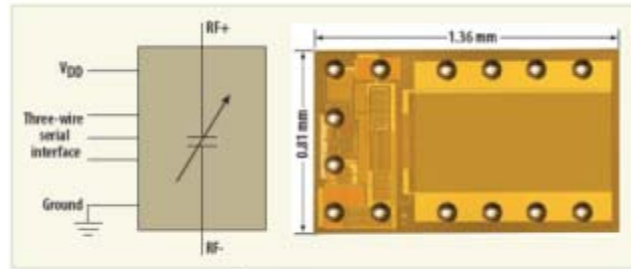
Figure 2. PZN IDC structure (reproduced from [2]). Figure 3. PZN IDC performance (reproduced from [2]).

(c) *DuNE™ capacitors* are a new patent-pending technology developed by Peregrine Semiconductor [3] for DTCs (Digitally Tunable Capacitors). The manufacturing process is based on Peregrine’s proprietary UltraCMOS™ technology supplemented by its HaRP™ design methodology. UltraCMOS™ is a patented low-power SOI (silicon on insulator) variant chip architecture that reduces transistor capacitance resulting in increased switching speed. HaRP™ is a design technology that produces significant improvements in harmonic results, linearity and overall RF performance.

The company claims that its DTCs provide digitally controllable capacitances in the range 0.5 to 10 pF with either 3:1 or 6:1 tuning ratios and 32 addressable states (5 bits). Q_s range from 40 to 80 between 1 and 2 GHz with device switching times below 5 μ sec. Power handling capability is quite good (+38 dBm @ 50 Ω), while power consumption is low (100 μ amps @ 2.4-3.5 volts DC). The manufacturer claims its DTCs provide better performance than currently available MEMS (*microelectromechanical system*) or BST devices, and they are readily available as off-the-shelf components.

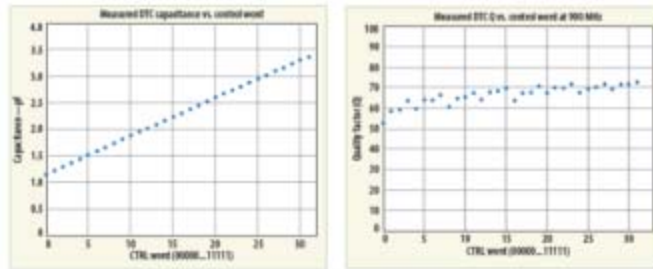
The digitally tuned capacitor schematic diagram and its “flip-chip” package appear in Figure 4. The DTC acts as a series capacitor with two RF terminals. It is powered by a single DC line, and controlled by a three-wire serial interface. The control word is five bits long. The device is extremely small (1.26 mm x 0.81 mm) and thus well-

suitable for use in TV set-top antennas. Measured performance is shown in Figure 5. Capacitance variation is very linear with control state (32 increments), and the variation ratio is 3:1, from 1.15 pF to 3.4 pF. The DTC Q-factor at 900 MHz, a representative cellular frequency, varies from about 53 to about 72, which is quite good.



5. The schematic diagram shows the DuNE DTC (left) while the photograph (right) shows a flip-chip DuNE DTC prototype that measures just 1.36 x 0.81 mm.

Figure 4. Digitally Tuned Capacitor (reproduced from [4]).



6. The measured performance of a 5-b DuNE DTC prototype shows linear tuning characteristic and a 3:1 capacitance range from 1.15 to 3.4 pF.

7. These measurements show the DuNE DTC prototype with quality factor (Q) designed to be in the range of 60 to 70 at 900 MHz.

Figure 5. DTC measured performance (reproduced from [4]).

DTCs have been effectively applied in cellular phone ATs. A typical configuration is shown in Figure 6. The transceiver, in this case a cellular handset, is connect to its antenna through an AT comprising four main elements: (1) serial interface; (2) digital mismatch sensor; (3) tuning algorithm; and (4) DTC core. This structure is representative of ATs based on other tuning technologies besides DTCs. For example, this same architecture would be used with MEMS-based or tunable thin film capacitor ATs. Note that the diagram does not show the RF path between the antenna and transceiver, only the AT control data path. The serial interface exchanges digital data with the transceiver on the AT status. The mismatch sensor responds to reflected power resulting from any impedance mismatch between the antenna and the system's characteristic impedance. Digital mismatch level data are processed by the tuning algorithm that determines which DTCs should be activated and at what capacitance level. Control words are sent to the DTCs in the matching network (DTC core) to effect the impedance match between the antenna and transceiver.

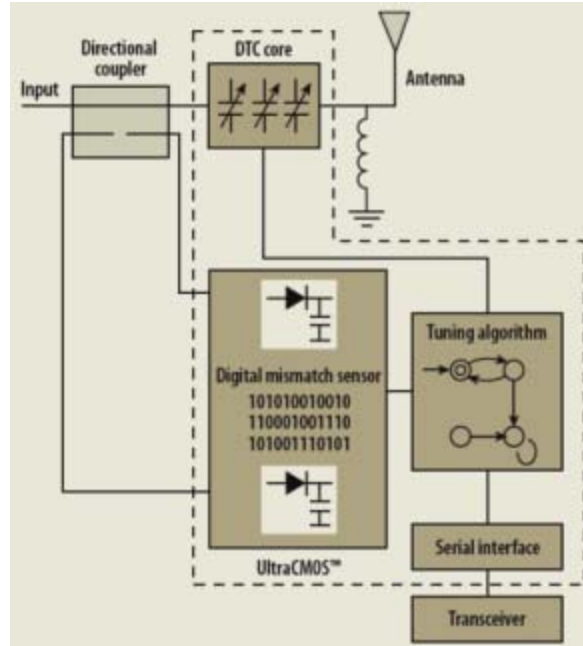


Figure 6. DTC-based AT (reproduced from [4]).

(d) *Dual-gap Tunable MEMS Capacitors* are made using a novel fabrication process that creates two gap device that has an extremely wide tuning range (as much as a factor of 15) with high Q [5]. Figure 1 shows the dual-gap structure schematically and as implemented using a “two hump” sacrificial layer which, when removed, creates two MEMS gaps instead of one. In the schematic, the two moveable electrodes are indicated by the double downward arrows. As these suspended elements move closer to the substrate electrodes the capacitance increases. The structure is a MEMS device designed for a linear capacitance variation with applied control voltage.

In the fabricated prototype, the central region (E_c) is $250\mu\text{m} \times 80\mu\text{m}$ ($L \times W$) with a $1.5\mu\text{m}$ fixed gap. The two “beams” are $800\mu\text{m}$ long by $80\mu\text{m}$ wide creating a variable gap because they are movable. The “actuation area” patches (E_a) are $200\mu\text{m}$ long and $80\mu\text{m}$ wide with a gap of $4.5\mu\text{m}$ with the beams not deflected. This structure produces a minimum capacitance of 0.12 pF that is voltage controllable to a maximum capacitance of 1.77 pF . The resulting tuning range is $\frac{C_{\max} - C_0}{C_0} = 1375\%$, which is quite remarkable. The required bias (“pull in”) voltage is less than 12 volts. This device is not commercially available, but it represents a class of tunable devices that should be very useful in the set-top AT when (and if) they become COTS (commercial off-the-shelf) items.

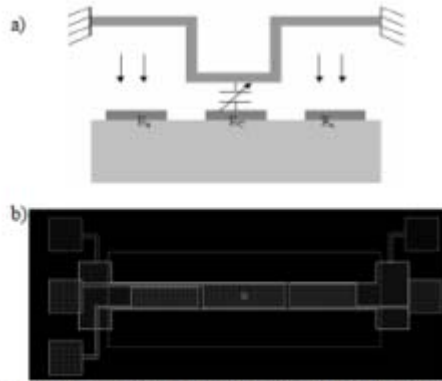


Figure 1: Schematic representation of dual gap tuneable capacitor - a) Cross section - b) Layout top view.

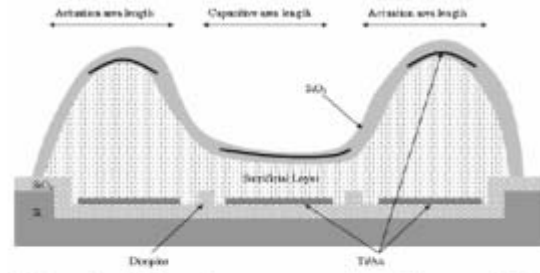


Figure 2 : Schematic representation of the tuneable capacitor based on dual pick profile of the sacrificial layer

Figure 7. Dual-gap tuneable MEMS capacitor (reproduced from [5]).

(e) *MEMS floating dielectric capacitors* (MFDCs) are a recent promising development [6]. The movable dielectric is a new actuation principle in which a floating movable dielectric is electrostatically maneuvered to vary the capacitance. Figure 8 shows the new concept schematically. A mechanical spring returns the movable dielectric to its undisturbed position when no force is applied by the electrostatic comb drive. When the drive is activated, the dielectric moves closer to the top and bottom capacitor plates thereby increasing the capacitance. Preferentially the RF path is through the plates, not through the dielectric and spring, which increases losses.

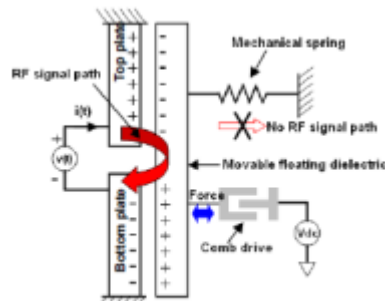


Fig. 1: Conceptual schematic view of the proposed tunable capacitor with an electrically floating dielectric.

Figure 8. MFDC concept (reproduced from [6]).

Figure 9 shows schematic RF signal path superimposed on the MFDC's actual structure as fabricated. In the left pane the signal flows through the spring, which increases the capacitance at the expense of increased losses. In the right pane the signal flows between the top and bottom plates through the movable dielectric. This configuration results in lower losses, but lower capacitance as well. Of course, either configuration can be used, depending upon the specific application.

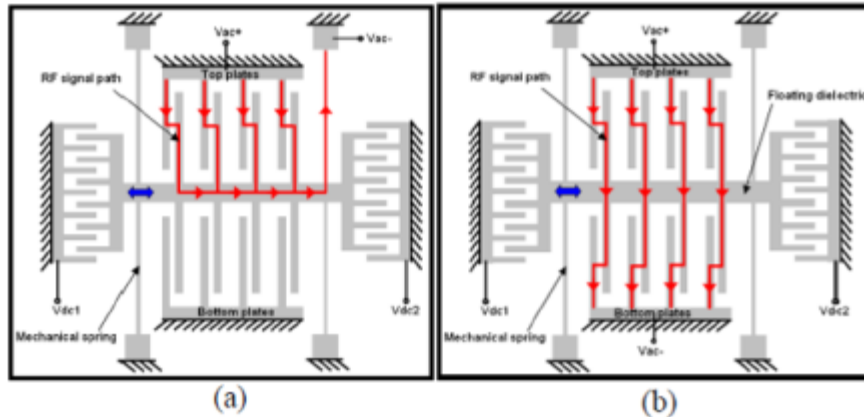


Fig. 2: Schematic views of tunable capacitor design with RF signal through spring (a) and dielectric (b).

Figure 9. MFDC as fabricated and measured data (reproduced from [6]).

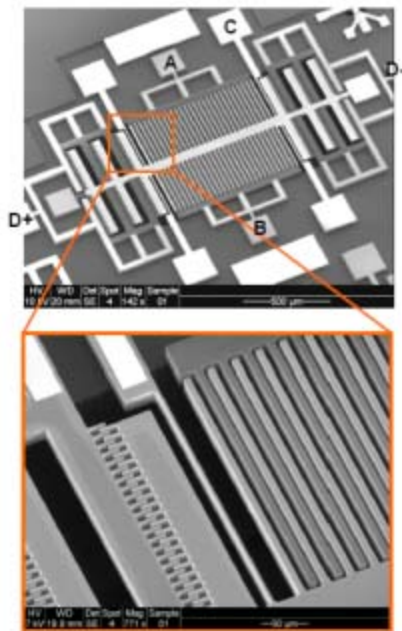


Fig. 4: SEM image of the micromachined tunable capacitor.

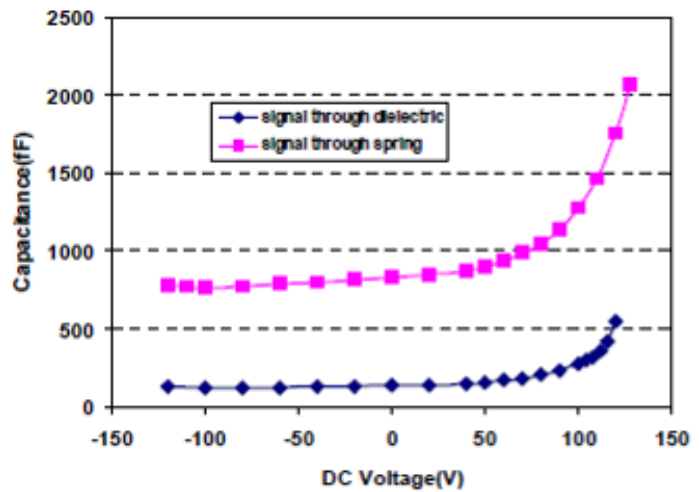


Fig. 5: Measured capacitor changes vs. applied dc bias

Figure 10. MFDC as fabricated and measured data (reproduced from [6]).

Figure 10 provides a scanning electron (SEM) microscope image of a fabricated MFDC (the area outlined in orange, lower pane) and measured performance data. Comparing Figs. 9 and 10, the features in the schematic are readily identifiable in the SEM photo. The actuator pads are labeled D+ and D- in the photo, while the spring is attached to pad C. Pads A and B are the connections for their associated comb plates.

The applied bias voltage ranged from -120 VDC to +120VDC, resulting in capacitance ranges of about 760 fF (femtoFarad) to 2100 fF for RF signals passing through the spring element (pink curve). The initial capacitance (no bias voltage) was 830 fF, leading to a tuning range of approximately 170%. The 1 GHz Q -factor was 0.35, which is low by comparison to other technologies. When the RF path is through the movable dielectric (blue curve), capacitance ranged from just over 100 fF to about 550 fF yielding a tuning range of approximately 370% with an initial capacitance of 135 fF. As expected, the reduced loss resulting from routing the signal away from the spring results in a much better Q -factor of 56 at 1 GHz. Overall, this performance is not as good as that provided by other technologies, but MFDCs are a new concept that requires further development. The MFDC approach certainly merits consideration as a potentially useful future technology for the set-top AT.

(f) The *voltage controlled semiconductor inductor* (VCSI) is another reactive component that should be useful in set-top ATs. Inductor values are usually fixed, so that obtaining specific value of inductance in an AT is usually accomplished by mechanically switching small inductors in and out of the matching circuit using relays or MEMS RF switches. Recently disclosed VCSI devices [7] should be particularly useful at broadcast TV frequencies. The device addresses the problem of limited tuning range provided by voltage tunable capacitors by varying the inductance instead.

Generally it comprises regular coil turns of wire interconnected by semiconductor diodes that can connect individual turn to create a VCSI. Including a resistor and capacitor creates a complete tunable RLC circuit. Figure 11 illustrates this patented technology. The left pane shows a perspective view of the device, which includes conductive loops (205) connected to a semiconductor bar comprising P- and N-type regions at each end (208 and 210, respectively) connected by a depletion region (212). Applying a voltage across terminals L_A and L_B varies the length of the depletion region which acts as an insulator. Because its size is proportional to the applied bias voltage, individual coil turns are either connected or disconnected in proportion to the voltage, thereby creating a voltage-variable inductor.

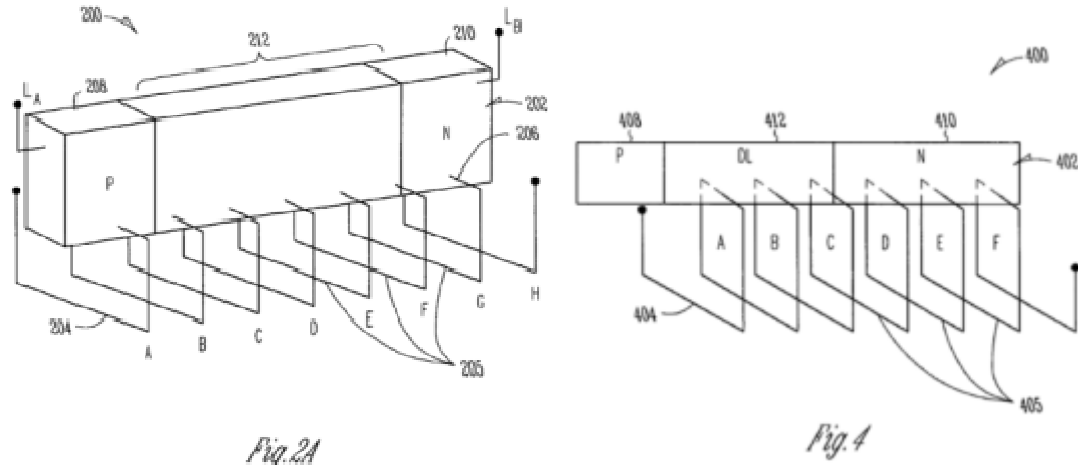


Figure 11. Voltage controlled semiconductor inductor (reproduced from [7]).

A helical-turn implementation of the VCSI is shown in the right pane of Figure 11. The same semiconductor diode structure comprising P- and N-type end regions connected to a central depletion layer (DL) whose length is voltage-variable. The figure provides a schematic representation of how the three regions' lengths vary with bias voltage compared to the "off" state shown in the left pane. In the diagram, coil turns C through F are electrically short-circuited because they are outside the insulating DL. In this case, only turns A and B are active elements in the inductor.

The VCSI may become an important element in set-top ATs because it provides a complete RLC tuning in a single chip-level device. A bank of VCSIs, for example, could comprise the switchable reactive elements in a set-top AT that are completely voltage-controllable, thereby eliminating the need for mechanical switching relays. VCSI therefore is an attractive emerging technology that merits watching.

2.5.1.2 Fully Integrated ATs

In addition to the emerging component-level technologies described in §1, fully integrated ATs have been developed that also merit consideration for set-top tuners. This section examines developments in that area.

(a) A *reconfigurable RF-MEMS-based matching network* is described in [8]. The chip-level device's circuit diagram is shown in Figure 12. It comprises two stages, the first of which is a Pi-match section with four shunt capacitor-series inductor (CL) sections. A total of eight RF-MEMS switches are employed yielding 2^8 impedances. The shunt capacitors are formed from bi-valued MEMS varactors. The variable capacitor in series with each fixed inductor, also a MEMS varactor, has the effect of adjusting the series inductance. The second section is a phase-shifter comprising a 3-dB 90-degree coupler connected to a reflective load. MEMS varactors adjust the load reflection

coefficient to control the overall phase shift. A total of 2^3 phase rotations are possible in the phase shifter, resulting in as much as 340 degrees of total phase shift that can be applied to the impedances at the output of the Pi-match. The network is designed to work at a 50 Ω impedance level.

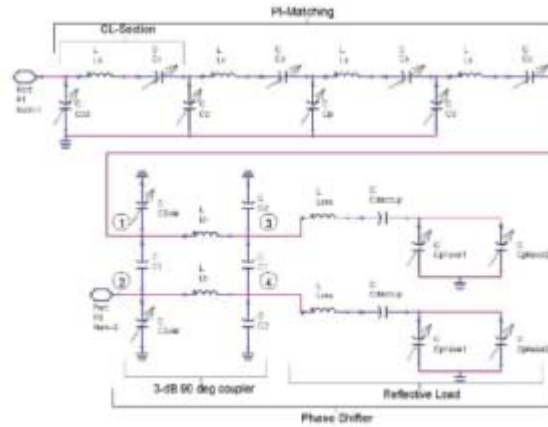


Figure 1 : Circuit topology of the reconfigurable matching network.

Figure 12. Reconfigurable RF-MEMS-based matching network circuit (reproduced from [8]).

The chip layout and fabricated device are shown in Figure 13 with the major sections being labeled on the layout diagram. The chip area is extremely small, only 40 mm² (slightly larger than 3x12 mm). The published report indicates that the chip has been fabricated and was undergoing testing, but no actual measured data were reported. Instead simulated performance at a single frequency (620 MHz) was calculated at each of the possible 2,048 impedance combinations and plotted on a Smith chart as shown in Figure 14. The circles are impedance values computed for the first stage alone, while the dots represent the show the performance of the complete reconfigurable matching circuit. The fairly uniform distribution of dots throughout the Smith chart suggest that the matching circuit will effectively match an extremely wide range of impedances to 50 Ω . This technology is directly applicable to the set-top AT and appears to be on the verge of realization. Future published results for reconfigurable RF-MEMS-based matching networks clearly bear watching.

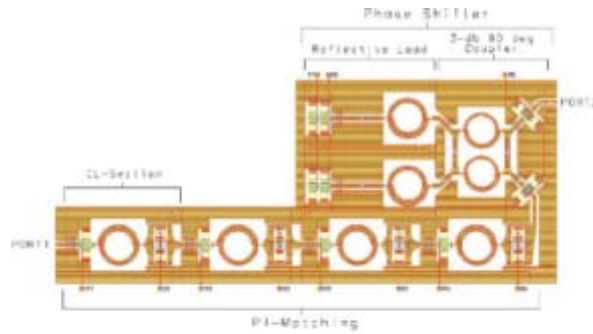


Figure 3 : Layout of the circuit as implemented in ADS

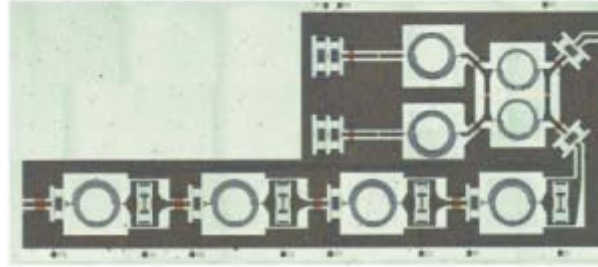


Figure 4 : Photograph of the fabricated circuit

Figure 13. Reconfigurable RF-MEMS-based matching network layout & fabrication (reproduced from [8]).

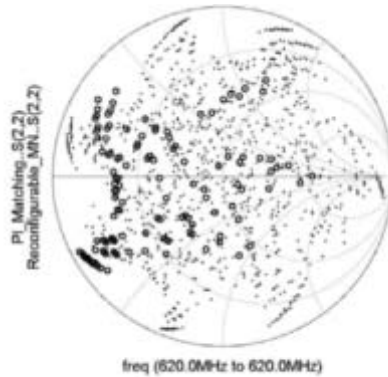


Figure 2 : Simulated impedance values (circles: first stage; dots: full reconfigurable matching network).

Figure 14. Reconfigurable RF-MEMS-based matching network performance (reproduced from [8]).

(b) The AT using only RF signal amplitudes described in [9] may be useful for the set-top application because it specifically addresses the issue of highly variable, unpredictable and uncontrollable environments. This new technology was developed for mobile applications such as cellular transceivers because their fluctuating environment often causes VSWR spikes approaching 10:1 in nominal 50 Ω systems. These fluctuations are frequently transient on time scales in the millisecond range. The new AT design accommodates this environment, and it may be useful in the highly variable TV set-top antenna environment as well.

The architecture appears in Figure 15, which includes schematic Smith chart representations of the impedance at various points. ATs generally comprise an impedance sensor, a tunable matching network, and control circuitry that changes the network parameters in order to achieve an acceptable VSWR (usually relative to 50 Ω with VSWR < 2-3:1). The general approach shown in Figure 15 therefore is applicable to any matching network. The new matching concept involves a two-step process: (1) the reactance is essentially tuned out using a series or shunt reactance; and (2) a tunable “transformer” changes the remaining resistive component to the desired value of impedance.

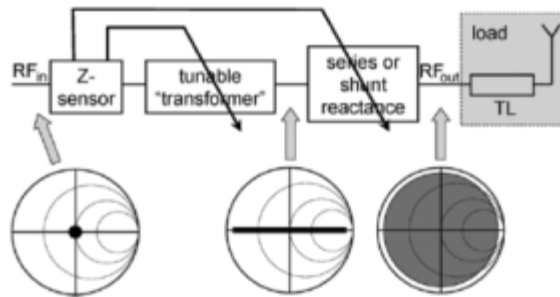


Fig. 2. Basic concept of the automatic antenna tuning system: tune out the imaginary part and tune the real part separately.

Figure 15. New AT architecture for fluctuating environment (reproduced from [9]).

In the new AT, the antenna impedance sensor makes a quasi-DC log-peak measurement of the RF signal amplitude at three points in the signal chain (V1, V2, V3 in Figure 16). Details of the log-peak detector circuit are shown in Figure 17. These data combined with the known transfer functions of the reactive elements (jX_{ext}) permit a calculation of the impedance’s imaginary part. The real part of the impedance is determined from the signal level $V_{\Delta R}$ and an offset voltage that brings this level to a target value corresponding to 1:1 VSWR. The tunable transformer comprises a T-network lumped transmission line made of two adjustable inductors and an adjustable capacitor. Any appropriate device can be used to implement these elements.

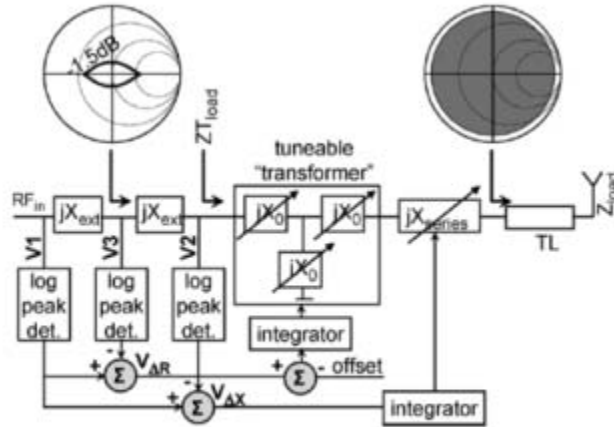


Fig. 3. Automatic antenna tuning system with low-frequency impedance detection; the target impedance (-1.5 -dB contour) is used in Section IV-A.

Figure 16. AT functional block diagram (reproduced from [9]).

Two demonstration versions of this new AT design was built and tested at 900 MHz. Measurements confirmed that they could reliably and quickly automatically tune antennas with $Z_{in} = [5 - 500] + j[15.8 - 158] \Omega$ (10:1 VSWR). Although the sizes were not reported, these demonstration units were intended for use in cellular handsets, so that the size is certainly consistent with use in a set-top television AT.

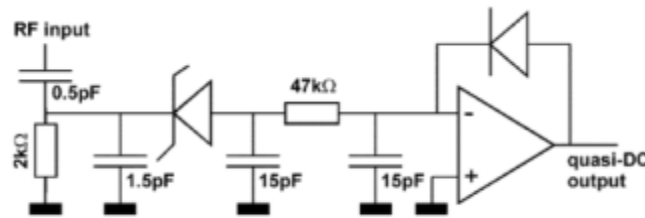


Fig. 4. Schematic diagram of the log-peak detector implementation.

Figure 17. Details of log-peak detector circuit in Figure 16 (reproduced from [9]).

2.5.1.3 On-Chip Tracking Filters

While tracking filters are not AT's, their technology likely is applicable to antenna tuners ATs, and consequently should be monitored for application in set-top devices. This section describes three different types of tracking filter.

A device developed specifically for DTV tuners is described in [10]. A new architecture is proposed that includes two separate filters, a harmonic rejection tracking filter (HRTF) and an RF tracking filter (RTF) that are controlled by complementary digital switches. The new architecture is shown in Figure 18. The entire device is fabricated as a single integrated circuit (IC) chip. The filter stage is shown in blue located between the low noise amplifier (LNA) connected to the antenna and the DTV tuner.

Unlike narrowband RF receivers, wideband DTV tuners are prone to interference from local oscillator odd harmonics mixing with signals at the lower television channels (48-287 MHz). This problem is addressed by the HRTF that provides a high-order band-pass tracking filter with 3rd-order harmonic rejection greater than 60 dB. On the UHF television channels the RFTF tunes 287-860 MHz with narrow band response (20 MHz at -3 dB). This stage is implemented using a cascade of tunable 2nd-order bandpass tracking filters.

Computer simulation of the new architecture's performance predict 48-860 MHz operation with tunable adjustable bandwidth of 8-20 MHz, 5-15 dB N+2 channel rejection (16 MHz offset), and 3rd-order harmonic rejection of 60 dB from the HRTF. The RFTF stage provides 4.2 dB of N+2 channel rejection above 287 MHz. This device can be fabricated on-chip using 0.13 μm CMOS technology with 1.2 VDC supply voltage and 19.8 mA current draw (total of 24 mW power consumption).

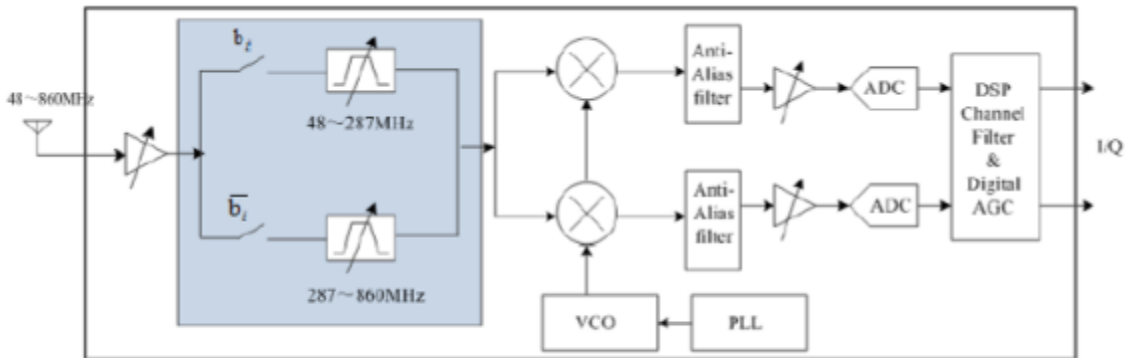


Figure 1. Direct Conversion TV tuner architecture

Figure 18. New DTV tracking filter architecture (reproduced from [10]).

Another potentially important emerging filter technology is the use of low-temperature co-fired ceramic (LTCC) technology to fabricate fully integrated multi-layer tunable filters for RF and microwave use. A typical device is shown in Figure 18. Passive

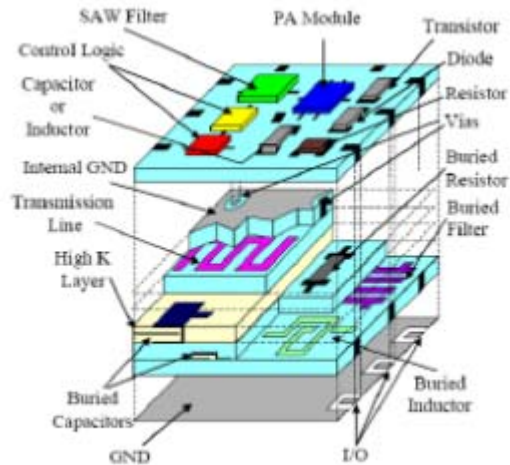


Figure 1. A typical LTCC structure

Figure 18. LTCC filter structure (reproduced from [11]).

Elements (resistors, inductors, capacitors) are integrated on the surface or embedded in a multilayer substrate. Various configurations have been demonstrated, including bandpass filters (380 MHz-2.4 GHz), 3-stage Butterworth bandpass filters (1.2 GHz), and an electronically tunable microstrip combline filter. These prototype devices point to LTCC technology's utility for RF and microwave applications. At this point the new multilayer architecture proposed in [11] that involves switching between layers for tuning is being computer-modeled, but working devices based on that approach have not been fabricated. LTCC technology may be very attractive in the television frequency range because of its potential for very high levels of integration resulting from the multilayer design.

A third example of an on-chip tracking filter is provided by [12]. A complete tunable structure was fabricated and tested. This chip occupied an area of only 2.8 mm² (fabricated with 0.18 μm CMOS) requiring 34-120 mA at 1.8 VDC. A photomicrograph of the chip appears in Figure 19, and its architecture in Figure 20. The device comprises cascaded RLC sections as shown in Figure 20, each containing a digitally programmable on-chip capacitor and resistor, and an off-chip fixed inductor. The resistor is adjusted with 8-bit resolution, while the capacitor uses a 10-bit control signal.

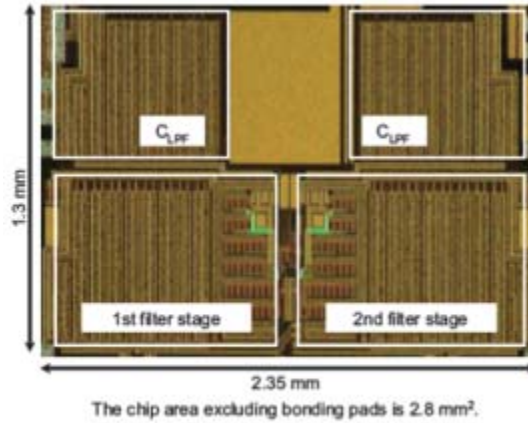


Fig. 7. Chip micrograph

Figure 19. Tunable LC-Tracking filter as fabricated (reproduced from [12]).

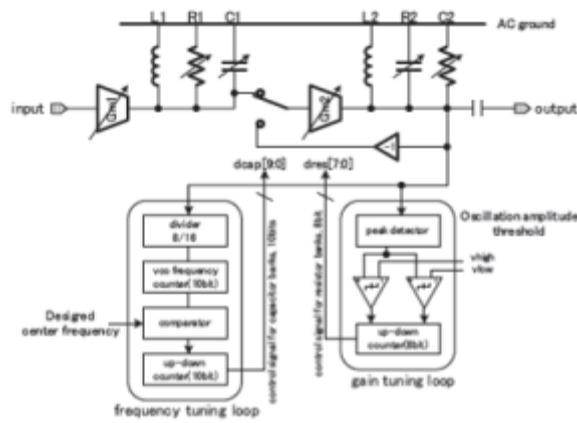


Fig. 1. RF tracking filter architecture

Figure 20. Tunable LC-Tracking filter architecture (reproduced from [12]).

Figure 21 shows the tracking filter's measured performance data from 125 MHz to 1.06 GHz. Its response in the 5.6 MHz passband is very flat with a ripple less than 0.2 dB. The noise figure in this device appears to be somewhat high (16.8-19.5 dB), but the third-order intercept points are good ($\sim 128/167$ dB μ V, in/out of band). Frequency selectivity is good at > 36 dB, and the power consumption quite low ($< \sim 0.2$ W maximum). This example shows that very effective single-chip RF tracking filters with minimal off-chip components (in this case two inductors) can be designed and fabricated for set-top use using currently available technologies.

TABLE I
PERFORMANCE SUMMARY

Parameter		Measured value
Center frequency(f_c)		125 MHz – 1.06 GHz
Passband ripple	$f_c = 125\text{MHz}$ (BAND1)	< 0.2 dB
Signal bandwidth		5.6 MHz
Noise Figure (Input referred noise)	$f_c = 430\text{MHz}$ (BAND2)	16.8dB (17.4 dBuV)
	$f_c = 1.06\text{GHz}$ (BAND2)	19.5 dB (20.1 dBuV)
in-band IIP3		127.7 dBuV
out-of-band IIP2		167.0 dBuV
Frequency selectivity at 3rd LO freq.		> 36dB
Power consumption	$f_c = 380\text{MHz}$ (BAND2)	120mA @ 1.8V
	$f_c = 430\text{MHz}$ (BAND1)	34mA @ 1.8V
Si-area		2.8 mm ²
Process		0.18 μm CMOS 1P6M with MIM cap

Figure 21. Measured performance of tunable LC-Tracking filter (reproduced from [12]).

2.5.1.4 Software Defined Radios

A software defined radio (SDR) is an element of a wireless communication network whose operational modes and parameters can be changed or augmented post-manufacture via software. The essential idea is that a flexible hardware layer exists whose function can be controlled and modified entirely by a computer program, as opposed to requiring hardware modifications of any kind. The SDR concept spans many radio network technologies including cellular systems, personal communications services (PCS), 3rd and 4th generation wireless (3G and 4G), mobile data, emergency services, paging, messaging, and military/government communications, and any future modifications to these existing services or entirely new ones. The FCC (Federal Communications Commission) definition is more restrictive in that it applies only to the transmitter side of an SDR. But, as a practical matter, the SDR concept applies to any wireless device whose characteristics are software-controllable, whether it be the transmitter, receiver, both, or some other element such as a modem.

SDR technology is relevant to the television set-top AT because there is a developing standard that specifically addresses the issue of “smart antennas” (SAs) in the context of SDR. This type of antenna and its associated AT may be useful for the set-top application and consequently should be monitored as an emerging technology. The high-level SDR smart antenna architecture appears in Figure 22. The hardware layer comprises M transmit antennas and N receive antennas because SDR in general supports two-way communication (in the set-top TV receive application, of course, there are no transmit antennas). Each antenna is has a separate RF/IF processing chain with the smart antenna signal processing (“waveform application”) being applied to the

baseband signal. Device drivers in the middleware layer control various programmable hardware devices, such as ASSPs (application-specific standard processors), FPGAs (field-programmable gate arrays), DSPs (digital signal processors), and GPPs (general purpose processors).

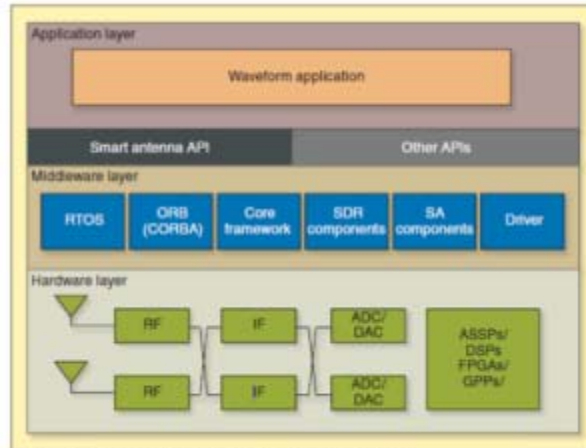


Figure 1. Example of an SDR-based smart antenna open architecture.

Figure 22. SDR smart antenna high-level architecture (reproduced from [13]).

Figure 23 illustrates a typical deployment of an SA API (application program interface). The SA control device (for example, an antenna tuner, tracking filter, MEMS-based controller, fluidic element controller, and so on) is operated by a GPP controlled by a CORBA interface (common object request broker architecture). The high-level SA algorithm controls appropriate CORBA-compatible drivers for DSP baseband processing, antenna control, and other functions such as synchronization and other SDR devices that may be controlled by the SA algorithm. The basic concept in this structure is that any hardware module involved in controlling the SA or processing its signal is controllable by the API with variable parameters.

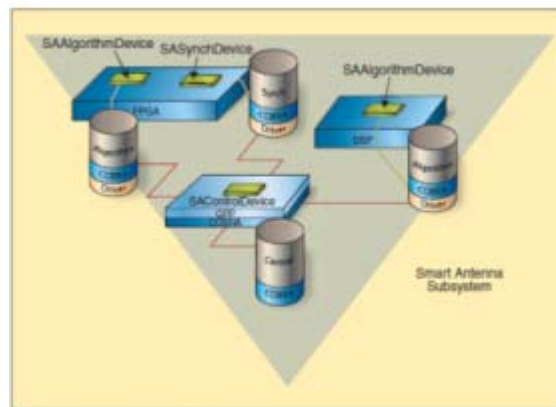


Figure 6. Deployment diagram of SA API.

Figure 23. SDR Smart Antenna API deployment (reproduced from [13]).

A typical SA hardware implementation for the SDR baseband signal processing module is shown in Figure 24. The two DSP integrated circuits (ICs), the GPP, and the FPGA ICs are labeled. This type of module is simply inserted into a backplane containing the other SDR modules to create a complete SDR. All chip-level functions are fully controllable by the SA API. As modifications are required, a simple download of the updated API is all that is necessary. No hardware modifications or swaps are necessary. The SDR approach thus provides exceptional flexibility in customizing radio performance and it well may be a very useful approach to developing effective set-top television ATs.



Figure 6: Photograph of implemented Baseband Signal Processing part of SDR smart antenna system.

Figure 24. Typical SDR smart antenna hardware implementation (reproduced from [14]).

2.5.2 References

- [1] Stemmer, S., "Structure-Property Relationships of Tunable Thin Film Dielectrics for Microwave Applications," *Ferroelectrics UK Conference*, Birmingham, UK, May 23-26, 2006.
- [2] Lee, Y. C., Hong, Y. P., and Ko, K. H., "Low-voltage and High-tunability Interdigital Capacitors Employing Lead Zinc Niobate Thin Films," *Applied Physics Letters*, **90**, 182908 (2007).
- [3] Peregrine Semiconductor Corp., 9380 Carroll Park Drive, San Diego, CA 92121 USA (www.psemi.com).
- [4] Ranta, T., and Novak, R., "Antenna Tuning Approach Aids Cellular Handsets," *Microwaves & RF*, p. 82, November, 2008.

- [5] Soulimane, S., Casset, F., Chapuis, F., Charvet, P. L., and Aid, M., "Tuneable Capacitor based on Dual Picks Profile of the Sacrificial Layer," *DTIP of MEMS & MOEMS*, Stresa, Italy, 25-27 April 2007 (EDA Publishing/DTIP 2007, ISBN: 978-2-35500-000-3).
- [6] Zhu, Y., Yuce, M. R., Moheimani, S. O. R., "A Low-Loss MEMS Tunable Capacitor with Movable Dielectric," *IEEE Conference on Sensors (IEEE SENSORS 2009)*, pp. 651-654, October, 2009.
- [7] Subramanian, K. M., "Voltage-Controlled Semiconductor Inductor and Method," U.S. Patent No. US 7,511,356 B2, Mar. 31, 2009.
- [8] Bedani, M., Carozza, F., Gaddi, R., Gnudi, A., Margesin, B., Giacomozzi, F., "A Reconfigurable Impedance Matching Network Employing RF-MEMS Switches," *DTIP of MEMS & MOEMS*, Stresa, Italy, 25-27 April 2007 (EDA Publishing/DTIP 2007, ISBN: 978-2-35500-000-3).
- [9] Firrao, E. L., Annema, A-J., Nauta, B., "An Automatic Antenna Tuning System Using only RF Signal Amplitudes," *IEEE Trans. Circuits and Systems – II: Express Briefs*, 55, No. 9, pp. 833-837, Sept. 2008.
- [10] Sun, Y., Lee, J-s., Lee, S-g., "On-chip Active RF Tracking Filter with 60dB 3rd-Order Harmonic Rejection for Digital TV Tuners," *SoC Design Conference, 2008. ISOC '08*, 24-25 Nov. 2008, Busan, vol. 01, pp I_406-I_409.
DOI: 10.1109/SOCCDC.2008.4815658
- [11] Suma, M. N., and Suhas, K., "Performance Analysis and Process Parameters of Novel LTCC Filters," *International Journal of Recent Trends in Engineering*, **1**, No. 3, p. 346, May 2009.
- [12] Kanmazawa, Y., Fujimoto, Y., Izuka, K., "A 130M to 1GHz Digitally Tunable RF LC-Tracking Filter for CMOS RF Receivers," *IEEE Asian Solid-State Circuits Conference*, Fukuoka, Japan, pp., 469-472, November 3-5, 2008 (978-1-4244-2605-8/08/\$25.00 ©2008 IEEE)
- [13] Hyun, S., Kim, J., Choi, S., Pucker, L., Fette, B., "Standardizing Smart Antenna API for SDR Networks," *RF Design*, p. 34, Sept. 2007.
- [14] Hyeon, S., kim, J., Choi, S., "Smart Antenna APIS: From Concept to Practice," *Proc. SDR 07 Technical Conference and Product Exposition*, SDR Forum, <http://www.wirelessinnovation.org>

2.6 Physically Reconfigurable Antenna Elements

2.6.1 Summary

A *reconfigurable antenna* (RA) is an antenna whose physical and/or electrical properties can be changed in real time in order to achieve certain performance characteristics. The panoply of possible RA implementations makes RAs especially attractive for the television set-top antenna application. This section discusses some of the “typical” RA implementations, as well as some rather unusual technologies that may point the way to future developments that could be useful for set-top devices.

The essential concept underlying RAs is that some antenna property is changed “on the fly” to accomplish some objective, say tuning. An example is the tunable antenna in which the electrical length of a radiating element is changed by switching in and out reactive elements (capacitors/inductors) or remotely moving the tap on a roller-type tuning inductor. This type of reconfigurable antenna has been used for at least fifty years (see, for example, [1] p. 20.46 *et seq.*).

While an RA may be any electrical size, typically they are a substantial fraction of a wavelength, so that they are not (necessarily) electrically small antennas (ESAs). The problems associated with ESAs, narrow bandwidth, low radiation efficiency, highly reactive input impedance, are mitigated in RAs that are a substantial fraction of a wavelength in size. Nevertheless, the RA concept is applicable to ESAs as well, and it may be useful for ESA candidates for the set-top application. As a general proposition, RA technology is applicable across the entire range of antenna electrical sizes, which makes it particularly attractive for set-top devices.

Most recent examples of effective RAs are at frequencies well above the broadcast television channels, typically in the microwave region. However, because these RAs often are comparable to the operating wavelength in size, they may be readily used at lower frequencies, especially at UHF TV channel frequencies. On the lower VHF channels, RA approaches may be effective when applied to standard antennas such as bowties or spirals whose size is consistent with set-top requirements.

Five candidate RA technologies hold promise for short or long term application to television set-top antennas:

(a) *Microelectromechanical System* (MEMS) RAs are antennas based on MEMS RF switches. These devices, which have been fabricated for well over a decade, have come to the foreground as the preferred approach for RAs. They can be used in all frequency ranges, and, in fact, perform better at lower frequencies, although current applications emphasize the high UHF and microwave ranges. Other similar switching

devices such as PIN diodes or GaAs (gallium arsenide) solid-state switches also are used to build RAs, but these technologies are older and perform less well. The latest developments in MEMS, nano-MEMS and the use of carbon nano-tubes (CNT), reduce sizes and improve performance to the point where there seems essentially no question that MEMS-based set-top RAs will be achievable in the near future.

(b) *Fluidic* RAs are a very recent development that promises simple, cost-effective, rugged reconfigurable wire antenna structures in almost any shape imaginable. Fluidic elements are fabricated from a flexible elastomer enclosing human-hair-thin channels filled with eutectic gallium/indium (EGaln), a liquid metal. The resulting “wire” provides electrical performance similar to copper and can be stretched, bent, rolled, or twisted into almost any shape simply by applying mechanical stress. The wire returns to its original linear structure upon relieving the stress. These elements have been used to fabricate a simple center-fed dipole that is tuned by stretching. A similar approach using a multiplicity of wires or other geometries (for example, bow ties or spirals) may well be the basis of a simple, effective set-top antenna. This technology has only recently been reported, and it certainly bears watching as a candidate for set-top RAs.

(c) *Pixelated piston* RAs comprise small individually controllable and addressable “pistons” in a two-dimensional matrix. Each piston is controlled by an actuator which, in turn, is operated by an electronic controller. A conductive patch is mounted on the end of each piston, which in their quiescent position form a continuous, flat ground plane. Each piston moves back and forth above and below the ground plane to form reconfigurable antenna radiating elements or transmission lines. This technology, which is patented, has been demonstrated to provide high-gain, beam steerable, antennas operating from 500 MHz to 18 GHz with reconfiguration times less than one millisecond. Its utility for the set-top application is self-evident, but at this point in its development the cost likely is prohibitive.

(d) *Liquid crystal* (LC) RAs are fabricated using LC substrates sandwiched between two electrodes that apply a DC bias voltage to control the LC’s dielectric constant by deforming its molecules. Very small unit cells are fabricated that can be formed or applied onto surfaces of various shapes. At this point in its development, LC RAs have been demonstrated only on planar surfaces, and only at extremely high frequencies (high microwave through millimeter wave ranges). An effective LC RA reflectarray antenna has been demonstrated at 77 GHz. It provided complete electronic beam steering over an angular range of 35 degrees with good gain and sidelobe performance. Whether or not this technology can be ported to low VHF television set-

top channels is not clear, but the technology bears watching because it is demonstrably effective for designing and building reconfigurable antennas.

(e) *Plasma* RAs are similar to the pixilated piston antennas, but instead of using conductive patches, they utilize ionized gas (plasma) as the conductive element. Each plasma element is turned “on” (ionized) or “off” (non-conducting) by a control voltage, so that the entire antenna aperture is electronically reconfigurable. Unlike pixilated piston RAs, the plasma elements lie in a single plane and cannot be positioned above or below the plane. This limitation, however, is minor in the context of set-top receive antennas because it is very likely that good receiving structures can be formed on a planar surface, which also simplifies the RA. The plasma RA has another potentially significant advantage over other candidate technologies. Existing plasma display technology, which is very highly developed and sophisticated, may be directly applicable to the design and manufacture of plasma RAs for the set-top application. Leveraging this existing technology may speed time to market and reduce costs substantially.

2.6.2 MEMS-based RAs

Microelectromechanical system (MEMS) radio-frequency switches have gained widespread acceptance as a standard element for implementing in RA structures. RF MEMS are routinely used to change both antenna feed networks to accomplish impedance matching and radiating element topology to control radiation pattern and efficiency. Most applications are in the microwave range, but MEMS use is not frequency-limited.

While there are other switching elements besides MEMS, notably solid-state PIN diodes and GaAs switches, MEMS offer several advantages. They are inexpensive, which is a major advantage for set-top applications, and they exhibit low insertion loss and low power consumption [2]. In recent years their availability as a commercial item has grown considerably, and they are now readily available as off-the-shelf components [3,4,5]. Demonstrated lifetimes exceed 100 billion cycles, which is consistent with consumer levels of usage over periods of several years.

Figure 1 shows a typical bi-layer curled MEMS structure. It is extremely small in size (300x1500 μ m). The two-layer switch element comprises materials with different thermal coefficients of expansion that pull it up away from the contact after annealing as shown in (a). The switch therefore is normally open (NO) when no control voltage is applied. Applying a DC voltage between the switch post and bottom electrode (1.5 μ m thick polysilicon) creates an electrostatic field that pulls the switch element onto the contact as shown in (b). The microphotograph below the switch diagram shows its structure as actually fabricated.

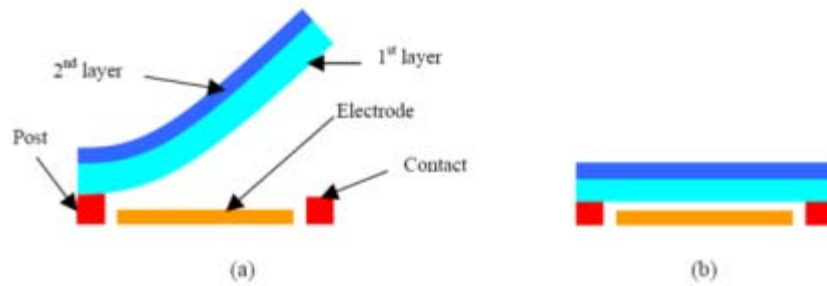


Figure 11. Operation of a bi-layer curled MEMS switch. (a) OFF state and (b) ON state.

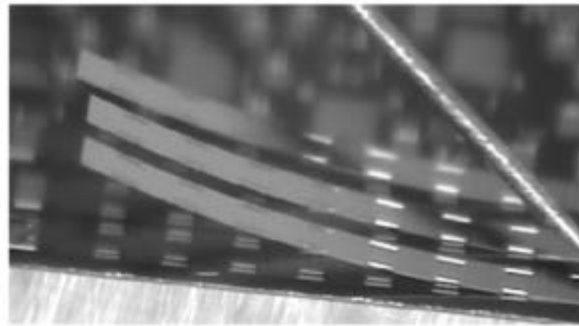


Figure 12. A photograph of the fabricated MEMS switches.

Figure 1. Typical RF MEMS switch (reproduced from [2]).

MEMS technology is improving at a rapid pace, and the latest generation of these switches are nano-scale [6]. *Nanoelectromechanical system* (NEMS) are laterally ~ 10 - 100 times smaller than a typical MEMS device, and they operate with actuation voltages below 10 volts, compared to 30-80 volts for MEMS switches. NEMS also provide faster switching times ($< \sim 1 \mu\text{sec}$) compared to MEMS (~ 10 - $20 \mu\text{sec}$). Figure 2 shows the new NEMS double-arm cantilevered switch schematically (a) and as fabricated (b) imaged by a scanning electron microscope.

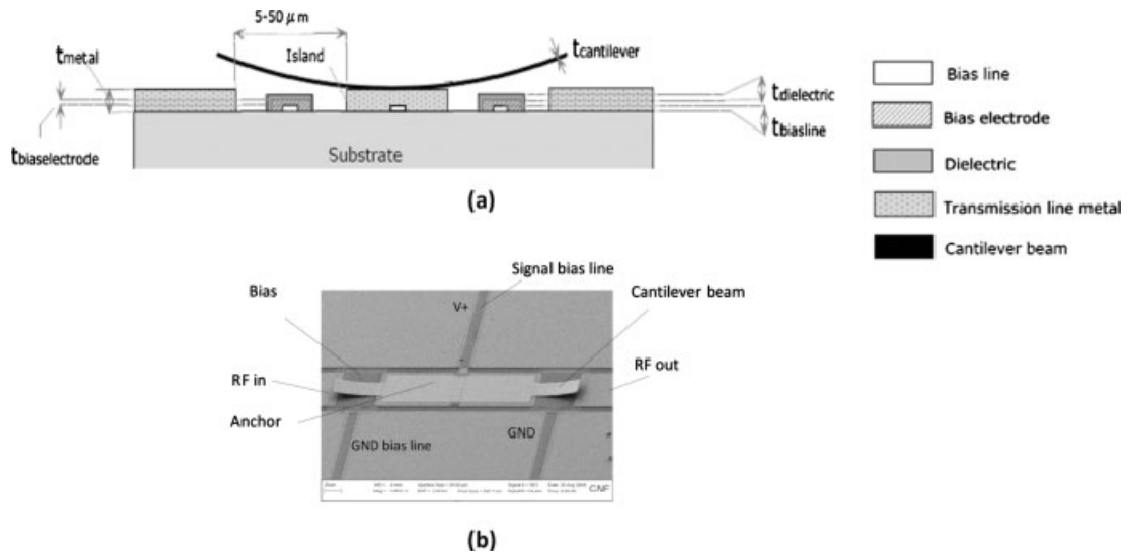


Figure 2. DC-contact NEMS switch (reproduced from [6]).

Another important recent development is the use of carbon nanotubes (CNT) to fabricate NEM switches [7]. These devices promise extreme longevity and reliability because of CNT's unusual physical and electrical properties. Carbon nanotubes are extremely strong with high electrical conductivity. In addition, their flexibility and extremely low mass suggest that switching speeds in the GHz range eventually may be attainable. Figure 3 shows two types of CNT-based NEM switches. Measured switching times were 26 ns for these devices, which while far short of the GHz range, are nonetheless faster than MEMS devices.

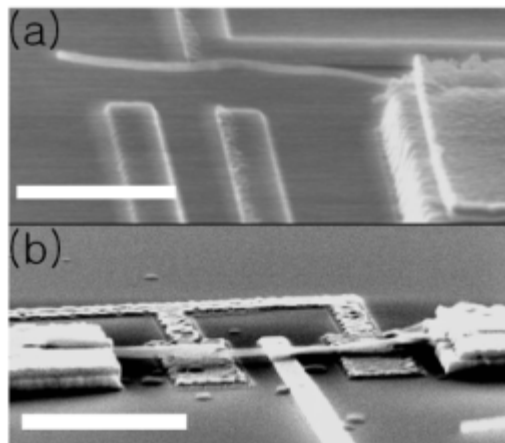


Figure 3. Two types of CNT-based NEMS switches (reproduced from [7]).

A typical MEMS-based reconfigurable array structure appears in Figure 4. This is an example of a complex RECAP (Reconfigurable Aperture) structure whose objective is wide bandwidth. Because a MEMS-based antenna can be reconfigured essentially in real-time, it can operate in multiple frequency bands. Aperture reconfiguration is achieved by switching in and out receiving and/or transmitting elements (radiating a signal, of course, is not an issue with set-top TV antennas). The structure shown in Figure 4 typically would be implemented using solid-state switches, but MEMS technology has leap-frogged that approach, so that MEMS provides better performance. In the array application, only the MEMS network departs from an otherwise standard design. The receiving/radiating element structure and its feed network are independent of the MEMS switch layer, as are the bias, FSS (frequency selective surface) and PBG (photonic band gap) layers. These last two elements may well not be required in an application like the set-top antenna because the operating frequencies are well below the microwave range where FSS and PBG structures are common.

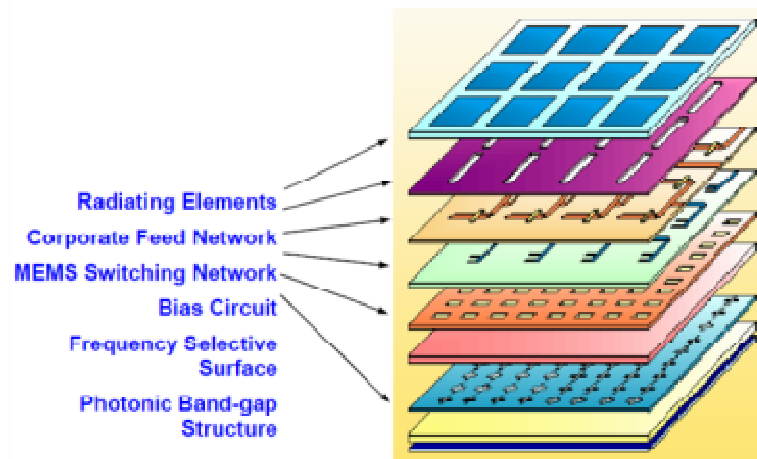


Figure 4. Reconfigurable MEMS-based antenna array (reproduced from [8]).

Another example of a state-of-the-art multiband MEMS-based antenna is reported in [9]. The design emphasizes a symmetric, repeatable topology which lends itself well to scalability, so that additional frequency bands are readily added. Scalability could be an important attribute in applying MEMS technology to the set-top environment, and this antenna demonstrates that scalability is achievable with MEMS. As configured the antenna covers four bands: 800-900 MHz; 1.7-2.5 GHz; 3.3-3.6 GHz; and 5.1-5.9 GHz. The lowest band lies just above the highest UHF television range, suggesting that this design likely could be easily modified to cover some portion of the upper TV channels. Table 2 reproduced below from [9] shows that this antenna indeed provides excellent performance in the four design bands. Its structure appears in Figure 5.

Table 2. Summary of Reconfigurable Antenna Performance

Band of interest	B1	B2	B3	B4
Frequencies covered (GHz)	0.8-0.9	1.7-2.5	3.3-3.6	5.1-5.9
Measured S11 (dB)	-13	-9	-7.7	-3.6
Measure Center Freq Gain	8.21 dB	7.96 dB	9.6 dB	8.4 dB

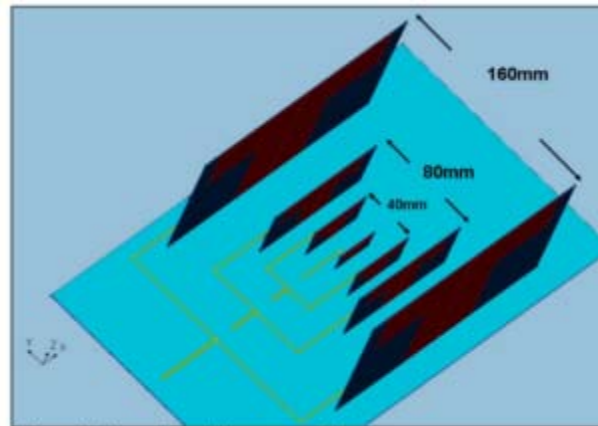


Figure 1. Reconfigurable antenna element.

Figure 5. Four band MEMS-based antenna (reproduced from [9]).

2.6.3 Fluidic RAs

An interesting new RA technology is the *fluidic* antenna. A fluid metallic alloy, eutectic gallium/indium (EGaln), comprising the metals gallium and indium, that remains liquid room temperature is injected into a microfluidic channel made from the silicone elastomer PDMS (polydimethylsiloxane). The channels are very small, about the width of a human hair, open at each end, and of any desired shape. After the channel is filled with EGaln, the alloy's surface oxidizes, creating a "skin" that holds the alloy in place while allowing it to retain its liquid properties. The alloy's mechanical properties are determined by the elastomer casing because it remains liquid.

The "wires" created by this process can be bent, stretched, rolled and twisted by applying a stress. Figure 6 shows a photograph of a twisted fluidic wire. Upon relieving the stress, the liquid conductor/elastomer reversibly returns to its original shape without hysteresis. An antenna fabricated of fluidic elements consequently is fully reconfigurable. The structure is self-healing to small cuts, and it is highly flexible and durable. Life expectancy therefore is very high, and fabrication costs reasonable because the elastomer's channels are formed using a technique known as "soft lithography" which avoids milling or etching in fabricating the fluidic antenna elements. However, the EGaln liquid metal is expensive, and at this time may be prohibitive for consumer applications.

A simple center-fed dipole was constructed from the fluidic element and tested. The antenna is shown in Figure 7. Its radiation efficiency was measured at approximately 90% over a frequency range of 1910-1990 MHz tuned by stretching the antenna. The efficiency is comparable to a copper element in this frequency range, so that the fluidic antenna is expected to perform as well as any metallic structure. In the television set-top application, this type of RA may be very attractive, especially if the price of EGaln alloy can be reduced because of volume. Of course, there are unanswered questions, for example, to what degree the elastomer casing can be stretched. The important conclusion that can be drawn from the reported research is that an entirely new fluidic technology may be close enough to maturity that it soon will be viable for reconfigurable set-top receive antennas.

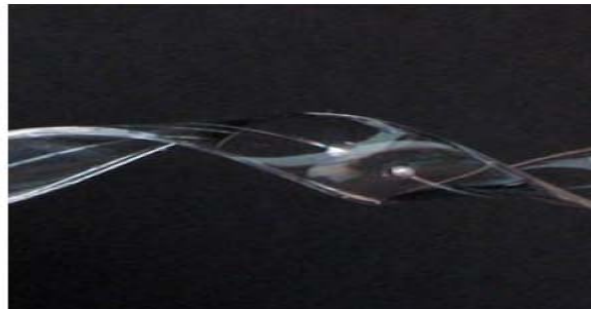


Figure 6. Twisted fluidic wire element.

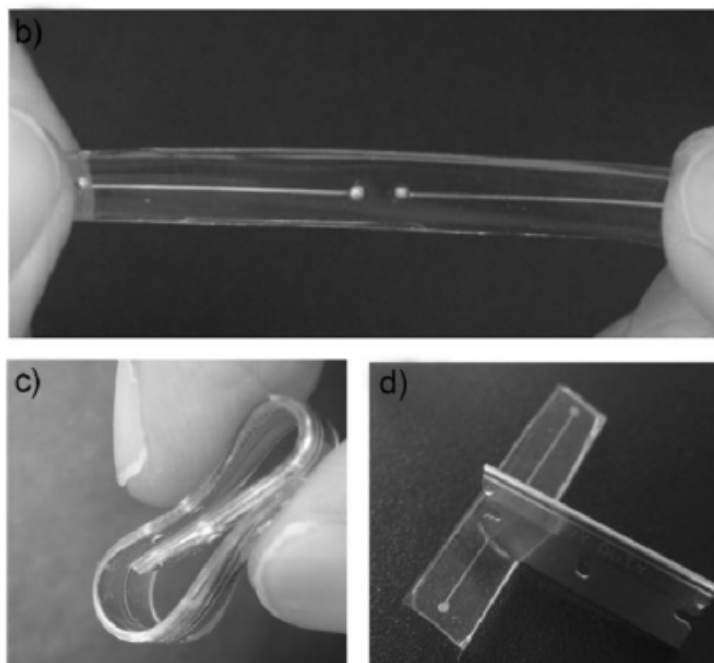


Figure 7 (a, b, c) Photographs of a prototype antenna being stretched and rolled. There is no hysteresis in the spectral properties of the antenna as it is returned to the “relaxed” state. d) The antenna self-heals in response to sharp cuts, such as those inflicted by a razor blade. Fluidic dipole antenna (reproduced from [10]).

2.6.4 Pixel Piston RAs

An interesting and potentially set-top feasible reconfigurable antenna comprises addressable conductive segments (“pixels”) attached to the top of a movable piston in a two-dimensional array of pistons [11]. This RA appears in Figure 8. The piston includes a conductive patch (1010) sitting on top of a dielectric section (1020) that is attached to a conductive segment of the same triangular shape (1030), although other shapes are possible as well. The lower circular shaft (1040) is a dielectric material. This antenna is designed to operate at very high frequencies, 20 GHz being representative, and its dimensions are consequently commensurate. Typically the conductive pixel is about $\lambda/20$ across (0.7 mm at 221 GHz), while the height of the dielectric segment is $\lambda/10$ (1.4 mm at 21 GHz) with an overall height of about 11 mm.

The reconfigurable antenna is created by raising and lowering the pistons to form a transmission line and radiating elements in any desirable allowable pattern. If a pixel is in its lower position, it comprises an element in the array’s ground plane. Otherwise, it is part of a transmission line or radiating element as shown in Figure 8 on the right. The entire structure is addressable on a pixel-by-pixel basis by a controller that operates a two-dimensional actuator for each pixel. Typical reconfiguration times are less than one millisecond, which is consistent with consumer requirements for the set-top application.

While the objective of this patented technology is electronically reconfigurable microwave patch antenna arrays, it may also be applicable to the set-top TV receive antenna if alternative element configurations are considered. For example, the pixel piston structure could be useful in creating folded element antennas, spirals, or bow-tie type elements. Each of these could be tuned to the required channel by sizing it appropriately.

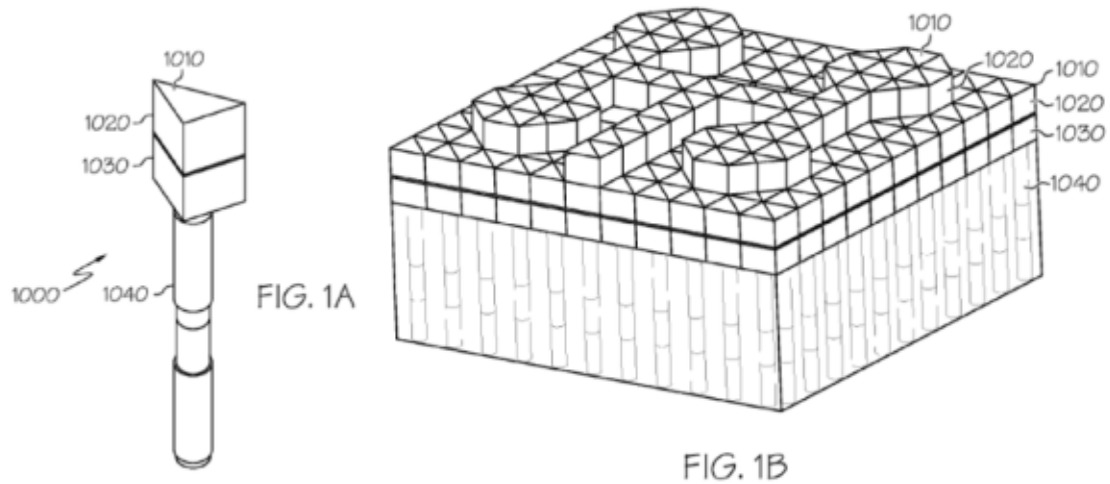


Figure 8. Pixel piston reconfigurable array (reproduced from [11]).

This technology has been implemented in commercially available antennas [12]. PARCA (Pixel-Addressable Reconfigurable Conformal Antenna) arrays are being developed for military applications requiring UWB (ultra wide-band) transmit antennas that adaptively reconfigure operating frequency, gain (beam width), and polarization while handling high power (~2 KW). A typical implementation operating from 1 to 18 GHz using approximately 100,000 ~1.65 mm diameter pixels would be 0.5 meter (20.5 in) square in size with a thickness of about 20 mm (0.8 in). Approximate weight is 12 lbs. This PARCA array would provide gain of 15 dBi and 40 dBi at 1 GHz and 18 GHz, respectively. The antenna is shown schematically in Figure 9.

Testing of microstrip transmission line and patch pixelated antennas has been done with good performance being demonstrated from 500 MHz to 18 GHz [13]. Whether or not this technology can be extended an order or magnitude lower in frequency for the set-top application with reasonable overall size is an open question. But it is clear from the current state-of-the-art that pixelated RAs constitute a technology to watch for the set-top receive antenna.

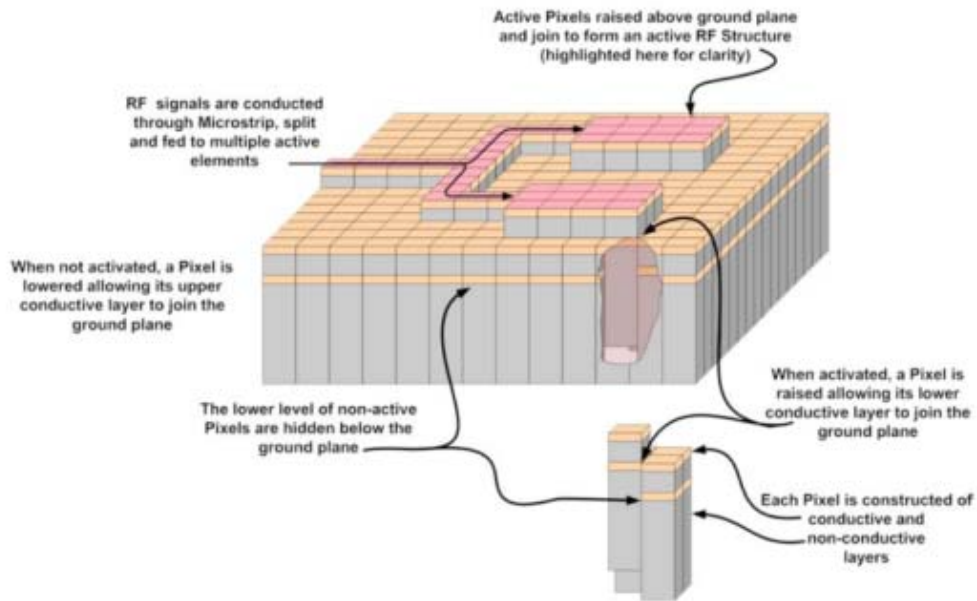


Figure 9. UWB PARCA array (reproduced from [13]).

2.6.5 Liquid Crystal Reconfigurable Antennas

Liquid crystal (LC) technology has recently been applied to RF front end components and array antennas for satellite applications, typically at quite high frequencies (> 20 GHz). Porting this technology to the low VHF range for a television set-top receive antenna simply may not be possible. Nevertheless, LC technology is worth monitoring because it may migrate to substantially lower frequencies, or it may inspire development of similar crystal-based technologies that are applicable in the VHF range.

Liquid crystals are inherently anisotropic and are so named because they simultaneously exhibit properties of liquid and crystalline materials. The class of *nematic* LCs provide the best dielectric characteristics from the microwave through millimeter wave bands, and therefore are the material of choice for very short wavelength RAs. A nematic LC molecule has a more or less rod-like shape as shown in Figure 10. Anisotropy is reflected in different perpendicular and parallel (relative to an incident electric field) dielectric constants, typical values being ~ 2.5 and ~ 2.8 - 3.5 , respectively. Application of a bias voltage to an LC causes a deformation of the molecular alignment as shown schematically in Figure 10, the effect of which is to change the LC's dielectric properties. These changes, in turn, constitute the basis of a reconfigurable antenna element.

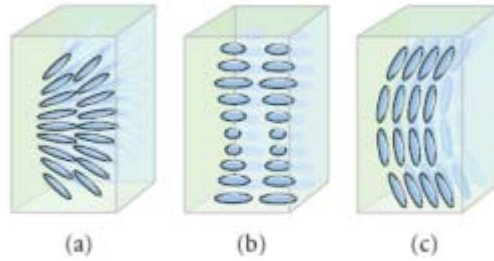


FIGURE 3: (a) The splay, (b) twist, and (c) bend deformation.

Figure 10. LC deformation modes (reproduced from [14]).

A reflectarray RA was fabricated using a dielectric substrate whose properties could be tuned using a bias voltage less than about 20 volts. The RA is a waveguide-fed planar reflecting surface capable of accurately steering the radiated beam into a wide range of directions. A unit cell comprising a single microstrip patch of dielectric sandwiched between two parallel plate electrodes is shown in cross-section in Figure 7 (left). The upper electrode patch is printed onto the dielectric substrate as is the lower electrode which acts as the antenna's ground plane. Initial LC molecule alignment is achieved using a thin (~ 300 nm) polyimide film on the electrode patch and ground plane. The applied external electric field created by the bias voltage reorients the LC molecules, thereby changing its dielectric properties. The figure shows the variation of dielectric constant as the bias voltage increases from zero to a value slightly exceeding the LC's threshold voltage, V_{th} , and then to a value that is much greater. As the effective dielectric constant changes, so does the capacitance per unit length of the microstrip patch, which allows the cell to be voltage-tunable as a reconfigurable antenna element.

The reflectarray antenna comprises 16×16 unit cells spaced 0.55λ . Each cell is 2.2 mm across with an LC cavity height of $50 \mu\text{m}$. The complete antenna is shown in Figure 11, in which the individual cells are clearly visible, as are the control lines (bias lines). The antenna is fed using a right-angle bent WR-10 open-ended waveguide as shown in the figure. Figure 12 shows measured pattern data for different bias voltage levels. The main lobe is clearly steered into the desired directions of zero (blue), +25 (black), and -10 (red) degrees with good relative main lobe gain and sidelobe suppression.

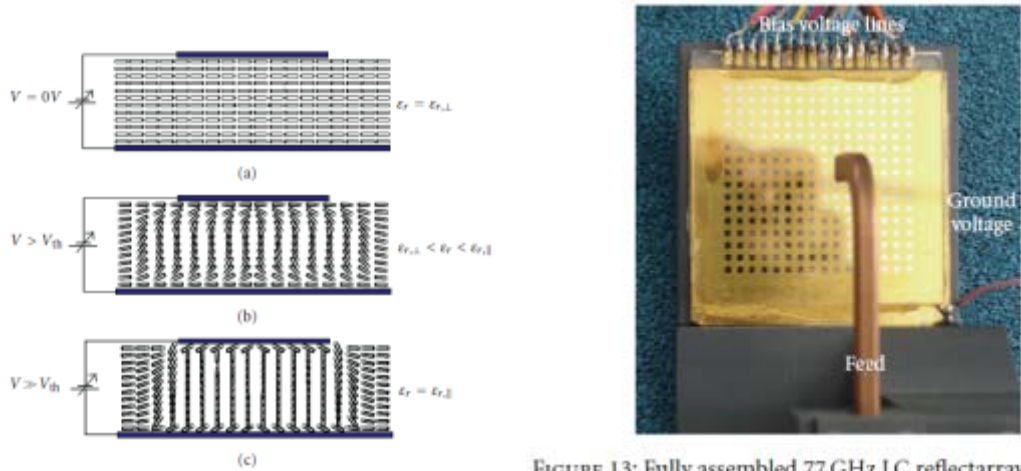


FIGURE 13: Fully assembled 77 GHz LC reflectarray with feed.

Figure 11. 77 GHz LC reconfigurable reflectarray (reproduced from [14]).

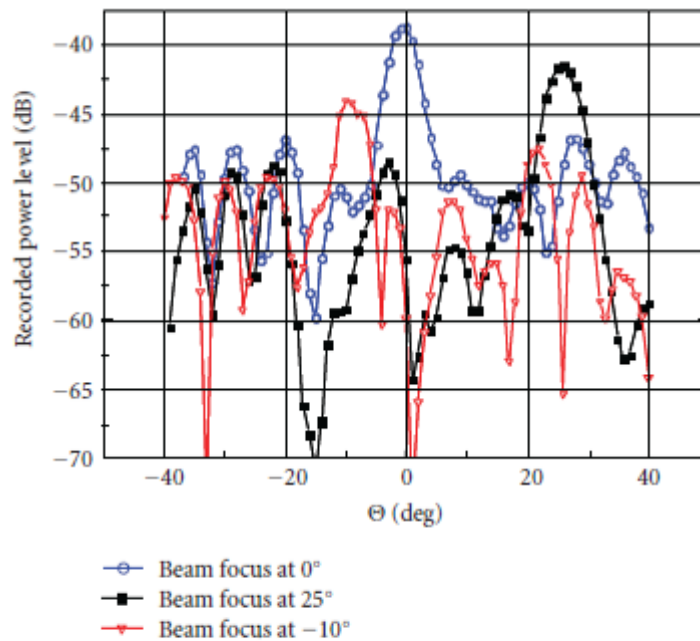


FIGURE 14: Three recorded E-plane patterns for three different voltage configurations, with the main beam pointing at different angles: -10° , 0° , and $+25^\circ$ (at 77.2 GHz).

Figure 12. LC reflectarray measured patterns (reproduced from [14]).

2.6.6 Plasma Reconfigurable Antennas

The plasma RA [15] is conceptually similar to the PARCA antenna in §4. It also uses electrically conductive/non-conductive surfaces to create radiating elements and associated components. But instead of conductive metallic patches, the plasma RA utilizes gas enclosures in which the gas can be made electrically conductive (plasma state) or non-conductive. The enclosures are interconnected and can be turned on (conducting) and off (non-conducting) by applying a control voltage. Figure 13 shows the basic plasma RA structure. It comprises square cells that contain four control electrodes, one on each edge. In the diagram, a cell that is turned on is shown by wavy lines between the electrodes. For example, cell 110 is “on” as shown by the wavy lines which indicate that the gas within the cell has been ionized into a plasma state. By contrast, cell 202 is “off” as indicated by the absence of wavy lines; its gaseous contents have not been ionized. Turning individual cells on and off in the manner forms the basis for a reconfigurable antenna system.

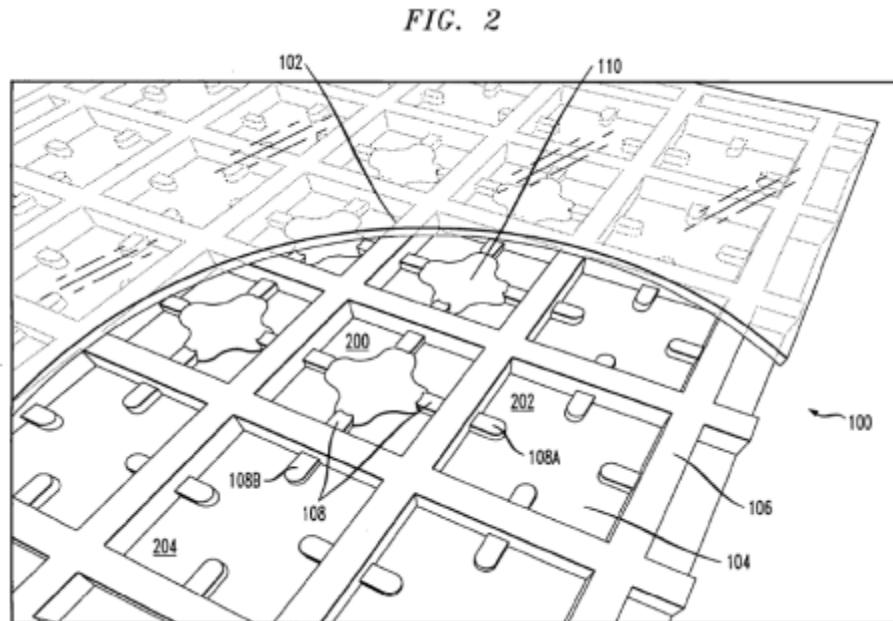


Figure 13. Plasma RA structure (reproduced from [15]).

While the reconfigurable aperture in Figure 13 can be used on a stand-alone basis, it frequently is coupled to backplane as shown in Figure 14. The backplane comprises control elements (304) that are arrayed on an insulating substrate (302) with conductive traces (312) that form the control lines. When mated with the plasma structure, the control elements turn individual gas enclosures on and off. A typical

complete plasma RA is shown in Figure 15, which adds a ground plane (404) printed on a dielectric substrate (402). The sandwich comprising the individually controllable plasma enclosures, the groundplane, and the backplane form an electronically reconfigurable antenna system.

The plasma RA may be particularly useful as a set-top antenna. One advantage is has over other approaches is that it almost certainly can benefit from the highly developed plasma screen technology used in consumer televisions. A plasma RA should be much simpler in structure and fabrication than a large plasma screen display. Applying existing display technology to manufacturing plasma RAs may be only an incremental step, thereby reducing time to market and costs.

FIG. 3

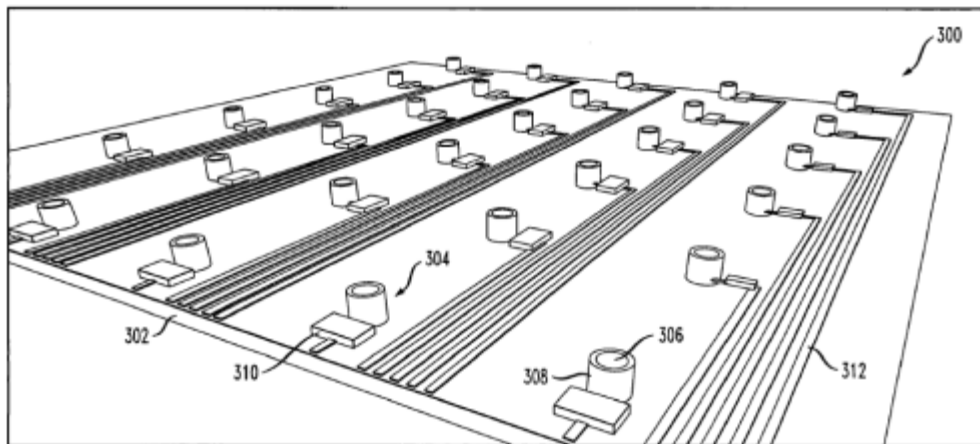


Figure 14. Plasma RA backplane (reproduced from [15]).

FIG. 4

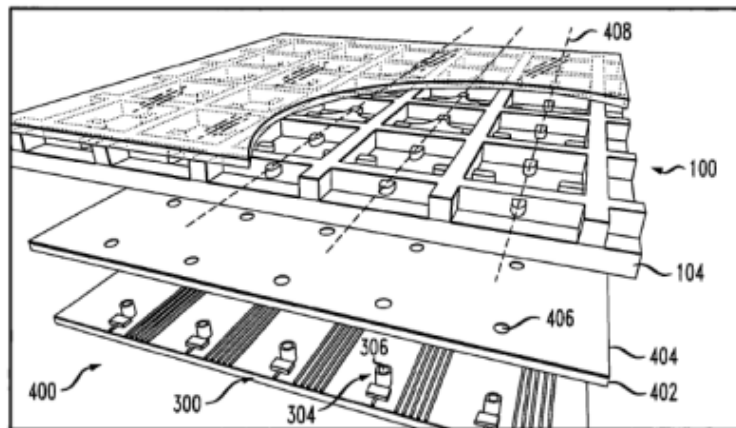


Figure 15. Complete plasma RA (reproduced from [15]).

2.6.7 References

- [1] Reed, D. (ed.), **The ARRL Handbook (2004)**, American Radio Relay League, Newington, CT 06111 USA.
- [2] Ativanichayaphong, T., Cai, Y., Wang, J., Chiao, M., and Chiao, J.-C., "Design Considerations of Reconfigurable Antennas using MEMS Switches," SPOIE 2005 Microelectronics, MEMS, and Nanotechnology Symposium, Brisbane, Australia, Dec. 11-15, 2005.
- [3] RadantMEMS, Inc., 255 Hudson Road, Stow, MA 01775 USA.
- [4] DowKey Microwave Corp., 4822 McGrath Street, Ventura, CA 93003 USA.
- [5] MEMScomm, LLC, 419r East Main Street, Morehead, KY 40351 USA.
- [6] Cetiner, B., Biyikli, N., Yildirim, B. S., and Damgaci, "Nanoelectromechanical Switches for Reconfigurable Antennas," *Microwave and Optical Technology Letters*, **52**, No. 1, January 2010.
- [7] Lee, S., Eriksson, A., Abdelrahim, A. S., Campbell, E. E. B., "Carbon-nanotube-based Nano Electromechanical Switches," *Jour. Korean Physical Society*, 55, No. 3, pp. 957-961, Sept. 2009.
- [8] Sabel, K. F., Katehi, L. P. B., Sarabandi, K., "Modeling and Design of MEMS-Based Reconfigurable Antenna Arrays," *IEEE Aerospace Conference, 2003. Proceedings*, p. 2-1135. DOI: 10.1109/AERO.2003.1235528
- [9] Wu, T., Li, R. L., Eom, S. Y., Lim, K., Jeon, S. I., Laskar, J., and Tentzeris, M. M., "A Multiband/Scalable Reconfigurable Antenna for Cognitive Radio Base Stations," *IEEE Antennas and Propagation Society International Symposium, 2008. AP-S 2008*, 5-11 July 2008, pp. 1-4. DOI: 10.1109/APS.2008.4619490.
- [10] So, J-H., Thelen, J., Qusba, A., Hayes, G. J., and Dickey, M. D., "**Reversibly Deformable and Mechanically Tunable Fluidic Antennas**," *Advanced Functional Materials*, **19**, pp. 3632-3637 (2009). DOI: 10.1002/adfm.200900604.
- [11] **Walton, et al., "Reconfigurable Antenna Using Addressable Pixel Pistons," U.S. Patent No. 7,561,109 B2, July 14, 2009.**
- [12] Syntonics, LLC, 9160 Red Branch Road, Columbia, MD 21045 USA.
- [13] Syntonics, <http://www.syntonicscorp.com/>
- [14] Gaebler, A., Moessinger, A., Goelden, F., Manabe, A., Goebel, M., Follmann, R., Koether, D., Modes, C., Kipka, A., Deckelmann, M., Rabe, T., Schulz, B., Kuchenbecker, P., Lapanik, A., Mueller, S., Haase, W., and Jakoby, R., "Liquid Crystal-Reconfigurable Antenna Concepts for Space Applications at Microwave

and MillimeterWaves,” *International Journal of Antennas and Propagation*,
Volume 2009, Article ID 876989, 7 pp. DOI:10.1155/2009/876989.

- [15] Metz, C., “Reconfigurable Plasma Antenna with Interconnected Gas Enclosures,”
U.S. Patent Application Publication No. US 2006/0220980 A1, Oct. 5, 2006.

2.7 Use of Metamaterials in Antenna Systems

2.7.1 Summary

Traditional antennas are fabricated from electrical conductors such as copper or aluminum and insulators such as plastic or rubber. Their performance is limited by their electrical size, that is, the largest dimension measured in wavelengths. Electrically small antennas are narrow-band, inefficient, and difficult to impedance-match. The demands on a television set-top antenna are for the most part antithetical. It must be small, but it requires a very wide bandwidth to cover all VHF/UHF broadcast channels with good gain and efficiency. Traditional antennas therefore have fallen short of providing good set-top performance.

A very promising emerging technology that may soon well address this limitation is the use of *metamaterials* (MTM) in the set-top antenna. This section examines whether or not MTM can sufficiently improve the performance of electrically small antennas to make MTM-based designs attractive for set-top use. While MTM have been available since the mid-1990s and the subject of much literature, they have not gained widespread commercial acceptance until recently. A recent survey paper examines this question and suggests some explanations for the MTM's slow acceptance, much of which is not based on the technology itself.

More recent developments show that well-designed MTM-based antennas indeed can provide significantly improved performance over traditional designs, but the reported designs are in frequency bands well above the TV VHF band. Wireless communication antennas have been designed, fabricated, and measured that improve on the "Chu limit" for small antenna performance by orders of magnitude using MTM. Substantially improved bandwidth, high efficiency, and good gain are available from antennas with maximum dimensions less than one-tenth wavelength. The question is whether or not this technology can be ported to the low end of the television broadcast band; and, while the answer is not guaranteed, it appears to be in the affirmative.

The MTM-based antenna is an attractive candidate for the set-top application, and it should be vigorously studied as a candidate architecture. Because MTM typically are formed from simple wire structures, they likely can be optimized for the set-top application, which may lead to designs that are different than those used at higher frequencies that still meet set-top performance objectives.

2.7.2 What is a metamaterial?

The term *metamaterial* (MTM) applied to antennas does not connote a material in its commonly used sense. The materials used to fabricate an antenna broadly fall into the categories of conductors (metallic elements), insulators (non-conductors), and, occasionally, semiconductors. Materials like copper, aluminum, silver, various plastics, rubber, paper, and so on, are what come to mind as typical antenna materials; and all of these share some common features. Whether naturally occurring or man-made, they are homogeneous with electrical properties determined by their chemical structure. Like all other naturally occurring substances (at least all that are known at this time), antenna materials exhibit positive relative permittivity (dielectric constant), $\epsilon_r \geq 1$, and positive relative permeability, $\mu_r \geq 1$. Their electrical performance in the antenna is determined by these fundamental physical parameters.

In sharp contrast, a *metamaterial* is a “composite” whose electrical properties are not determined by chemical structure, but instead by the shapes and patterns of inclusions that often are imbedded in some other material or simply arrayed in a pattern on a substrate [1]. A common inclusion is the split-ring resonator (SRR), and often combinations of SRRs and small wires are arranged to create a “unit cell” from which the metamaterial is built. Arrays of cells on some surface or within some volume constitute the actual “metamaterial.” As a concrete example, Figure 1 shows a unit cell comprising a double SRR on an insulating substrate and a parallel wire. The SRR and wire are normally conducting materials such as copper or aluminum. An array of unit cells deployed on or embedded in a surface of any shape or throughout some volume becomes the *metamaterial*, which evidently is quite different from a homogeneous piece of plastic, for example, whatever its shape.

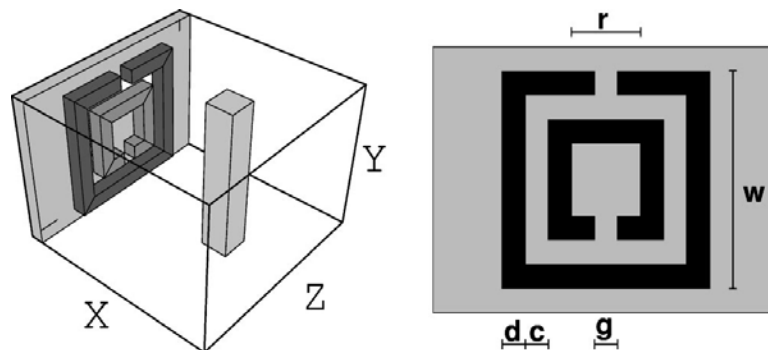


Figure 1. SRR/wire unit cell (reproduced from [1]).

What makes metamaterials attractive as antenna components is that they are *left-handed*, in distinction from all naturally occurring materials, which are *right-handed*. In right-handed materials (RHM), the electric field, \vec{E} , the magnetic intensity, \vec{H} , and

propagation (wave) vector, \vec{k} , are related by the “right-hand rule,” viz, $\vec{E} \times \vec{H} \approx \vec{k}$. The phase and group velocities in RHM are in the same direction, parallel to the wave vector. A *left-handed material* (LHM) obeys a “left-handed rule” in which the phase and group velocities propagate in *opposite* directions. Physically this results in energy flow (Poynting vector) antiparallel to the direction of wave propagation. For LHM, both the effective permittivity and permeability are negative, $\epsilon_r \leq 0$ and $\mu_r \leq 0$, which gives rise to LHM’s unusual electromagnetic (EM) properties.

While the notion that this type of behavior can arise from as simple a unit cell as an SRR close to a wire perhaps seems counter-intuitive, it is not. There are examples of very simple wire structures exhibiting similar behavior. For example, the three-dimensional mesh of orthogonal crossed wires in Figure 2 exhibits a negative dielectric constant for frequencies $\omega < \omega_p$ where $\omega = 2\pi f$, $\omega_p = (c/d)[2\pi/\ln(d/w)]^{1/2}$, and c is the velocity of light [2]. Thus, properly arrayed unit cell structures comprising conducting and insulating elements simply exhibit a similar behavior that is determined by the specific details of how the unit cell is structured.

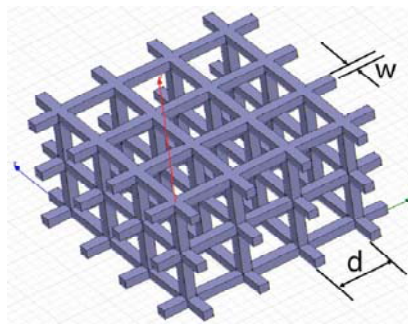


Figure 2. Crossed-wires metamaterial (reproduced from [2]).

Without doubt, the most important consequence of having $\epsilon_r \leq 0$ and $\mu_r \leq 0$ is that the metamaterial’s refractive index is negative, $n < 0$, which leads to some very non-intuitive EM effects. Besides energy flow opposite to the propagation direction, $n < 0$ results in *negative refraction* as shown in Figure 3. In the figure, air lies above the interface with either LHM or RHM. For both types of lower materials, a reflection takes place at the interface that follows the usual law of reflection (incidence and reflection angles being equal, rays 1 and 2). If the lower medium is RHM (normal material), the propagating ray (#4) is bent towards the normal. This is the usual refraction that takes place with all normal materials, and, for example, bends the image of a pencil in water towards the vertical. But, if the lower medium is LHM, just the opposite occurs. The propagating ray (#3) is bent *away* from the vertical, not towards it.

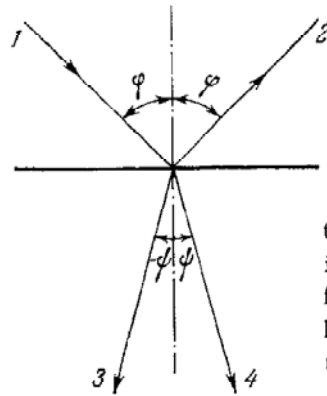


FIG. 3. Passage of a ray through the boundary between two media. 1 – incident ray; 2 – reflected ray; 3 – reflected ray if the second medium is left-handed; 4 – refracted ray if the second medium is right-handed.

Figure 3. LHM and RHM rays at air-metamaterial interface (reproduced from [3]).

2.7.3 Slow Acceptance of LHM Cellular Antennas

While there is no question that metamaterials offer intriguing possibilities for novel antennas, their use has not become widespread. Some possible explanations for this situation are offered in [4], which specifically addresses application to mobile-phone antennas. Because the cellular band (825-894 MHz, $\lambda = 0.36 - 0.335m$) lies just above the broadcast television band (54-806 MHz, $\lambda = 5.55 - 0.37m$), the issues raised in [4] are largely applicable to TV antennas.

An important consideration in whether or not LHM are useful is the antenna's *electrical size*, that is, its size measured in wavelength, λ . The wavelength at the highest TV channel 69 is the same order as the cell phone wavelengths, whereas TV channel 2 has a wavelength about 15 times larger than the longest cellular wavelength. This observation raises the question of whether or not general statements or conclusions made about antennas for cellular frequencies hold up for low-band TV antennas. The answer is a clear "maybe."

A typical cell phone antenna with a largest dimension of 0.1m has an electrical size of 0.28λ at 825 MHz. A channel 2 TV antenna has the same electrical size if its largest dimension is 1.55m, which is too large for a set-top antenna. A more reasonable set-top dimension might be 0.5m, which is 0.09λ at 54 MHz. So the question is whether or not observations about a 0.28λ antenna can be applied to one that is about three times smaller. There is no definitive answer, but the electrical sizes are close enough that some attributes of metamaterials applied to cellular antennas can be ascribed to TV antennas as well. Thus, some of the reasons in [4] why LHM are not widely used in cellular antennas may apply to TV antennas as well. Among those limitations are:

1. *Bandwidth.* Metamaterials tend to exhibit strong resonances accompanied by substantial dispersion and losses. The result is a high- Q , narrow-band structure that makes it very difficult to cover the entire range of VHF and UHF television frequencies. An antenna covering all cellular frequencies has a fractional bandwidth (BW) of 8% (relative to band center). If a set-top TV antenna contains two antennas, one low-band (channels 2-13, 54-216 MHz) and the other high-band (channels 14-69, 470-806 MHz), they must have fractional bandwidths of 120% and 53%, respectively, to cover all channels. If achieving 8% BW in a LHM cellular antenna is difficult, then meeting the requirements of a set-top antenna is even more difficult.

2. *Other Factors.* Whether or not an antenna is “good” for a specific application depends on many factors, many of which are not electrical in nature. Antennas that perform well electrically (gain, bandwidth, efficiency) may be too costly, too large, too heavy, too difficult to manufacture, and so on. Reports of successful LHM-based antennas usually do not address these factors, and as a result it may be difficult to analyze the benefits and risks associated with that type of antenna. This consideration has slowed the adoption of LHM antennas for mobile phones and likely applies to TV set-top antennas as well.

3. *Marketing.* Like any consumer product or component thereof, LHM antennas must be properly marketed to be effectively used. Many types of man-made materials are used in antennas, especially in the microwave range, and the resulting designs are considered “traditional.” LHM-based designs often resemble traditional ones, so that they share many common features. Yet LHM antennas are frequently described as being fundamentally “different,” which leads to some measure of reluctance in adopting them. A better approach would be to characterize LHM antennas as *alternatives* to traditional designs rather than a fundamental departure.

2.7.4 Examples of LHM Antennas

Even though the speculation in [4] provides possible reasons why MTM-based antennas are not more widely used, recent developments show rather convincingly that technical objections are not valid reasons. Quite to the contrary, state-of-the-art MTM antenna designs support the view that they well may be able to meet set-top TV performance requirements. This section consequently examines some typical designs in the context of porting them to the low VHF television channels.

(a) *Compact Broadband Monopole.* An example of the state-of-the-art in small broadband LHM antennas is shown in Figure 4(a), which is reproduced from [5]. The antenna comprises a PCB (printed circuit board) monopole loaded with a left-handed

negative-refractive-index transmission-line (NRI-TL) metamaterial. The loading reduces the electrical size of the antenna while providing large bandwidth.

This particular antenna was designed for dual-band use in the WiMax and WiFi bands [3.3-3.8 GHz, ($\lambda = 0.09\text{m} - 0.08\text{m}$) and 5.15-5.85 GHz ($\lambda = 0.06\text{m} - 0.05\text{m}$), respectively]. Its physical size of 0.03m [W_g in Figure 4(a)] corresponds to 0.3λ at the lowest frequency, which is comparable to the electrical size of a cellular antenna and about three times larger than a typical 0.5m set-top antenna at channel 2. Adding NRI-TL loading increased BW over the unloaded structure by approximately 1.5 GHz without increasing its size. The LHM monopole's BW (return loss below -10 dB) is 3.84 GHz from 3.15-6.99 GHz (fractional BW of 76%). The computed radiation efficiency is close to 90% across both the WiMax and WiFi bands. Input impedance is plotted in Figure 4(b), and it shows moderate values across a very wide frequency range, from about 5GHz to 10 GHz, so that good impedance matching should be readily achievable without requiring a balun.

The compact LHM monopole provides a good example of enhancements directly attributable to NRI-TL loading of a simple structure: excellent impedance bandwidth and high efficiency in an electrically small structure. Although this particular antenna would not meet a set-top TV antenna's requirement of 120% BW (see §3), it certainly suggests that with further improvements that objective might be reached.

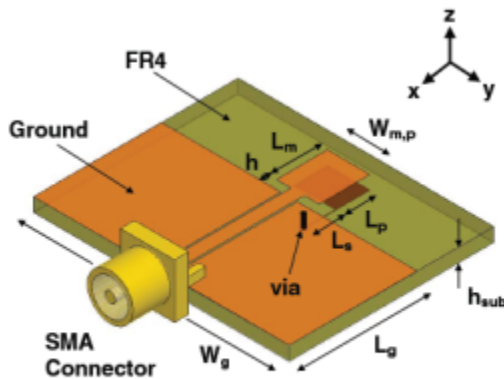


Fig. 1. NRI-TL metamaterial monopole antenna. All dimensions are in mm: $L_m = 6$, $W_m = 5$, $L_g = 15$, $W_g = 30$, $h = 1$, $L_p = 4$, $W_p = 5$, $L_s = 3.45$, $W_s = 0.1$, $h_{sub} = 1.59$, $S_{open} = 0.2$, $W_{open} = 1.55$, via diam. = 0.5.

(a)

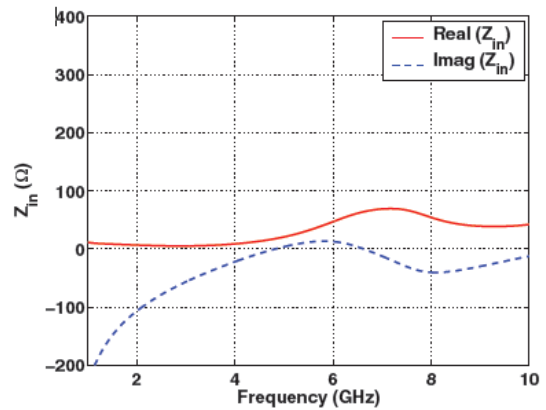


Fig. 4. Simulated input impedance characteristics of the unloaded monopole antenna from Ansoft HFSS.

(b)

Figure 4. Broadband LHM monopole: Structure (a); Input impedance (b) (reproduced from [5]).

(b) *Efficient Electrically Small Antenna (EESA)*. An MTM-based Efficient Electrical Small Antenna (ESSA) [6] is shown in Figure 5. It provides another example of how LHM antennas can achieve performance that is not possible with traditional designs, and suggests that porting MTM designs to TV set-top antennas is a viable approach to achieving improved performance.

The ESSA comprises a monopole surrounded by an SNG (single negative) MTM structure mounted on a plane substrate. It achieves a voltage standing wave (VSWR) bandwidth ≤ 2 of 470 MHz (1.75-2.22 GHz) [fractional VSWR bandwidth of 24%] in a package with an electrical size of only 0.07λ . The addition of LHM in this case resulted in a much broader bandwidth than could be achieved otherwise because the effect of MTM's is to lower the system Q -factor from the theoretical "Chu limit" of 16.72 for traditional materials to 2.23. Significantly, the increased bandwidth is not accomplished at the expense of radiation efficiency or gain, which often must be sacrificed in traditional designs. The ESSA's measured maximum gain and efficiency were 2.44 dBi and 83.61%, respectively.

The radiation patterns generally exhibited broad lobes with fairly shallow nulls ($< \approx -25$ dB, Figure 6), which lend themselves well to omnidirectional reception as required in a set-top antenna. Because the ESSA's electrical size is comparable to that required for a set-top antenna (see §3), it may be possible to "stack" several ESSA's covering different band segments in a fairly small set-top package. This particular ESSA design suggests that MTM-based antennas may well meet TV set-top reception requirements.

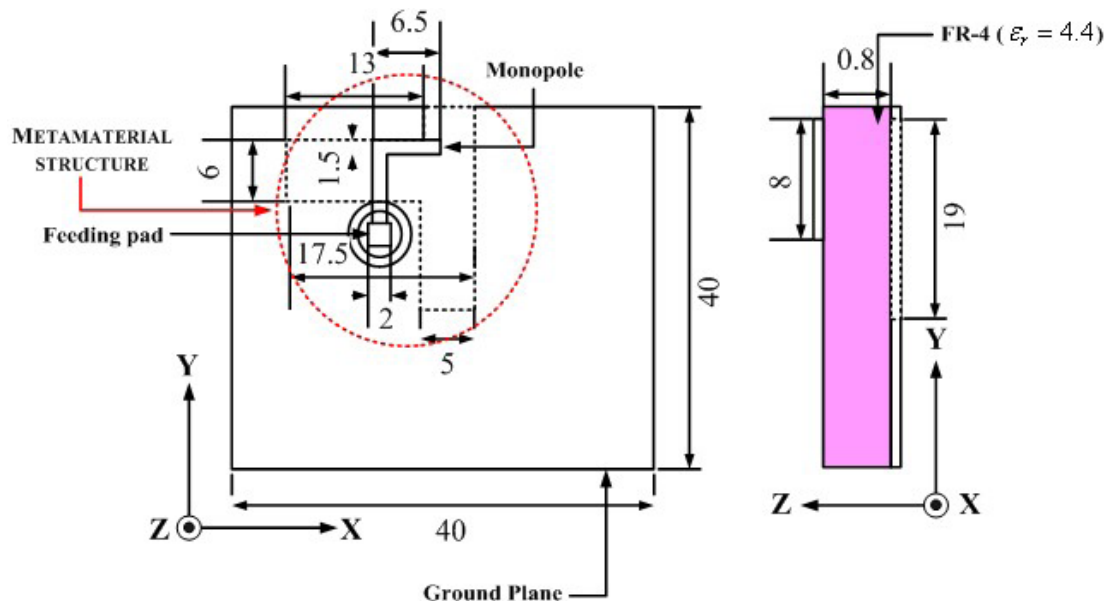


Figure 5. MTM ESSA geometry (reproduced from [6])

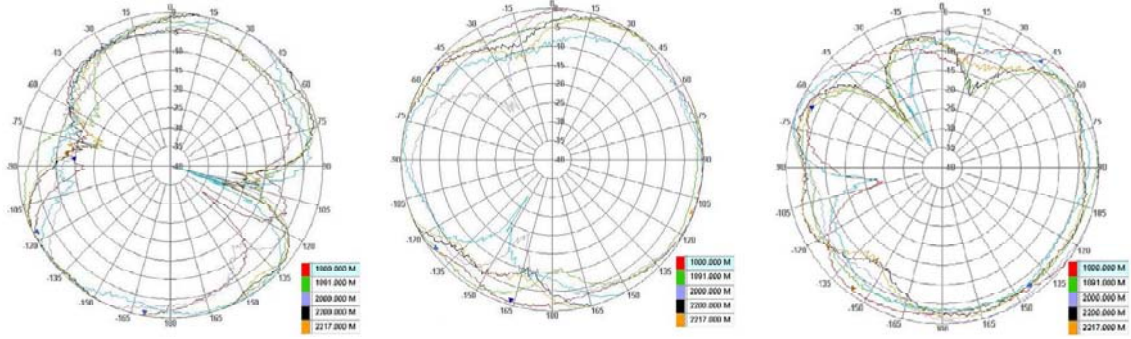


Figure 6. ESSA measured radiation patterns (reproduced from [6]).

(c) *LHM Topologies*. There are some general approaches to MTM-based antennas that appear to be useful regardless of the specific type of radiating element [7], and these likely should be the focus of future efforts to apply LHM to television set-top antennas. Various types of materials are available as shown in Figure 7. “Normal” materials have positive permittivity and permeability, and are referred to as Double Positive (DPS). “Epsilon negative” (ENG) materials can occur naturally in unusual states of matter (for example, plasmas), while *homogeneous* “mu negative” (MNG) materials can be man-made (for example, ferrite). LHM materials, on the other hand, do not occur in Nature and are “Double Negative” (DNG) because both permittivity and permeability are negative. While composite MTMs usually are DNG, ENG and MNG types also can be made and sometimes are desirable in antenna applications.

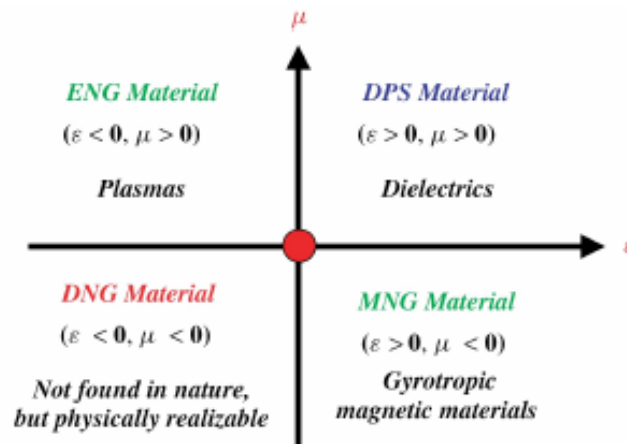


Figure 7. Material classification (reproduced from [7]).

Figure 8 shows two LHM configurations that should be useful in a wide range of applications and, in particular, TV set-top antennas. In Figure 8(a) a PCB antenna is placed on an MTM substrate in order to decrease radiating element size while increasing radiation efficiency and bandwidth. In this example, the substrate is an MNG

array of square SRRs imbedded in a homogeneous dielectric medium. Figure 8(b) shows an ENG shell surrounding a radiator fed against a PEC (perfectly electrically conducting) ground plane. The shell can be very thin ($\approx 0.01\lambda$) so that it has little effect on attenuating signal level, yet it substantially reduces antenna input reactance over a fairly wide range of frequencies. While the “Chu Q -factor” is the recognized theoretical limit for antennas made from normal materials, the ENG shell can lower Q by a factor of 1,583 while providing a good match to 50Ω and efficiencies approaching 98%, at least over some range of frequencies. These examples illustrate LHM’s potential benefits for TV set-top antennas, and they should be vigorously pursued for the next generation of set-top antennas.

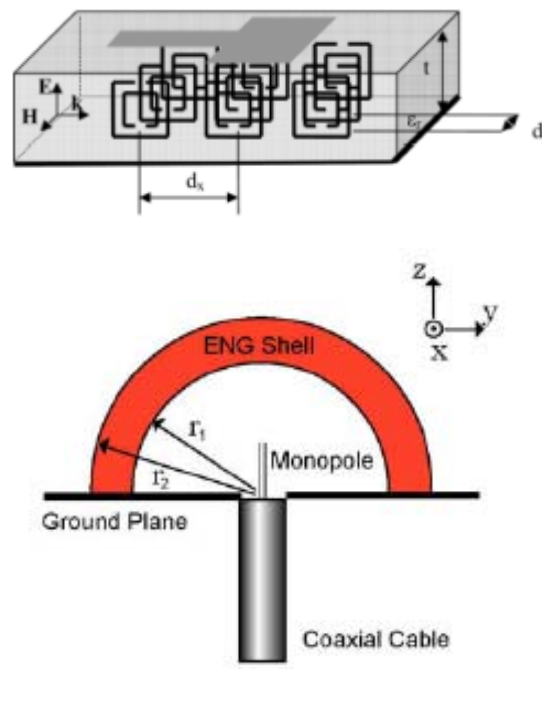


Figure 8. Generally useful LHM configurations (reproduced from [7]).

2.7.5 LHM Antenna Patents

An online search at Patent Storm (<http://www.patentstorm.us/>) using the keyword ‘metamaterial’ returns 521 U.S. issued patents and applications, many of which are related to antennas or optics. The application of MTM to antennas is a very active technology area, both in the scientific and engineering literature and in the realm of patented proprietary technology. While a thorough review of the patent literature is beyond the scope of this report, it is instructive to examine a specific development as representative of the state-of-the-art.

Figure 9 shows a typical implementation disclosed in U.S. patent #7,592,957 B2, which issued recently (Sept. 22, 2009) and consequently representative of the state-of-the-art. The figure illustrates one implementation of many described in the patent (forty-nine drawing sheets, many with multiple figures). This patent discloses composite right- and left-handed (CRLH) MTM structures as the basis of electrically small antennas and antenna arrays for use in wideband multi-band communications. One design, for example, provides 5.6 dBi gain with a 2.35-4.42 GHz BW ($S_{11} < -10$ dB). This level of performance is representative of what can be achieved today for wireless communication applications, and it is quite good compared to the performance of traditional antennas. It bodes well that LHM-based antenna designs likely can be useful for the TV set-top application.

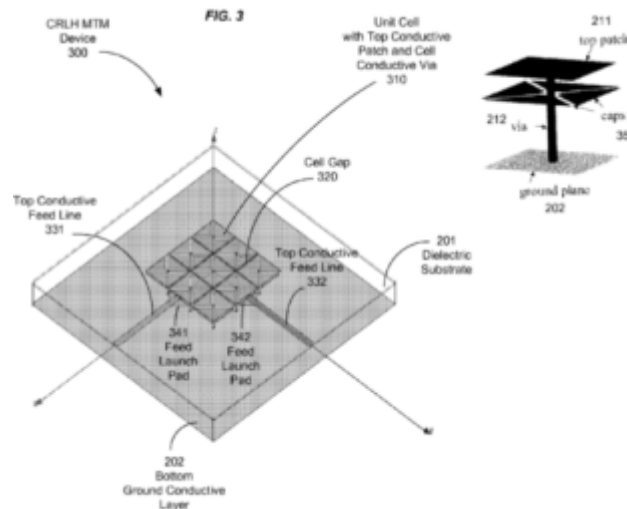


Figure 9. Typical CRLH MTM 2-D array (reproduced from U.S. patent #7592957)

2.7.6 Theory of LHM

A *metamaterial* (MTM) or *left-handed material* (LHM) has simultaneously negative values of relative permittivity (ϵ_r) and permeability (μ_r). There are no known naturally occurring substances with this attribute, but there are artificial media exhibiting left-handedness. MTM are useful antenna components because unusual electromagnetic effects occur when ϵ_r and μ_r are both negative. For example, the direction of power flow, wave refraction, Doppler shift, and the direction of Cherenkov radiation are all dramatically different than they are in “normal” media. These and perhaps other unusual electromagnetic properties of MTM may be useful in antenna system design, particularly in the microwave region.

Artificial MTM can be manufactured from arrays of conducting elements, such as small wire segments, split ring resonators, or other similar structures. These discrete elements may mimic continuous media, because, surprisingly, their left-handedness can extend to frequencies where the wavelength is much larger than either the element size or spacing. MTM slabs may be useful as coatings on metallic antenna parts. If the metamaterial can be “worked” appropriately, then major antenna components might be fabricated from it directly. The utility of these materials is an open question, because they are not well understood either theoretically or experimentally. In fact, serious investigation of these materials has occurred only in about the past decade. What follows is a discussion of how metamaterials behave and some of the issues in using them as antenna components.

Maxwell’s Equations

All electromagnetic (EM) phenomena, including the EM behavior of metamaterials, are described by Maxwell’s equations. Maxwell’s equations are completely general, and apply to EM phenomena in all media at all frequencies, including electrostatics (“zero” frequency). MTM behavior must be consistent with Maxwell’s equations in every limiting case for which theoretical results are available, whether electrostatic or time-varying. Limiting cases may be useful in understanding the counter-intuitive behavior of metamaterials.

Maxwell’s equations are:

$$\nabla \cdot \mathbf{E} = \frac{\rho_t}{\epsilon_r \epsilon_0} \quad (1)$$

$$\nabla \cdot \mathbf{B} = 0 \quad (2)$$

$$\nabla \times \mathbf{E} + \frac{\partial \mathbf{B}}{\partial t} = 0 \quad (3)$$

$$\nabla \times \mathbf{B} - \epsilon_r \epsilon_0 \mu_r \mu_0 \frac{\partial \mathbf{E}}{\partial t} = \mu_r \mu_0 \mathbf{J}_m \quad (4)$$

in which: \mathbf{E} is the electric field (volts/meter).

$\rho_t = \rho_f + \rho_b$ is the total charge density (coulombs/cubic meter).

ρ_f is the free charge density, and ρ_b is the bound charge density.

\vec{B} is the magnetic induction (teslas or webers/square meter).

$\mathbf{J}_m = \mathbf{J}_f + \frac{\partial \mathbf{P}}{\partial t} + \nabla \times \mathbf{M}$ is the total current density (amperes/square

meter), consisting of \mathbf{J}_f , the current density of free charges; $\partial\mathbf{P}/\partial t$, the polarization current density; and $\nabla \times \mathbf{M}$, the magnetization current density.

\mathbf{M} is the magnetization (amperes/meter).

ϵ_0 is the permittivity of free space (farads/meter).

ϵ_r is the relative permittivity, or dielectric constant.

μ_0 is the permeability of free space, which is arbitrarily set equal to

$4\pi \times 10^{-7}$ teslas meter/ampere (henrys/meter).

μ_r is the relative permeability.

In materials where Ohm's law applies, the free current density is related to the electric field by $\mathbf{J}_f = \sigma\mathbf{E}$, where σ is the conductivity (Siemens/meter).

Physically, the two fundamental vector fields are \mathbf{E} and \mathbf{B} , because it is these fields that produce forces on electric charge according to the Lorentz force law $\mathbf{F} = q(\mathbf{E} + \mathbf{v} \times \mathbf{B})$. It is customary, however, to write Maxwell's equations in terms of the fields \mathbf{E} and \mathbf{H} , where \mathbf{H} , the "magnetic field" or "magnetic intensity" (amperes/meter), is proportional to \mathbf{B} . The primary reason for doing this is that the quantity $\mathbf{E} \times \mathbf{H}$ is the energy flux density, which is of paramount importance in determining a system's electromagnetic behavior.

Media Parameters

It is necessary to specify the electrical and magnetic properties of the medium supporting the electromagnetic field in order to solve the field equations, subject to appropriate boundary conditions. Without this information, Maxwell's equations do not form a determinate system.

The EM behavior of any medium is determined by its material properties, the electric permittivity and magnetic permeability. There are other material parameters, but they are secondary in nature. For example, in linear media the electric susceptibility is the proportionality factor between the applied electric field and induced polarization. Similarly, the magnetic susceptibility relates magnetization to the applied magnetic

field. Each of these parameters is included indirectly in the relative permittivity and permeability, respectively, and therefore they have no independent significance.

Various classes of media exist. The simplest is *free space*, in which the relative permittivity and permeability are both unity. The EM properties of *isotropic* media are independent of the direction of the EM fields. Media in which the electrical properties are the same everywhere are *spatially homogeneous*. In some media, the EM properties vary in time, and such media are described as *temporally inhomogeneous*. The most complex media are *anisotropic*. The EM properties are direction-dependent, and may also vary spatially or temporally. The permittivity and permeability of anisotropic media are described by tensors instead of real or, in the case of lossy media, complex scalars.

Wave Velocity and Refractive Index

Time-varying fields in the form of propagating electromagnetic waves follow directly from Maxwell's equations. The equations are combined to obtain a "wave equation" whose solutions are coupled electric and magnetic field that move through the medium carrying energy as they do.

In a lossless medium, ϵ_r and μ_r are real numbers. A monochromatic EM wave's phase velocity, the velocity at which the wavefront (surface of constant phase) propagates, is completely determined by these two material parameters. The propagation velocity is

$$v = \frac{1}{\sqrt{\epsilon_r \epsilon_0 \mu_r \mu_0}} = \frac{c}{\sqrt{\epsilon_r \mu_r}}, \quad (5)$$

where c is the velocity of light in free space, or simply "speed of light" (very nearly 3×10^8 meters/second).

In lossless "normal" media, ϵ_r and μ_r are positive real numbers greater than 1 (this is not true in a metamaterial). Waves in normal media always propagate slower than the speed of light. The velocity ratio is the medium's *refractive index*, given by

$$n = \frac{c}{v} = \sqrt{\epsilon_r \mu_r}. \quad (6)$$

When n is real, EM waves can propagate in the medium. If n is purely imaginary at some frequency, then no wave mode (field configuration) can propagate at that frequency.

In lossless anisotropic or inhomogeneous media, ϵ_r and μ_r vary with propagation direction or position, and are represented mathematically as matrices of positive real numbers. In lossy materials ϵ_r and μ_r are complex numbers with non-zero imaginary parts that result in energy dissipation as the wave propagates through the medium. In such media the refractive index varies with direction or position or both.

n^2 may be negative (n is imaginary) in some naturally occurring media. At frequencies below its plasma frequency, for example, a gaseous plasma has a negative dielectric constant but positive permeability, resulting in $n^2 < 0$. This situation occurs in the earth's ionosphere, and provides an example of unusual wave propagation resulting from the negative permittivity. Instead of being refracted, as it would be if n^2 were positive, below the plasma frequency an incident radio wave is instead reflected. This is the mechanism that supports long distance high-frequency (HF) radio communication.

In normal media, both ϵ_r and μ_r are frequency-dependent, often strongly so. For example, the dielectric constant of water decreases from 81 at DC and very low frequencies, to 78 at 1 Mhz, 34 at 10 Ghz, and about 2 at optical frequencies. The refractive index varies correspondingly from 9 at DC to 1.4 in the optical region. In magnetic materials (water is not one), the frequency variation of relative permeability can be several orders of magnitude.

The effective ϵ_r and μ_r of metamaterials are also are frequency-dependent (in fact they must be), and they change sign just as the dielectric constant does in a plasma. As a result, in certain frequency ranges the metamaterial's novel EM properties disappear, and there is a strong analogy between the behavior of a metamaterial and naturally occurring plasma. The variation of permittivity and permeability with frequency may be very important in practical antenna applications, particularly in view of the wide spectrum used by modern communication systems. Metamaterials may be quite useful in the microwave range, but less so at lower frequencies.

Right and Left Handed Media and Power Flow

Another important parameter describing the propagation of an EM wave is its *wave vector*, \mathbf{k} , whose magnitude is the *wavenumber*. \mathbf{k} is in the direction of propagation and perpendicular to the wavefront. In normal media, not in a metamaterial, it also coincides with the direction of energy flow.

The wavefront consists of electric and magnetic fields which are orthogonal to each other, and to the direction of propagation. The triad of vectors \mathbf{E} , \mathbf{H} , and \mathbf{k} constitute a mutually orthogonal set related by the "right hand rule". When the vector

\mathbf{E} is rotated into the direction of \mathbf{H} through the included angle ϕ in the plane containing \mathbf{E} and \mathbf{H} , curling one's fingers in the direction of rotation with the thumb extended perpendicular to the fingers determines the direction of the wave vector \mathbf{k} (hence, right "hand" rule). The *handedness* of a medium is determined by the vector triplet \mathbf{E} , \mathbf{H} , and \mathbf{k} . The right hand rule relationship holds in normal media, which are consequently described as *right handed*. A metamaterial, by contrast, is *left handed* as discussed below.

The direction of energy flow in the wavefront is $\mathbf{E} \times \mathbf{H}$, which for a plane wave in normal media corresponds to the direction of the wave vector \mathbf{k} . The vector $\mathbf{S} = \mathbf{E} \times \mathbf{H}$ is known as the *Poynting vector*, in units of watts/square meter. Integrating \mathbf{S} over a closed surface gives the amount of energy per unit time (joules/second) flowing out of that surface.

Theoretical Basis of Metamaterials

Veselago's Model: In a seminal paper published in the late 1960s, the Russian physicist V. G. Veselago theoretically investigated the effects on EM fields of negative values of relative permittivity and permeability [3]. Because the refractive index is equal to the square root of their product, changing the signs of *both* ϵ_r and μ_r produces no change in the refractive index. Veselago suggested three possible interpretations of what simultaneously negative values of ϵ_r and μ_r might mean:

- (1) The electromagnetic properties of any material are independent of whether or not ϵ_r and μ_r are both positive or both negative.
- (2) Having simultaneously negative values for ϵ_r and μ_r is inconsistent with the laws of physics, and no such material can ever exist.
- (3) Materials with negative permittivity and permeability may exist and possess unusual electromagnetic properties.

Veselago acknowledged that, at the time of his paper, there were no materials, naturally occurring or artificially made, with $\epsilon_r < 0$ and $\mu_r < 0$. He nevertheless proceeded to analyze the properties of such media in the event that they might be discovered or man-made.

In the case of a monochromatic plane wave described by the propagation factor $e^{-i(kz - \omega t)}$, Maxwell's equations lead to the following relationships:

$$\mathbf{k} \times \mathbf{E} = \frac{\omega}{c} \mu_r \mu_o \mathbf{H} \quad (7)$$

$$\mathbf{k} \times \mathbf{H} = -\frac{\omega}{c} \varepsilon_r \varepsilon_o \mathbf{E} \quad (8)$$

If $\varepsilon_r > 0$ and $\mu_r > 0$, then the triad \mathbf{E} , \mathbf{H} , and \mathbf{k} are related by the right hand rule. The medium is therefore *normal* or *right-handed* (RH). If, instead, $\varepsilon_r < 0$ and $\mu_r < 0$, the sign of the right hand side of equations (7) and (8) changes. As a result, the vector triplet is now left-handed (curling the fingers of the *left* hand). The direction of the wave vector \mathbf{k} therefore is reversed when the material parameters are both negative. A metamaterial with negative permittivity and permeability is consequently called a *left-handed* (LH) material (LHM).

Power Flow in LHM: Compared to its orientation in RHM, the wave vector \mathbf{k} in LHM points in the opposite direction relative to \mathbf{E} and \mathbf{H} . An immediate consequence is that the Poynting vector and wave vector are in opposite directions. Because the Poynting vector $\mathbf{S} = \mathbf{E} \times \mathbf{H}$ always forms a right-handed triad with \mathbf{E} and \mathbf{H} , regardless of the sign of the permittivity and permeability, allowing $\varepsilon_r < 0$ and $\mu_r < 0$ changes the direction of \mathbf{k} but not of \mathbf{S} .

The wave propagates in one direction, but the power flow is in the opposite direction. Veselago points out that this situation corresponds to a negative group velocity ($V_{group} = \frac{\partial \omega}{\partial k}$, computed at the average value of the wavenumber). While perhaps somewhat surprising, there are examples of just this effect. Some naturally occurring anisotropic media and certain media in which spatial dispersion exists exhibit negative group velocity.

Doppler Effect and Cherenkov Radiation in LHM: Other unusual effects occur in LHM. The Doppler effect is reversed. The measured frequency of an approaching emitter will be lower than the stationary frequency, not higher as in RHM. Cherenkov radiation, electromagnetic radiation emitted by a charged particle moving at high speed in a LHM, will be directed backward relative to the direction of motion, which is the opposite of what happens in RHM.

Reflection and Refraction at a Plane Interface: EM plane waves incident upon a plane material surface are *refracted* as they enter the medium. For waves propagating between normal media, the wave bends towards the normal upon entering a denser medium (higher refractive index), and away upon entering a less dense medium. Figure 10 shows this effect in which the upper medium is less dense than the lower one. Φ is

the incidence angle, and Ψ the refraction angle. If the wave propagates from a RHM into a denser LHM, the refracted wave is bent towards the normal, but on the opposite side of the normal as shown in Figure 2. Interestingly, the direction of the reflected wave is the same (reflection angle equals the incidence angle) regardless of the nature of the lower medium.

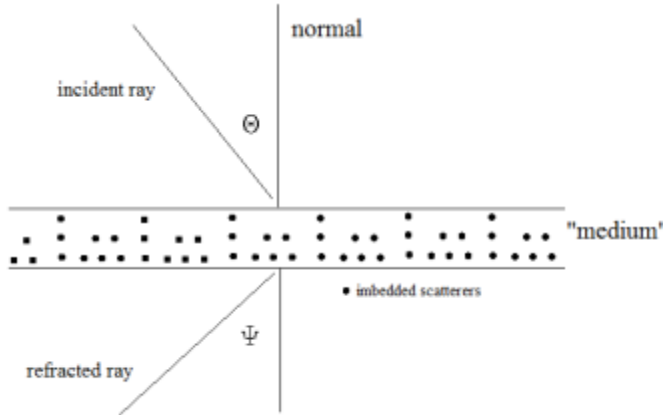


Figure 10. Refraction at MTM interface

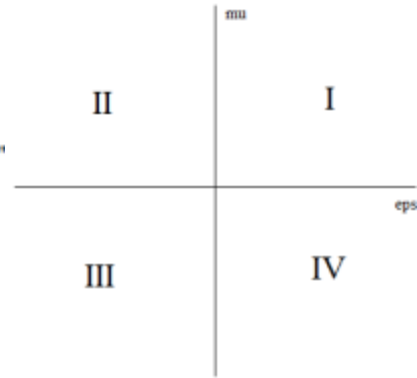


Figure 11. Media classification

Media Classification: In order to classify media based on permittivity and permeability, Veselago introduced the $\varepsilon - \mu$ diagram shown in Figure 11. The plane is divided into the four standard quadrants, labeled I through IV proceeding counter-clockwise from the upper right-most quadrant. Considering only isotropic materials, normal dielectrics with $\varepsilon_r > 0$ and $\mu_r > 0$ are contained in quadrant I. Quadrant II contains media with $\varepsilon_r < 0$ and $\mu_r > 0$, which is characteristic of gaseous and solid-state plasmas. The dielectric constant of a gaseous plasma is given by $\varepsilon = 1 - \sum \frac{\omega_o^2}{\omega^2}$, where ω_o is the plasma frequency, and the summation is over all species in the plasma. At sufficiently low frequencies, the second term in this expression becomes greater than 1, which leads to a negative permittivity. Quadrants II and IV, however, are unoccupied, at least by isotropic materials, because there is no known naturally occurring material with negative permeability.

The $\varepsilon - \mu$ diagram can be used only for scalar values of permittivity and permeability. Certain anisotropic materials with tensor permittivity and permeability fall into quadrants III and IV for propagation in specific directions within the medium, because in those directions ε_r and μ_r are scalars. An example is propagation along the magnetic field direction in a gyrotropic medium, such as a plasma in a magnetic field. In

the propagation direction ϵ_r and μ_r are scalars, while generally in the medium they are second-rank tensors (3x3 matrices).

Requirement of Dispersion: A non-dispersive LHM cannot exist. This result follows from the fact that the energy density of an electromagnetic field is given by $W = \epsilon_r \epsilon_o \mathbf{E} \cdot \mathbf{E} + \mu_r \mu_o \mathbf{H} \cdot \mathbf{H}$. If both ϵ_r and μ_r are negative, then the total energy is negative, which is not possible.

In order to assure positive total energy, the medium must be *dispersive*. In a dispersive material, the expression for energy density is different, and includes the variation of permittivity and permeability with frequency:

$$W = \epsilon_o \frac{\partial(\epsilon_r \omega)}{\partial \omega} E^2 + \mu_o \frac{\partial(\mu_r \omega)}{\partial \omega} H^2. \quad (9)$$

W is always positive if $\frac{\partial(\epsilon_r \omega)}{\partial \omega} > 0$ and $\frac{\partial(\mu_r \omega)}{\partial \omega} > 0$. In general, therefore, the permittivity and permeability must be frequency-dependent in LHM. Media in which both ϵ_r and μ_r are negative and constant with respect to frequency cannot exist. It does appear possible to have only one parameter depend on frequency, as long as its derivative is large enough to avoid a negative total energy; but Veselago did not consider this possibility.

The same conclusion about the necessity of dispersion can also be reached by considering the limiting case of a parallel plate capacitor at DC. Neglecting fringing, the capacitance is $C = \frac{\epsilon_r \epsilon_o A}{d}$, where A is the plate area, and d is the plate separation in consistent units. Physically, capacitance is the ratio of free charge on the plates, Q , to the potential difference (voltage) between them, V , taken as positive quantities. Thus, $C = \frac{Q}{V}$, must be positive at DC. If a metamaterial were used as a dielectric between the capacitor plates, its permittivity therefore must be positive in the limit of zero frequency (DC). This is necessary to avoid the physically impossible case of a negative capacitance. But, by definition, ϵ_r in a metamaterial must be negative at some frequency in order for the medium to be a metamaterial. Consequently, the metamaterial's relative permittivity must change sign with frequency, from a positive value at DC to a negative value at some non-zero frequency. This is dispersion. Note that this brief discussion does not address how the capacitor behaves as a circuit element at frequencies where $\epsilon_r < 0$. Doing so should be quite interesting.

Realization of Metamaterials

Because metamaterials do not occur naturally, the only way to obtain a metamaterial is to manufacture it. The very nomenclature, *metamaterial*, conjures up the image of a “substance”, generally a solid material with some specific chemical composition. Existing metamaterials, however, could not be further from that image.

Smith [8] recently described a LHM that was modeled theoretically and measured experimentally. Building upon the split ring resonator (SRR) medium created by Pendry [9], short, small-diameter wires were added to an array of SRRs to create the left-handed metamaterial. The medium is actually an array of discrete electromagnetic scatterers arranged so that the *effective* ϵ_r and μ_r are negative at some frequencies. It is not at all a “substance” in the usual sense.

Figure 10 represents this concept schematically. Imagine two parallel planes in space, between which an array of scattering elements is deployed. The scatterers, represented by dots in the figure, might be short wire segments, other geometrical shapes, SRRs, other resonant structures, or any number of EM elements fabricated from conductors and/or dielectrics.

In the realm of every possible configuration, it seems intuitively plausible that some arrangements will result in anomalous propagation such as seen in metamaterials. In Figure 10, for example, it is not difficult to imagine that there is some scatterer arrangement that will “refract” a wavefront incident at the angle Φ in the direction opposite to “normal” refraction as shown. This type of propagation is a characteristic of a left-handed material. If the volume between the planes is thought of as a “medium”, it would be properly described as one with negative effective permittivity and permeability, that is, a metamaterial.

Metamaterials that are “substances” may eventually be developed or discovered. But current research focuses on creating LHMs using imbedded scatterers. This is not a limitation, however, and indeed may actually provide more flexibility than attempting to create purely chemical substances. Designing the scattering matrix may permit engineering metamaterials whose properties could not exist in chemical substances. Creating solid materials consisting of a matrix containing small conductive scatterers, possibly even carbon nanotube scatterers, might permit the designer to actually tailor the LHM properties to the EM application.

The idea of using a matrix of scatterers to create a “medium” with a negative effective permittivity is not new. In the 1950s, Bracewell [10] and Rotman [11] experimentally investigated ionospheric propagation using a three-dimensional array of

intersecting thin, straight wires. Dispersion in this “medium” is similar to that in a neutral plasma, such as the ionosphere.

Just as the real ionosphere does, the artificial one has $\epsilon_r < 0$ for frequencies below the “plasma frequency”. However, unlike the ionosphere’s plasma frequency, which depends on the charged particle density, and particle charge and mass, the artificial medium’s “plasma frequency” depends on the arrangement and dimensions of the wires. Because LHM must exhibit $\epsilon_r < 0$ at some frequencies, and because the dispersion relation has the same form as a gaseous plasma’s, metamaterials made from scatterers are often described in terms of a *plasma frequency*. It is important to remember that the term used in the manner is a purely formal construct, not to be confused with the parameter of the same name describing a gaseous plasma.

The effective permittivity of Smith’s wire medium is given by

$$\epsilon_{eff}(\omega) = 1 - \frac{\omega_p^2}{\omega^2} \quad (10)$$

where ω_p is that medium’s plasma frequency. ω_p depends in a complicated way on the wire scatterers’ electrical properties and geometrical arrangement. At frequencies below ω_p , ϵ_{eff} is negative, which is one of the requirements for LHM. The other requirement is that μ_r simultaneously be negative. The SRR medium has an effective permeability given by

$$\mu_{eff}(\omega) = 1 - \frac{F\omega_o^2}{\omega^2 - \omega_o^2 - i\omega\Gamma} \quad (11)$$

where F is the fractional area of the unit cell occupied by the SRR’s interior, and Γ is the SRR dissipation factor. ω_o is the SRR medium’s plasma frequency. Equations (10) and (11) assume that the array of wires and the array of SRRs do not interact appreciably, which was true in Smith’s medium.

When the scatterer arrays are uncoupled, the wire array produces the medium’s ϵ_{eff} , and the SRR array produces its μ_{eff} . Under these conditions, the effective refractive index of the composite medium is $n_{eff}(\omega) = \sqrt{\epsilon_{eff}(\omega)\mu_{eff}(\omega)}$. If there is an overlapping band of frequencies in which the effective permittivity and permeability are both negative, then the effective index of refraction is real, and propagating modes exist. The medium is LH, however, because of the negative material parameters, so that the unusual propagation effects associated with LHM occur.

The SRR, wire segment, wire-SRR media were modeled using a commercial EM software package to generate dispersion curves (the problem is far too complex for an analytical solution). The SRR array alone showed a pronounced band gap from 4.2-4.6 GHz. No modes would propagate in this band. The wire array alone exhibited an even wider band gap, from just above DC to 13 GHz, the array's plasma frequency. No modes would propagate in this range. The reason propagation cannot occur is that μ_{eff} and ϵ_{eff} , respectively, are separately negative in these bands, which results in a purely imaginary refractive index.

A metamaterial is created by combining the wire and SRR arrays. The wire-SRR array has overlapping bands from 4.2-4.6 GHz where the simultaneously negative material parameters combine to create a metamaterial. Computer modeling of the dispersion characteristics of the combined arrays clearly showed propagation in the otherwise forbidden band. Experimental measurements further confirmed the LH nature of the medium by observing propagation between 4.2 and 4.6 GHz which was not possible in either array alone.

Analysis of Metamaterials

In calculating a metamaterial's performance, it is unlikely that analytical results are attainable for all but the simplest scatterer geometries. Analytically solving Maxwell's equations is almost certainly impractical. Computer modeling is likely to be the best approach, and possibly the only truly useful one. Metamaterials made of imbedded arrays of scattering elements can, in fact, be analyzed with existing modeling software, at least to some degree. Commercially available packages, and government-developed programs such as NEC-4, provide a starting point for modeling metamaterials. But many questions arise.

Most EM software approximates the modeled structure using some form of discretization. In NEC-4, for example, continuous wires are approximated by short segments. Continuous surfaces are approximated by patches of surface area. Other programs use the same or similar approaches.

One characteristic of the discretized models is that very substantial computer resources (memory and speed) are often required to obtain good results. In NEC-4, for example, the model size (a measure of required memory) is proportional to the square of the number of segments, and the computation time (a measure of required processor speed) scales similarly. Other types of models exhibit similar characteristics. Disproportionately greater resources are required with increasing complexity, modeling accuracy, and resolution in the frequency domain. It may be expected that these issues will be exacerbated for metamaterials, because LHMs fabricated from large numbers of

complex individual scatterers are indeed very complex structures. This level of complexity is likely to push existing modeling capabilities to the limit.

Metamaterials should be studied experimentally, not only to characterize available materials, but also to develop the experimental techniques and fixtures needed for such studies. Because of the anomalous propagation, it is likely that new measurement techniques will have to be developed to fully explore metamaterial properties. For example, direct measurement of the negative values of permittivity and permeability, key parameters in characterizing a metamaterial, is required. But it is not clear that suitable instrumentation or techniques for doing so exist.

Future of MTM

MTM hold great promise as components in antenna design, particularly at microwave frequencies. Whether or not they can be used effectively at low VHF frequencies is an open question because there simply is not enough data to reach a conclusion. At this time not enough is known about MTM's electromagnetic behavior. There are no "design handbooks" and essentially no low frequency data. Nevertheless, the performance of MTM-based antennas at microwave frequencies strongly suggests that MTM antennas will be useful at VHF as well.

2.7.7 References

- [1] Markos, P., and Soukoulis, C. M., "Numerical studies of left-handed materials and arrays of split ring resonators," *Physical Review E*, **65**, p. 036622-1 (2002). DOI: 10.1103/PhysRevE.65.036622.
- [2] Shapiro, M. A., Shvets, G., Sirigiri, J. R., and Temkin, R. J., "Spatial dispersion in metamaterials with negative dielectric permittivity and its effect on surface waves," *Optics Letters*, **31**, 13, p. 2051 (2006).
- [3] Veselago, V. G., "The electrodynamics of substances with simultaneously negative values of ϵ and μ ," *Soviet Physics Uspekhi*, **10**, 4, Jan.-Feb. 1968
- [4] Ikonen, P., "Electrically small metamaterial-based antennas – have we seen any real practical benefits?" arXiv:0902.1820v1 [cond-mat.mtrl-sci] (2009).
- [5] Antoniadis, M. A., and Eleftheriades, G. V., "A compact broadband NRI-TL metamaterial monopole antenna," *13th Annual International Symposium on Antenna Technology and Applied Electromagnetics and the Canadian Sciences Meeting* (2009).

- [6] Kim, J-H., Kim, H-Y., Lee, H-M., "Design of efficient electrically small dual band monopole antenna using negative permittivity metamaterial structures," *IEEE Antennas and Propagation Society International Symposium, 2008*, San Diego, CA, pp.1-4. DOI: 10.1109/APS.2008.4619487
- [7] Slyusar, V. I., "Metamaterials on antenna solutions," *International Conference on Antenna Theory and Techniques*, Lviv, Ukraine, pp. 19-24, 6-9 October 2009.
- [8] Smith, D. R., Padilla, W. J., Vier, D. C., Nemat-Nasser, S. C., Schultz, S., "Composite medium with simultaneously negative permeability and permittivity," *Phys. Rev. Lett.*, **84**, 18, 1 May 2000
- [9] Pendry, J. B., Holden, A. J., Robbins, D. J., Stewart, J., "Extremely low frequency plasmons in metallic microstructures," *Phys. Rev. Lett.*, **76**, 4773 (1996).
- [10] Bracewell, R. N., "Analogues of an ionized medium, applications to the ionosphere," *Wireless Engineer*, **31**, p. 320 (1954).
- [11] Rotman, W., "Plasma simulation by artificial dielectrics and parallel-plate media," *IRE Trans. Ant. Prop.*, **AP10**, p. 82 (1962).

2.8 Electronic Band-Gap and High Impedance Surfaces

Introduction

Electromagnetic band-gap (EBG) structures recently have attracted a great deal of interest among researchers because EBG structures can significantly reduce surface waves, thereby improving patch antenna performance [1]. Reflection phase characteristics also can have a pronounced negative effect on antenna performance [2,3]. It is well known that when a dipole antenna is operated near a metallic ground plane as shown in Figure 1, the radiated waves are reflected from the ground plane, so that interference may occur. Antenna bandwidth and gain are degraded, which is readily demonstrated by applying image theory.

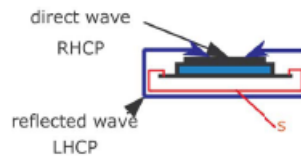


Figure 1. Antenna Near Ground Plane

To overcome these difficulties, dipoles are operated at a height of 0.2λ or higher above the ground plane. In [1] the concept and feasibility of developing wideband, ultra-thin (substrate thickness < 0.1λ) directional dipoles and dipole arrays using EBG structures are addressed. The reflection phase angle of an EBG surface varies from -180 to 180 degrees with frequency. The goal is to make the antenna operating frequency band coincide with the EBG stop band, and then to flatten the reflection phase curve within the stop-band region, which then will ensure wide-band operation of the antenna. This technology could be useful in an integral television antenna as well as set-top antennas that lay flat on the television.

The parameters generally adopted to characterize the performance of EBG structures include the surface wave attenuation and reflectivity. A double benefit can be derived from the use of artificial magnetic conductor type of EBGs because not only are surface waves suppressed, but also in-phase image currents are induced. The so-called reflection phase—frequency diagram gives information on how the structure reacts to a wave impinging on it. Normally, the configuration behaves similar to a metal plate (perfect electric conductor, “PEC”). However, another characteristic feature of EBGs is the existence of a certain frequency range over which an incident electromagnetic wave does not experience *any* phase reversal upon reflection (a rather remarkable phenomenon). In this range the structure behaves as a perfect magnetic conductor (“PMC”). The frequency range where the phase reversal is within from the PMC point (phase reversal) is conventionally used to define the bandwidth and is called the “bandgap.” The concept here is to introduce a ground plane for shielding purposes (reducing the contributions of LHCP signals), and cover this plate with EBG cells (cancelling out the surface currents)

Types of EGB-Cells

Various EBG structures from literature have been investigated. A small sample of different geometries is displayed in Figure 2. These EBG cells can be with or without vias to a ground plane on the opposite side of the substrate. A Mushroom EBG substrate is shown in figure 3. The EBG cells in this figure are shown with vias (each cell is shorted to the ground plane).

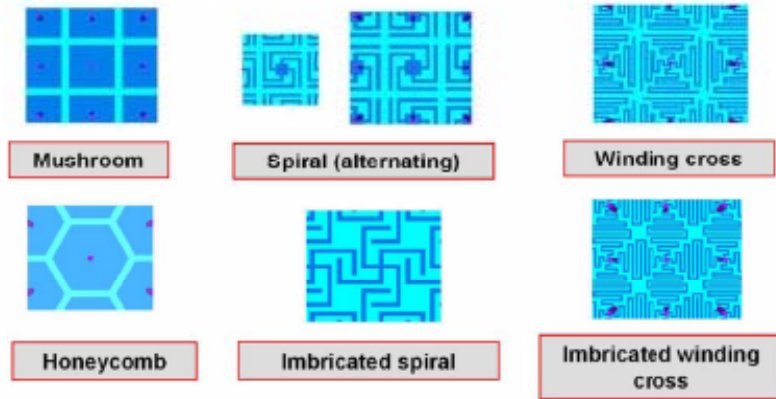


Figure 2. Different Types of EBG Structures.

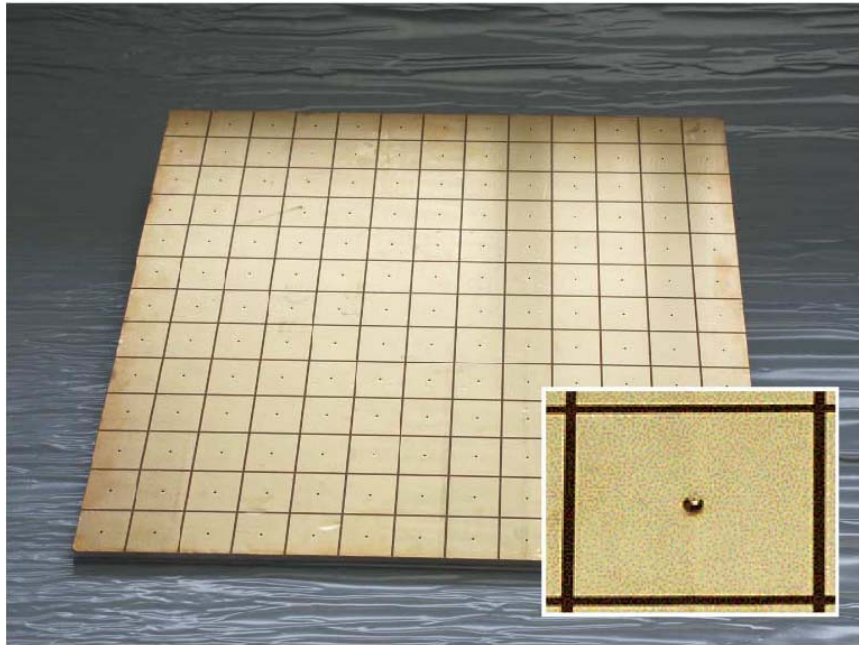


Figure 3 Mushroom EBG substrate (inset: Zoom on a single cell and a golden nail)

Performance of a Dipole Antenna on a Constant Reflection Phase EBG Surface

For a dipole antenna operating against a ground plane, the driving-point impedance is the algebraic sum of the self and mutual impedances when image theory is applied. For a PEC ground plane the driving point impedance is the self minus the mutual impedance since the reflection phase is 180 degrees. The driving point impedance of a dipole on an EBG structure with any other constant reflection phase characteristics can also be

calculated. For example, for a thin wire dipole the self and mutual impedances can be computed using the induced EMF theory. Of course, it may not be possible to achieve a constant reflection phase over a band of frequencies using an EBG structure, but that is the goal. As an example, the dipole under consideration is infinitely thin and resonant at 2.9 GHz in free-space with a 2:1 VSWR bandwidth of 5%. The driving point resistance is negative (at low frequencies) for phase angles of -100 degrees to -160 degrees because the mutual resistance is larger than the self resistance and adds destructively with it. But for phase angles of 40 degrees to 110 degrees the mutual resistance adds constructively with the self-resistance. Thus, the driving point reactance for different phase angles is capacitive at low frequencies and inductive at high frequencies.

An EBG surface can be characterized by its reflection phase angle given by

$$\phi(f) = \text{Im} \left[\ln \left(\frac{af^2 + bf - c}{af^2 + bf + c} \right) \right]$$

where a , b and c are the EBG design parameters with $a=4\pi^2\eta LC$, $b=2\pi L$ and $c=\eta$ [4]. Here L , C and η represent the inductance, capacitance and intrinsic impedance of free-space, respectively. The slope of the reflection phase curve can be changed by varying the values of a and b . The bandwidth of this dipole antenna has been enhanced by flattening out the reflection phase curve at the useful phase angle regions, which corresponds to the EBG surface of having a stop band center frequency at 2.82 GHz.

EBG Dipole

Work on an EBG Dipole was completed in the past by MegaWave Corp. Figure 4 shows an EBG structure modeled in XFDTD. It consists of a double layer, mushroom-like structure embedded in FR-4 substrate with the bottom layer consisting of an array of 6 by 12 square patches and the top layer of an array of 5 by 10 square patches. The overall dimensions are 2"x4" with a thickness of 0.18". The computed reflected phase of the EBG is plotted in Figure 5. The reflected phase was generated by comparing the phase of a plane wave scattered from the EBG surface with that from a PEC surface. The bandwidth of the EBG material was estimated to be from 1.66 to 2.35GHz as determined by the reflection phase being in the range of $90^\circ \pm 45^\circ$ [2].

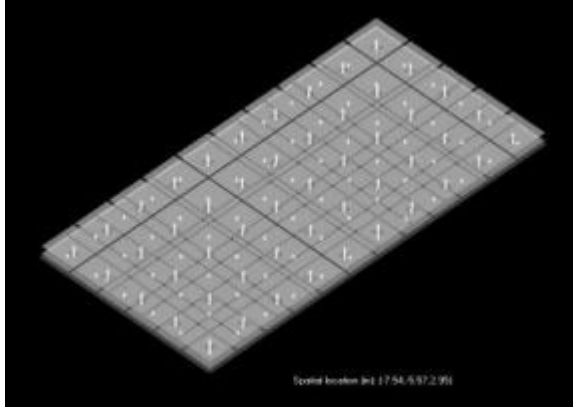


Figure 4: XFDTD Model of Dual Layer EBG Material

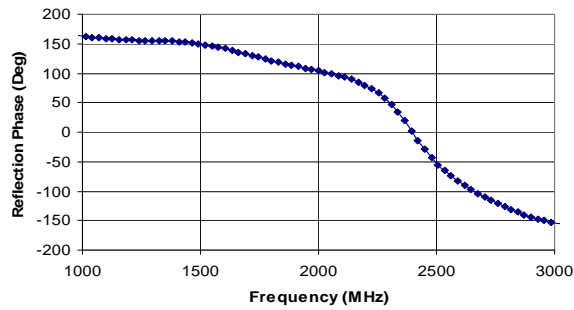


Figure 5: Computed Reflection Phase of EBG Material

A prototype of the MegaWave-designed EBG structure was fabricated as shown in Figure 6, and Figure 7 shows a wideband dipole placed 0.25" away from the EBG structure. The measured VSWR was less than 2.6:1 across a very wide operating frequency band from 1.35 to 2.7GHz as shown in Figure 8.

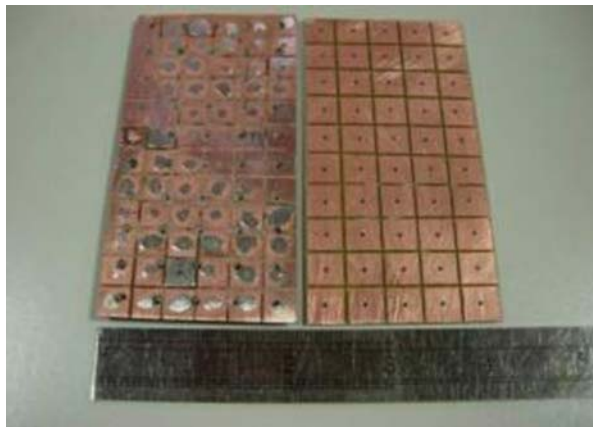


Figure 6: Lab Prototype of EBG Structure (Top and Bottom Layers Shown)



Figure 7: Lab Prototype of Wideband Dipole on EBG Material

The free space radiation patterns of both the wideband dipole on the EBG structure and the Phase I directional dipole antenna were measured and compared in MegaWave's laboratory. Figures 9 and 10 show the measured free-space patterns. This EBG technology could be implemented in the television UHF and VHF bands with an expectation of greatly improved set-top antenna performance.

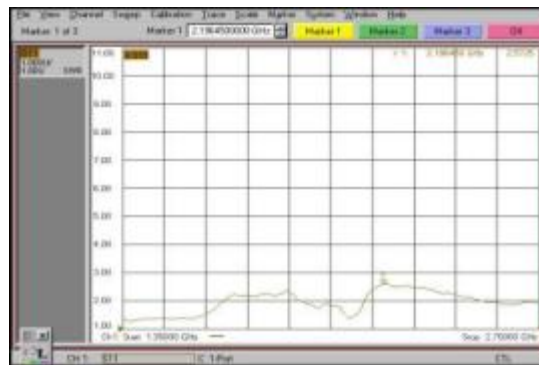


Figure 8: VSWR of Wideband Dipole on EBG Material

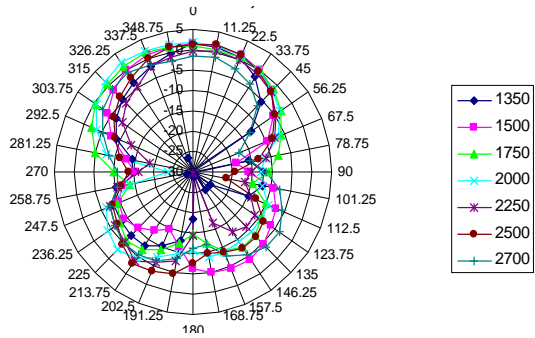


Figure 9: Measured Radiation Patterns of Antenna

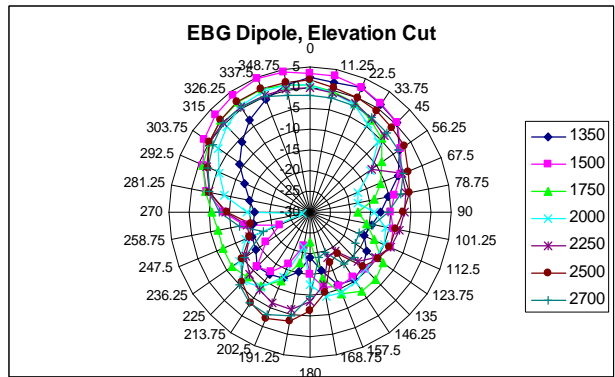


Figure 10: Measured Radiation Patterns of Wideband Dipole on EBG

References

- [1] R. Baggen, M. Martinez-Vazquez, J. Leiss, S. Holzwarth, L. S. Drioli and P. D.Maagt, "Low Profile GALILEO Antenna Using EBG Technology", IEEE, Antennas and Prop., Vol.56, Num. 3, March 2008, pp 667-673
- [2] Fan Yang and Yahya Rahmat-Samii, "Reflection Phase Characterization of the EBG Ground Plane for Low Profile Wire Antenna Applications", IEEE Transactions on Antennas and Propagation, Vol.51, No.10, October 2003.

2.9 Fractal and Self-Similar Antennas

There is no question that, among all the antennas existing today, one of the most interesting and visually appealing is the Fractal antenna. However it not clear exactly what benefits in bandwidth and gain they provide as compared to non-fractal elements of the same shape and area, but without the fine detailed geometries. The reader is directed to the section on pathological antennas (1.5) and its subsection 1.5.8 on fractals in Dr. R.C. Hansen's recent textbook, "Electrically Small, Superdirective, and Superconducting Antennas," Wiley Interscience, 2006.

First publications about electrodynamic characteristics of fractal structures were published in the 1980's, but first practical approach appeared 10 years later. Dr. Nathan Cohen, a professor at Boston University, designed, engineered and patented many fractal antenna designs, some of which are shown in Figure 1.

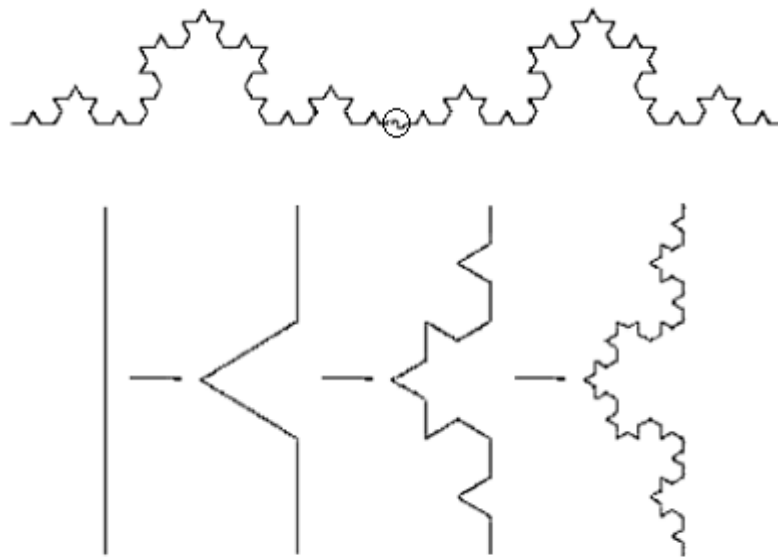


Figure 1. Fractal Designs

This fractal figure is built as follows: first line (length is z) is cut in 3 equal pieces $z/3$. In the middle the triangle is formed with same side lengths $z/3$ and same angles. This creates a single element template. This process is repeated with other segments in which sizes diminish 3 times ($z/9$), then again 3 times ($z/27$), and so on. A fractal antenna is created using fractal geometry, a self-similar pattern built from the repetition of a simple shape.

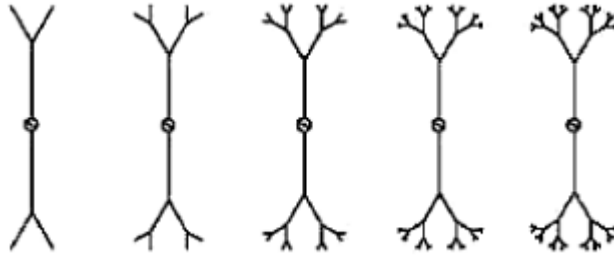


Figure 2. Fractal Dipole

The Fractal dipole as shown in Figure 2, is a recursive tree. Each of the new iterations multiplies the branches by two, in the process lowering the resonance frequency. By using many iterations, it is possible to use an antenna at lower frequencies without increasing the overall antenna size. Dipole antennas usually have narrow bandwidth, about 2.4% of the center frequency. If the 5th fractal iteration is used, then this parameter increases to 3.1%. If a 3D tree is used (when there are 4 branches used instead of 2) then this parameter increases 12.7%. Besides Dipole antennas there are resonant loop antennas used. Some typical loop fractal antennas built using Koch figures as shown in Figure 3 [7,8].

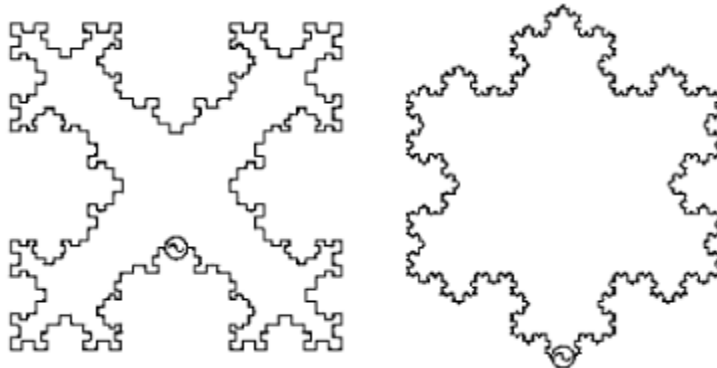


Figure 3. Fractal Loop Examples

RF MEMS could also be used in conjunction with fractal antenna structure as the basis of a new reconfigurable array antenna approach. The RF MEMS switches permit the connectivity of sections of the antenna's conductive parts, and therefore enhance the coupling between the fractal elements allowing multiple frequency operation with one antenna. Using this scheme a set-top antenna could be designed to change shape and/or size based upon which frequency (channel) the television was currently tuned to. The use of fractal shapes provides the multiband characteristic through the property of self similarity at equal or different physical scales. The electromagnetic performance of the RF MEMS switches is ideal for this application, and their placement is accomplished by small physical connections of the antenna's adjacent conducting pans [1].

Most fractal antennas, including the Sierpinski antenna, have been studied extensively over the last few years [3,4]. A modified Sierpinski antenna is shown in Figure 4. The centerline of the CPW [1] feed provides the RF input and dc voltage for MEMS switch actuation. Switches S1 and S1' actuate at a low voltage, switches S2 and S2' at a medium voltage, and switches S3 and S3' at a high voltage. Figure 5 shows the different states of the antenna. An alternate implementation could be for a bowtie antenna as shown in Figure 7.

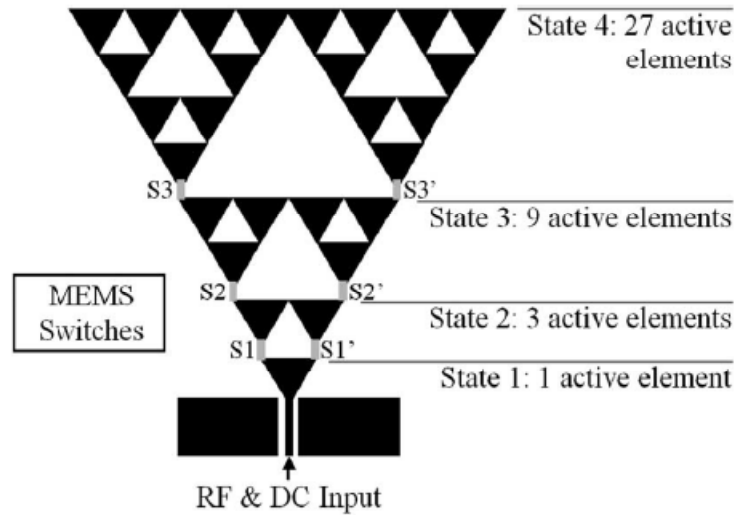


Figure 4. Illustration of a MEMS reconfigurable Sierpinski antenna.

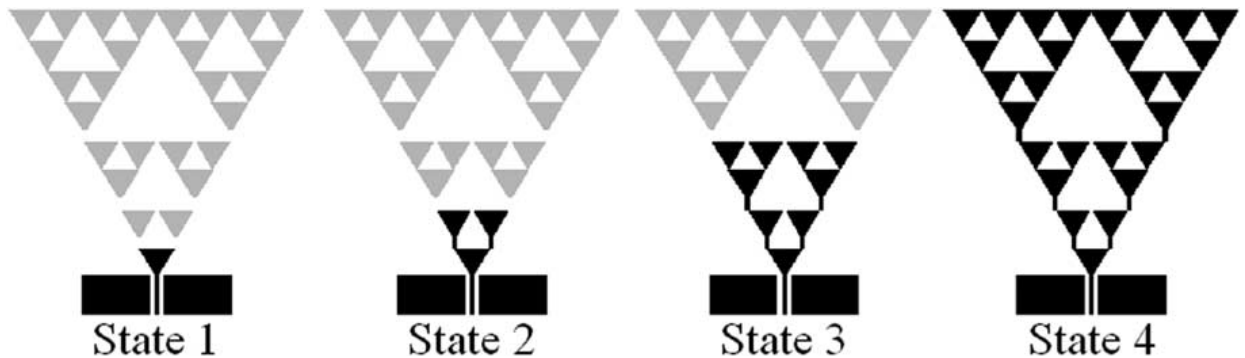


Figure 5. States of Reconfigurable Sierpinski Antenna

In most of the literature, integration has been accomplished on rigid and nonflexible semiconducting or organic polymer substrates such as silicon and FR-4. The idea of integrating RF MEMS switches into a multiband self-similar antenna was first implemented in [2], where the entire system, including the RF MEMS, the planar self-similar antenna, and the CPW-coplanar strip transition, was fabricated on silicon. The integration is achieved on a very thin and flexible liquid crystal polymer (LCP) substrate. Since the switches share a common dc feed, this technique provides reconfigurability

without the need for additional bias lines. This is advantageous since dc bias lines take up space, add loss, and reduce the bandwidth of a device. This technology is particularly useful for antennas where bias lines can have a pronounced effect on radiation patterns, and may be especially useful in the set-top application.

The implementation of a sequentially activated antenna is shown in Figure 5. All of the MEMS switches used are single supported (cantilever type) and ohmic. Regardless of the applied voltage, the triangular element that is closest to the RF/dc input is always active. When no dc voltage is applied, the antenna radiates at its highest frequency. When a low dc voltage is applied to the signal line, the first set of MEMS switches (S1 and S1') actuate, and this activates the second level of triangular elements. The antenna now radiates at a lower frequency. Since all of the switches are ohmic, the low voltage is also present at the membrane of the next set of switches (S2 and S2'). However, these switches are designed to actuate at a higher voltage so they are unaffected by the voltage present. When a higher dc voltage is applied, the first set of MEMS switches (S1 and S1') remains in the "ON" position while the second set of switches (S2 and S2') actuates. This activates the next iteration, consisting of six additional radiating elements. Again, this higher voltage is present at the next set of switch membranes (S3 and S3'), but the electrostatic force created is not sufficient for actuation. Finally, when the voltage is increased to its highest value, the first two sets of switches (S1 and S1' and S2 and S2') remain in the "ON" position while the remaining set of the switches (S3 and S3') actuates .

Thus, the voltage "cascades" from one state to the next like a sequence of overflowing buckets. This technique could not be used if the switches were capacitive since they do not pass dc voltage. The four different states are illustrated in Figure 8, where all of the activated regions for different voltages are dark in color. This biasing technique allows for direct actuation of the electrostatic MEMS switches through the RF feed structure. Since only the RF feed is dc grounded, the switches actuate with the use of a floating ground. That is, the signal pin of the CPW feed is connected to the dc cathode, and the ground pins are connected to the anode of a bias tee. The electrostatic charges that are created during switch actuation can dissipate through the substrate and be removed by the dc-grounded RF feed when in the "OFF" state. This method has been successfully documented in [5]. The reduction or elimination of bias lines is highly advantageous because they can significantly distort the radiation patterns and they can introduce additional unwanted resonances. To change the actuation voltage of a MEMS switch, there are four parameters that can be changed.

- 1) *Membrane material*: Switch membranes are almost always made of metal. This is due to their pliable nature. Stiffer metals (that is, those with a high Young's Modulus, E) will have a higher actuation voltage than those with a lower E .
- 2) *Bridge thickness*: The thicker the bridge, the stiffer the membrane, resulting in a higher actuation voltage.

- 3) *Bridge height*: The higher the bridge, the larger the gap between the metal layers, resulting in decreased the electrostatic force and increased actuation voltage.
- 4) *Membrane geometry*: Springs can be designed into the shape of the membrane to lower the actuation voltage.

Of these parameters, only the fourth does not require any fabrication changes. Making changes to a fabrication process can be a costly endeavor and may create additional variables of concern.

LCP was chosen as the substrate for its many advantages. LCP is a thin ($100\ \mu\text{m}$), flexible, low-loss ($\tan \delta \approx 0.004$), low-moisture absorbing material with low permittivity ($\epsilon_r \approx 3$) [9]. Since the material is a polymer, there are additional packaging and cost advantages. All of these characteristics make it an ideal substrate for antennas, particularly at high frequencies. With respect to the geometry, the antenna elements have a 60° flare angle and maintain the resonant structure's self similarity with a log-periodicity of $\delta = 2$. The antenna is fed through a 6-mm-long CPW transmission line with a $50\text{-}\mu\text{m}$ gap, a 1.3-mm signal conductor width, and a $1.5\text{-}\mu\text{m}$ -thick aluminum layer. The overall size of the antenna, including the feed, is $20 \times 25\ \text{mm}$. The CPW feed was chosen to facilitate the measurement setup. This reconfigurable antenna operates at four different principle frequencies. For each frequency, the antenna maintains its multiband performance. It was verified that the antenna has a different first resonant frequency for each of the four states. Since the antenna is self-similar with a log-periodicity of 2, each time the antenna transitions to the next state, the frequency should be halved. That is, the resonant frequency of state 2 should be half that of state 1. This is shown in Figure 6.

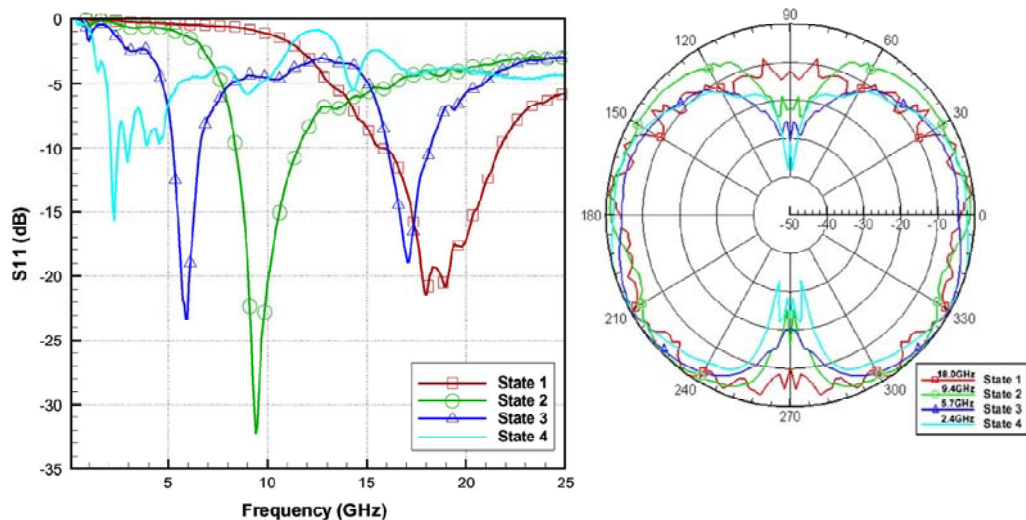


Figure 6. Measured Results of Built antenna for S11 and pattern

Fractal Antenna with RFID-MEM's

The general problem with using MEMS in a fractal antenna is how to power them. This was accomplished by putting DC on the RF of the feed of the antenna with a floating ground in the last section. If the goal is a dipole antenna as shown in Figure 7, then the floating ground would become a problem. One possible solution for this difficulty is known as "RFID-MEM's." The RFID could power the MEM to switch a section on and off. It would be controlled with a reader placed close to the antenna. If the television sends a digital signal back on the coaxial line that has information on what channel is currently tuned, then this information could be used by the reader to activate the correct switches to optimize the antenna for the best reception on the tuned channel. The RFID would need to operate either below the television spectrum, such as 13.56MHz, or above it, such as an UWB RFID. This system should have minimal effects on the antenna pattern of the bowtie antenna and could cover the entire VHF and UHF bands.

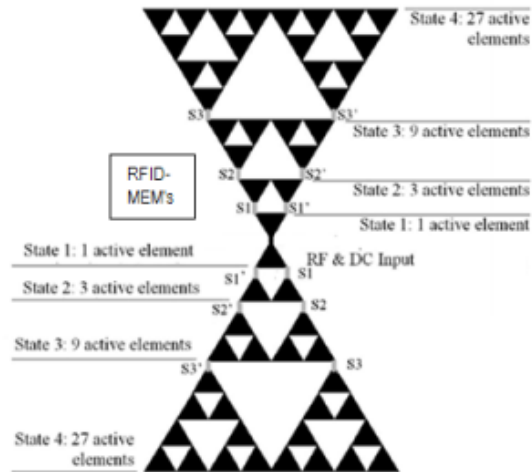


Figure 7. Bowtie Antenna

Fractennas

There have been some commercially available fractal/self similar antennas made by Fractal Antenna systems Inc. [10]. Fractal Antenna Systems has fabricated a wideband dipole as shown in Figure 8. The antenna has a self similar geometry present at multiple resolutions. Along two of the axes there is a substantial mirror image. Along the center there is a thin dipole that runs all the way through the antenna. The long thin dipole geometry creates a loading effect rather than predominately providing the function of radiating electromagnetic energy, which instead is provided by the more distinct V shaped dipole as shown in Figure 9. This antenna is claimed to radiate energy between 400 MHz and 6000MHz and are fabricated using deterministic fractal geometry.

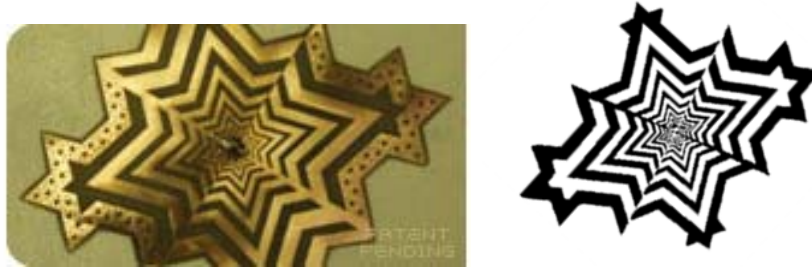


Figure 8 Wideband dipole by Fractenna



Figure 9 Wideband Dipole (Bowtie) by Fractenna

REFERENCES

- [1] N. Kingsley, D.E. Anagnostou, M. Tentzeris and J. Papapolymerou, "RF MEMS Sequentially Reconfigurable Sierpinski Antenna on a Flexible Organic Substrate With Novel DC-Biasing Technique", *J. OF MICROELECTROMECHANICAL SYSTEMS*, VOL. 16, NO. 5, OCTOBER 2007, pp. 1185-1192
- [2] D. E. Anagnostou *et al.*, "Design, fabrication, and measurements of an RF-MEMS-based self-similar reconfigurable antenna," *IEEE Trans. Antennas Propag.*, vol. 54, no. 2, pt. 1, pp. 422–432, Feb. 2006.
- [3] B. Cetiner, J. Qian, H. Chang, M. Bachman, G. Li, and F. DeFlaviis, "Monolithic integration of RF MEMS switches with a diversity antenna on PCB substrate," *IEEE Trans. Microw. Theory Tech.*, vol. 51, no. 1, pp. 332–334, Jan. 2003.
- [4] R. Jackson and R. Ramadoss, "A MEMS-based electrostatically tunable circular microstrip patch antenna," *J. Micromech. Microeng.*, vol. 17, no. 1, pp. 1–8, Jan. 2007.
- [5] N. Kingsley and J. Papapolymerou, "Organic 'wafer-scale' packaged miniature four-bit RF MEMS phase shifter," *IEEE Trans. Microw. Theory Tech.*, vol. 54, no. 3, pp. 1229–1236, Mar. 2006.
- [6] C. P. Baliarda, J. Romeu, and A. Cardama, "The Koch monopole: A small fractal antenna," *IEEE Trans. Antennas Propag.*, vol. 48, no. 11, pp. 1773–1781, Nov. 2000.
- [7] N. Cohen and R. Hohlfeld, "Fractal loops and the small loop approximation," *Commun. Q.*, pp. 77–81, Winter 1996.
- [8] J. Anguera, C. Puente, C. Borja, and J. Soler, "Fractal-shaped antennas: A review," in *Wiley Encyclopedia of RF and Microwave Engineering*, vol. 2, K. Chang, Ed. New York: Wiley, 2005, pp. 1620–1635.

- [9] D. Thompson, O. Tantot, H. Jallageas, G. Ponchak, M. Tentzeris, and J. Papapolymerou, "Characterization of liquid crystal polymer (LCP) material and transmission lines on LCP substrates from 30 to 110 GHz," *IEEE Trans. Microw. Theory Tech.*, vol. 52, no. 4, pp. 1343–1352, Apr. 2004.
- [10] Fractal Antenna Systems, Inc. 130 Third Avenue Waltham MA 02451, www.fractenna.com

2.10 Retrodirective Arrays

2.10.1 Summary

Retrodirective antennas are self-adapting systems that transmit a signal or direct their beam in the direction of an incoming signal without any prior knowledge of the signal's angle of arrival or intensive signal processing to determine the direction. Two types of retrodirective antennas have been developed, the Van Atta (VA) array and the Phase Conjugating (PC) array. The VA array is fundamentally a passive, planar structure (although active VA arrays exist as well). The PC array is an active antenna that can be fabricated on a non-planar surface. Thus, the VA array generally is simpler and, consequently, easier to design and fabricate. Retrodirective systems are attractive candidates for the set-top television antenna.

While existing retrodirective systems typically operate at frequencies well above the television band, the technology is advancing rapidly and much of it at this time or in the short-term future likely will be applicable to set-top antennas. This section describes several state-of-the-art implementations, mostly for VA systems, but some for PC systems. It also describes an important development in conformal PC array design using genetic algorithm optimization that allows a retrodirective array to be designed for a specific surface shape. Finally, some new work on near field scatterer effects is discussed that shows how a retrodirective antenna can mitigate near field phase distortions in environments such as the interior of a building (a typical set-top environment).

(a) Retrodirective Concept

A retrodirective antenna is conceptually similar to an optical corner reflector, three plane reflecting surfaces intersecting at right angles. A light beam incident onto the corner reflector, also known as a retroreflector or cataphote, is automatically reflected back along the direction from which it came. The basic retrodirective array concept is shown schematically in Figure 1. There are two basic structures: (1) the Van Atta array, and (2) the Phase Conjugating array. The VA array is simpler than the PC array because it does not require active devices, whereas the PC array does. VA and PC arrays operate differently, but both systems achieve the same goal of directing the antenna's beam in the direction of an incoming signal. Without any knowledge of the signal's direction of arrival, a retrodirective antenna is able to transmit a signal back toward the transmitter along the direction of that incoming signal without using phase shifters.

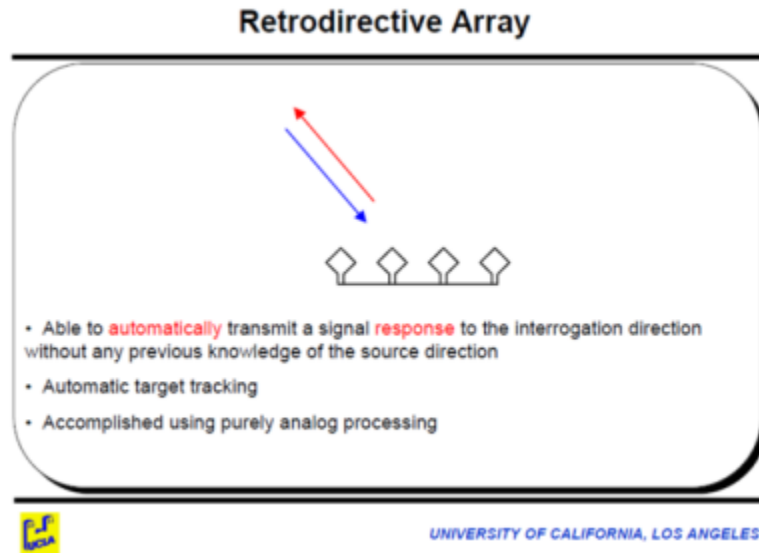


Figure 1. Basic retrodirective concept (reproduced from [1]).

(b) Van Atta Array

The VA concept [2] is shown in Figure 2. Pairs of antenna elements, which can be any type of radiator (in this case horns), are equally spaced about the array's center point and interconnected with waveguides (or transmission lines) that have equal length or are multiples of a wavelength. Each antenna element acts as both a receiving antenna and a transmitting antenna. The incident field received by each element is reradiated by its paired counterpart after propagating along the interconnecting transmission line or waveguide. The effect of the resulting propagation delay is to reverse the phase of the reradiated field distribution relative to the received field distribution, causing the reradiated field to be directed back along the line of sight of the incident field. While Van Atta's original antenna was strictly a passive retroreflector, active systems have been developed that utilize the basic Van Atta structure [3,4,5]. Figure 3 provides a schematic illustration of the Van Atta concept for passive and active implementations.

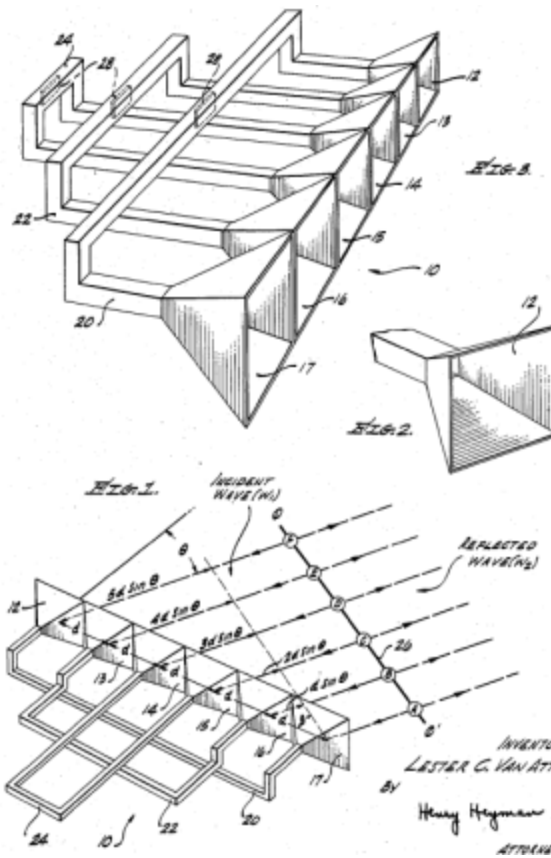


Figure 2. Van Atta retrodirective array (reproduced from [2]).

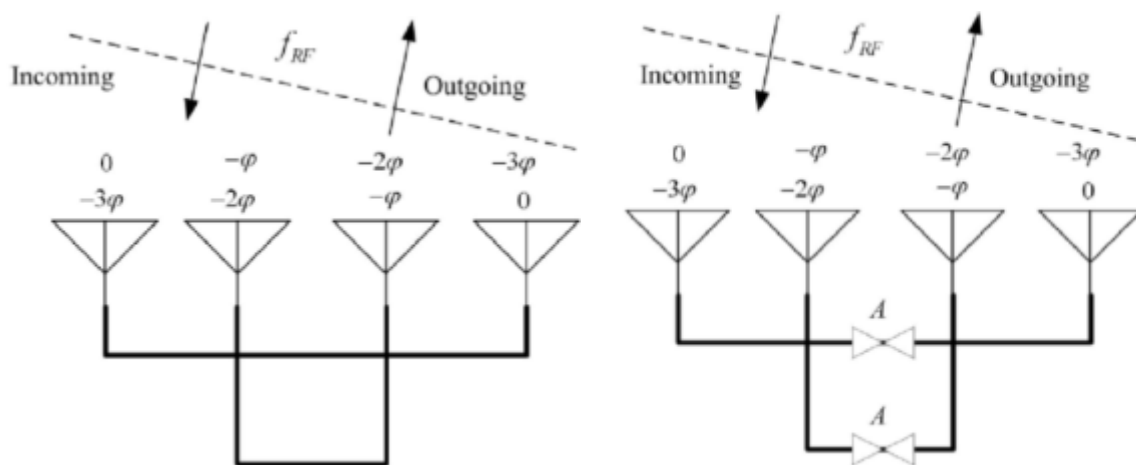


Figure 3. Passive (a) and active (b) Van Atta array phase front (reproduced from [3]).

(c) Phase-Conjugating Array

Unlike the Van Atta array, the PC retrodirective array requires active elements because its operation relies on actively changing the relative phase of its elements. The direction of an emitted signal, or, by reciprocity, the maximum directivity for received signals, is controlled by the relative phase and amplitude of the individual radiating sources or receiving elements in a multi-element array as shown in Figure 4. By operating a local oscillator (LO) at twice the received signal's radio frequency (RF), mixing the LO and RF signals results in a lower sideband product whose frequency is the same as the incident signal's but whose phase is conjugated (reflected about the real axis as shown in Figure 5).

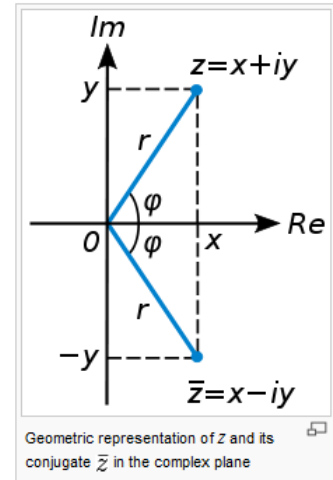
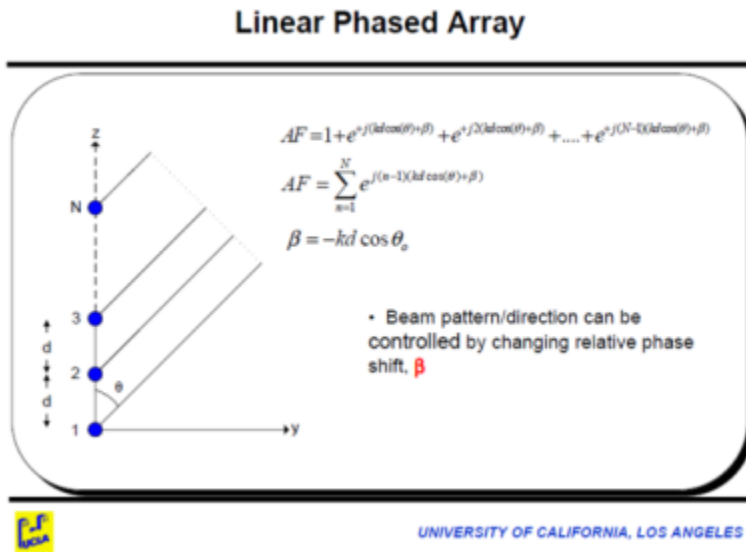


Figure 4. Beam direction control (reproduced from [1]).
Phase conjugation.

Figure 5.

Conjugating the phase for each antenna element steers the antenna beam back along the direction of the incoming signal as shown in Figure 6. If the antenna is used for transmitting, then the radiated signal is transmitted along back along the direction of the received signal. If the antenna is used for receiving, then the radiation pattern is steered with is maximum directivity in the direction of the received signal.

A conjugating retrodirective antenna, whether VA or PC, could be very useful as a set-top television antenna because it provides optimal gain in the direction of the received signal regardless of its incidence direction. A retro receive antenna would automatically adapt itself to the signal environment allowing a fixed antenna to provide maximum response to signals from any direction. The following sections describe some state-of-the-art implementations that may be applicable in the set-top television environment.

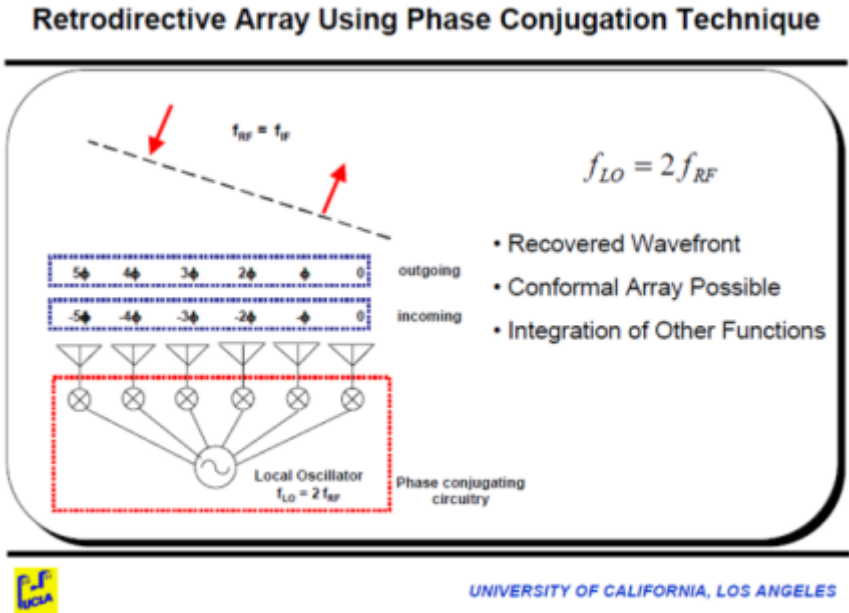


Figure 6. Retrodirective phase conjugating architecture (reproduced from [1]).

(d) Retrodirective Array Implementations

Broadband Van Atta Array. Figure 7 shows the schematic diagram for a frequency-offset broadband Van Atta array [6]. While the VA architecture is inherently more broadband than PC arrays because bandwidth-limiting LO and phase conjugation mixers are not required, there nevertheless are active-element implementations that improve performance while maintaining substantial bandwidth as shown in the figure. In this particular application, the antenna is used for two-way communication, which is why optional amplifiers that increase effective radiated power are included and dual-polarized antennas are used (orthogonal polarizations for transmission/reception to increase isolation).

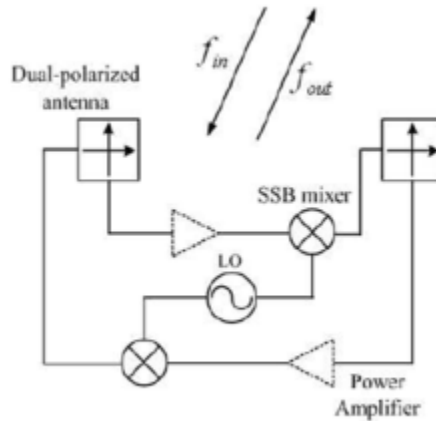


Figure 7. Diagram of broadband two-way Van Atta array (reproduced from [6]).

Figure 8 shows the structure of the prototype broadband VA array antenna. A patch radiator is fed by two excitation slots at right angles to provide orthogonal polarization. Microstrip feed lines excite the apertures and are deposited as shown the opposite side of the aperture substrate. The reflecting plane is included to improve front-to-back ratio. Two such antennas comprise the prototype array which operates from 2.8 to 3.4 GHz. The antenna as fabricated is shown in Figure 9. The patch antennas are evident on the surface of the front circuit board substrate, while the separate SSB mixer circuit boards are seen in the background. This antenna achieved beam steering over approximately $\pm 30^\circ$ from the broadside direction (perpendicular to the plane of the antenna patches). This active VA array shows that substantial retrodirectivity can be achieved even in a simple two-element array. It perhaps points the way towards retrodirective set-top antennas based on the same or similar architecture that utilize different antenna elements, such as dipoles or bow-ties, that are better suited to the lower television frequencies.

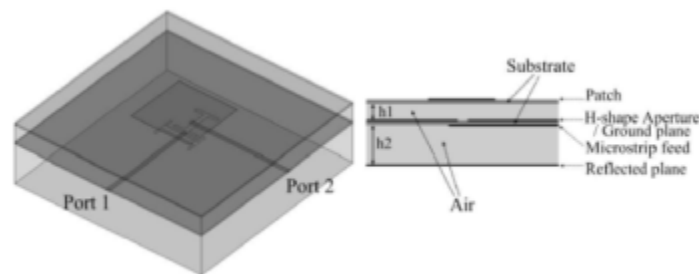


Figure 8. Broadband two-way Van Atta array antenna element (reproduced from [6]).

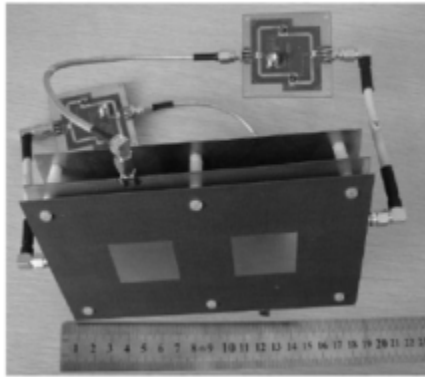


Figure 9. Broadband two-way Van Atta array as fabricated (reproduced from [6]).

Passive Array with Hybrids. An interesting example of a passive VA array implementation involves using 90° hybrid couplers as the phasing elements [7]. This design relies on a clever use of hybrid couplers whose incident and reflected signals' phases are reversed when the coupler is terminated with loads having the same reflection coefficient. Figure 10 shows how a phase difference $\Delta\phi$ between signals into ports 1 and 2 (input/isolated ports, respectively) is transformed into a phase difference of $-\Delta\phi$ between the reflected signals at those ports as long as ports 3 and 4 (direct/coupled, respectively) are terminated with the same reflection coefficient. In practice, these ports simply float unterminated because Γ then is the same for each (~ 1).

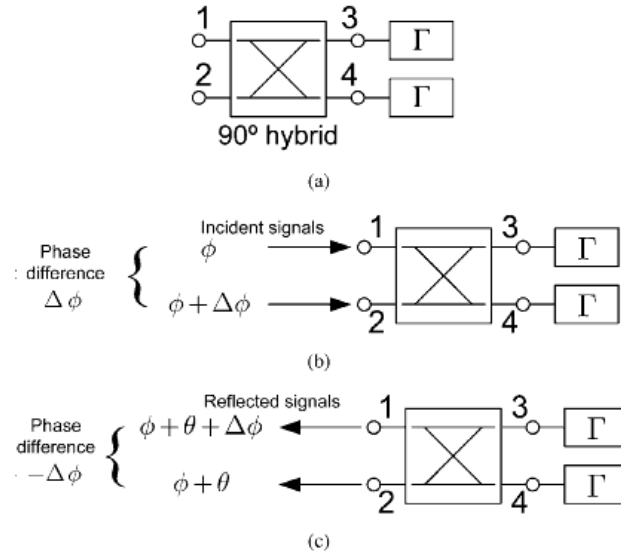


Fig. 2. (a) A terminated 90° hybrid with (b) and (c) to illustrate the phase difference reversal characteristics of the input signals and the reflected signals.

Figure 10. Passive VA array using hybrid couplers (reproduced from [7]).

A particularly attractive feature of this design is ease of implementation. Figure 11 shows 3-, 4- and 6-element retrodirective array circuits fabricated on 1.6 mm thick FR4 substrate using planar 90° microstrip branch line couplers. It is significant, too, that this retrodirective design does not require an even number of array elements as does the basic Van Atta design. The prototype array was fabricated with 2.9 GHz patch antenna elements on the same type substrate spaced 0.48λ . Measurements showed effective beam steering over a range of $\pm 40^\circ$. This type of retrodirective antenna may be particularly attractive for the set-top application because of its simplicity.

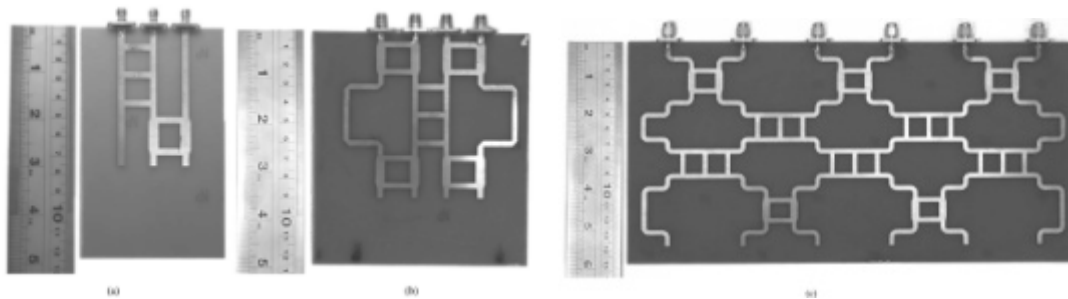


Figure 11. Passive 3/4/6-element VA array circuits as fabricated on PCB (reproduced from [7]).

Feed Systems for Van Atta Arrays. Two interesting and potentially useful VA array designs are described in [8]. Two planar VA arrays were designed and simulated using commercially available electromagnetic modeling software (ANSOFT HFSS). The first antenna (Figure 12, (a)/(b) left) used a microstrip line edge-fed patch at 7.58 GHz as the antenna element (overall dimensions $\sim 13 \times 30$ mm). This element was arrayed in a two-dimensional 4x4 grid and evaluated for bandwidth and radiation characteristics. The second antenna comprised aperture-coupled microstrip patch antenna elements operating at 9 GHz also arrayed in a 4x4 2-D grid (Figure 12, (a)/(b) right). The second design was found to be superior because it could be more easily fabricated using both sides of the substrate and it provided better beam steering ($\pm 80^\circ$ @ -10 dB). This simulation shows that very effective designs with small footprints are possible at very short wavelengths. This technology may be applicable directly or with modification or extension to set-top antenna requirements.

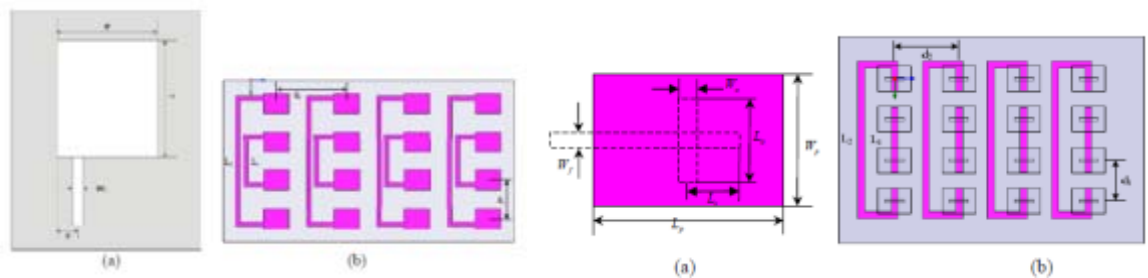


Figure 12. Planar edge-fed VA arrays (reproduced from [8]).

A Fractal VA Antenna Element. Dual-polarized Van Atta array antenna elements provide advantages over singly polarized elements, in particular increased transmit/receive (T/R) isolation on two-way links, multipath mitigation, and polarization diversity. While T/R isolation is not a consideration in the set-top television antenna, the other factors are. Additionally, size is a concern, and newer antenna element designs emphasize small size. An interesting fractal-based element is reported in [9] that may be useful for set-top VA arrays. Figure 13 shows the overall antenna in perspective and plan views. There are two square (40 mm) 1-mm thick material dielectric substrates, the top one being PTFE material ($\epsilon_r = 2.65$), and the bottom FR3 ($\epsilon_r = 4.4$). The First Minkowski fractal patch is shown on the right with the vertical and horizontal polarization feed ports marked V and H, respectively.

Details of the patch, which is designed to operate from ~ 4.4 to 5 GHz, appear in Figure 14. Its overall size is quite small at 21 x 16.8 mm, and it provides similar electrical performance to a square patch that is about 20% larger. Figure 15 shows details for the H-shaped slots that function as aperture coupling structures to excite the fractal patch. It is evident that, once dimensions are specified, the components are readily fabricated and easily assembled, which are very desirable characteristics for the set-top television antenna.

Computed data show that the antenna element exhibits H-polarization VSWR < 2 from ~ 4.82 -5.17 GHz with 16.8% impedance bandwidth. The corresponding V-polarization figures are ~ 4.27 -5.2 GHz, bandwidth 19.8%. Measured results confirm the modeling with bandwidth figures of 19.7% and 20.5%, respectively, which is good agreement. Directive gain is ~ 8 dB with >20 dB front-to-back ratio. These results clearly show that the microstrip Minkowski fractal antenna element is useful in VA arrays at microwave frequencies, and that it well may provide excellent performance for the higher television bands as well.

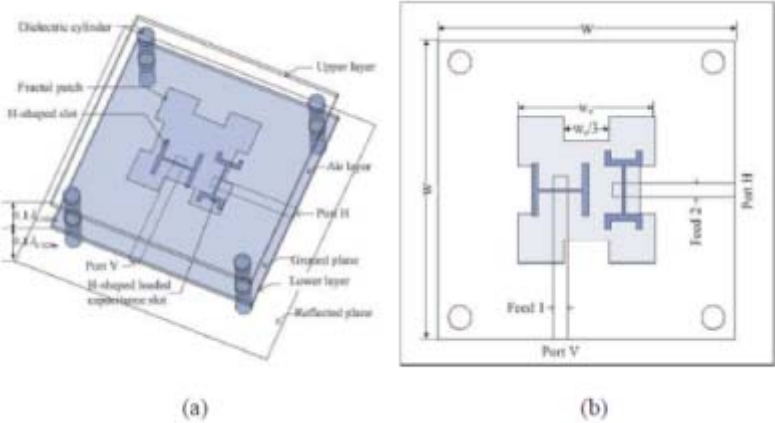


Figure 13. Proposed microstrip fractal antenna element (reproduced from [9]).

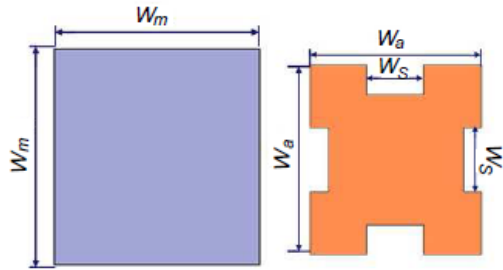


Figure 2. Structure of the conventional square patch and the Minkowski fractal patch ($w_m = 21$ mm, $w_a = 16.8$ mm).

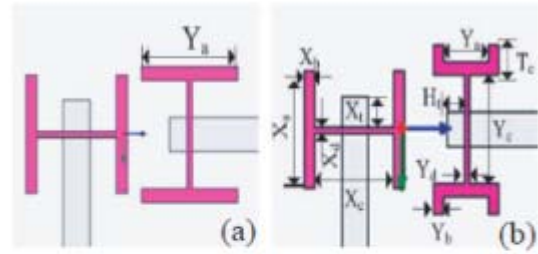


Figure 3. The aperture-coupled structures. (a) Double H-shaped slots, (b) H-shaped and H-shaped loaded capacitance slots.

Figure 14. Fractal patch (reproduced from [9]).

Figure 15. Aperture details (reproduced from [9]).

Dual-Ring Antenna Elements. The dual-ring antenna element proposed in [10] is another novel device that can be used in retrodirective Van Atta arrays. Inner and outer concentric rings form an inherently two resonant-frequency structure. Each of the rings is parasitic with the other ring excited, and by properly choosing dimensions fairly widely separated resonance points can mark the upper and lower limits of a fairly flat response curve. The structure of the dual-ring element is shown in Figure 16. It is implemented in a two-layer microstrip structure with the rings deposited on the outer surface of an upper substrate underlain by a transmission line for feeding and a ground plane as shown. Element dimensions were optimized using HFSS modeling software, and the fabricated element tested. The measured bandwidth (-10 dB) was just under 34% (31-42.8 GHz), which agreed quite well with the predicted value of 34.3% (30-42 GHz). Between 30 and 40 GHz the average measured gain was ~ 4.5 dBi.

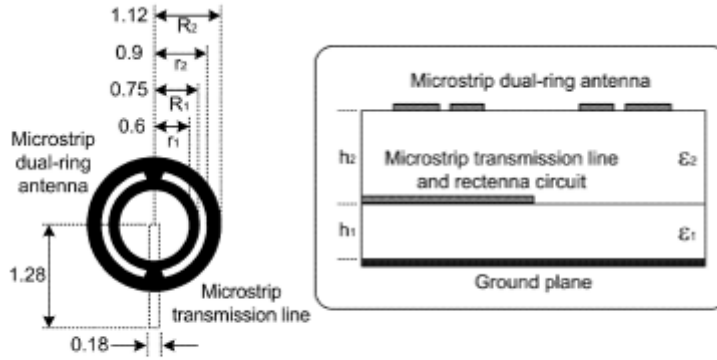


Fig. 3. Geometry of the broadband proximity-coupled dual-ring antenna and the two-layer dielectric structure. All dimensions are in mm.

Figure 16. Dual ring antenna element (reproduced from [10]).

The Van Atta array implemented using dual-ring elements was fabricated using 8 sub-arrays comprising 16 dual-ring elements in a 4 x 4 2-D grid. Figs. 17 and 18 show the sub-array and complete array structures, respectively. Measurements confirm the new array's predicted performance, which shows excellent beam steerability out to about

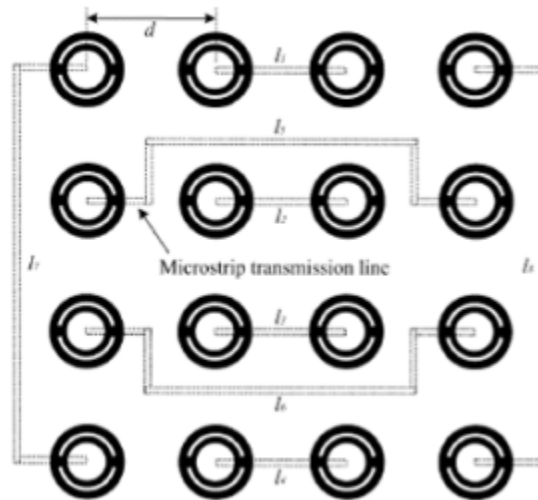


Fig. 5. Geometry of the 4x4 retrodirective sub-array where the dash-lines are the microstrip transmission line networks.

Figure 17. Dual ring element sub-array (reproduced from [10]).

$\pm 45^\circ$. The large array exhibits a very narrow main half-power beamwidth on the order of $\sim 2^\circ$ that is very stable between 32 and 49 GHz. Of course, this prototype antenna operates far beyond the highest television operating frequency, but its technology may be applicable to the TV set-top antenna with appropriate modifications.

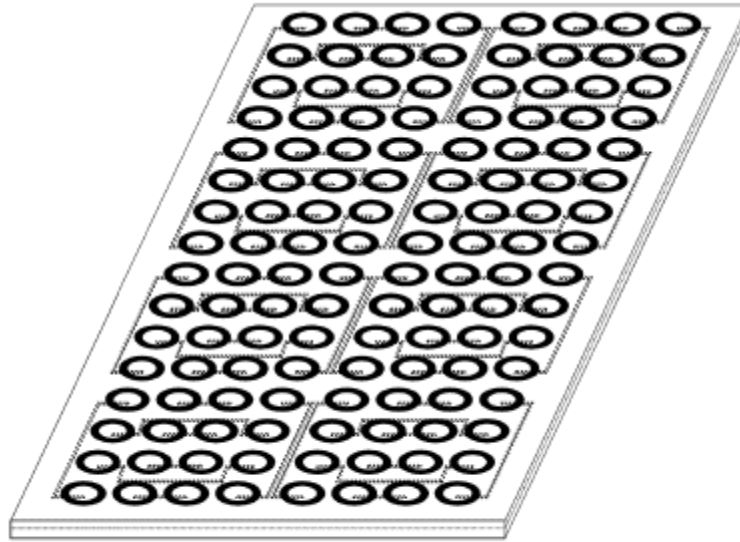


Fig. 6. Geometry of the 8x16 retrodirective array that consists of eight 4x4 sub-arrays.

Figure 18. Retrodirective array of dual ring elements (reproduced from [10]).

Conformal Retrodirective Arrays. In some cases it may be desirable to deploy a retrodirective antenna on a non-planar surface (the systems described above all utilize planar structures). Unfortunately the simpler Van Atta design cannot be used in such cases, so that Phase Conjugating systems are required instead. An interesting example of a genetically optimized, thinned PC array is described in [11]. The array's schematic representation appears in Figure 19, and its final physical configuration in Figure 20.

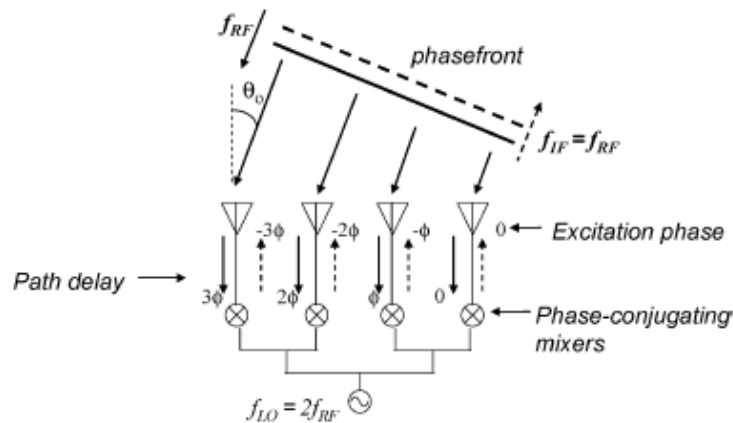


Fig. 1. A retrodirective array using heterodyne technique [5].

Figure 19. Conformal PC retrodirective array schematic diagram (reproduced from [11]).

In this example, the array was thinned to a total of 16 elements whose positions were optimized to achieve reasonable sidelobe levels over a scanning range of $\sim\pm 120^\circ$. The shape and size of the optimized array aperture cannot be determined analytically, but a suitable optimization algorithm permits design of conformal PC arrays. This type of structure could be important in the set-top environment as a space-saving measure, but it would incur the additional expense and complexity associated with active PC arrays compared to the simpler passive Van Atta design.

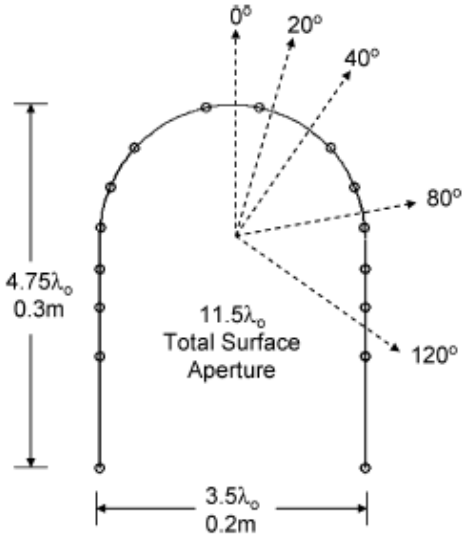


Fig. 2. The shape and the physical size of the aperture [4].

Figure 20. Conformal PC array structure (reproduced from [11]).

Near-Field Effects. Retrodirective antennas typically operate primarily in free space or near-free space environments, so that near field obstructions are not a factor in antenna performance. This typical environment is quite different from the set-top environment in which nearby objects and structures will definitely be in the antenna’s near field and consequently a potential source of interference. Near field effects were studied in [12] in order to investigate these effects. Figure 21 shows the experimental antenna in an anechoic chamber and typical measured data. Three different near field scatterers were studied: (a) straight wire grid; (b) partially obscuring low loss MDF (medium density fiberboard); and (c) partially or totally obscuring concrete blocks.

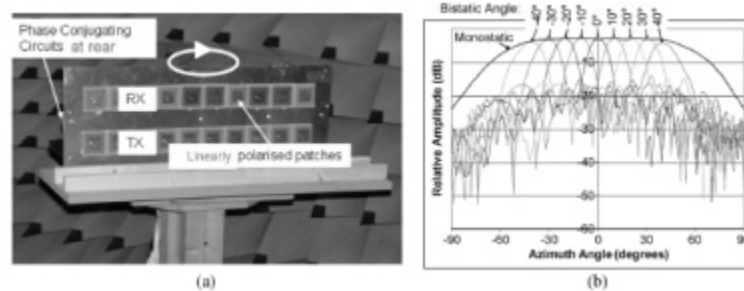


Figure 21. Measurement system for near field effects (reproduced from [12]).

Measurements were made at 2.4 GHz using a 10-element retrodirective array scanning $\pm 40^\circ$ with a half-power beamwidth of $\sim 12^\circ$. The retrodirective antenna performed quite well in the presence of obstructions. For example, using gapped concrete block scatterers, it was able to fully compensate for phase distortions that reduced a basic reference antenna's gain by 11 dB. This study was the first to demonstrate that retrodirective antennas offer demonstrable performance advantages over other antennas in difficult propagation environments such as the interior of a building. This finding is an important reason for exploring retrodirective technology as it might be used in a television set-top antenna.

2.10.2 References

- [1] Leong, K., and Itoh, T., "Active Retrodirective Arrays," Electrical Engineering Dept., Univ. of California Los Angeles, available online: <http://www.rish.kyoto-u.ac.jp/jusps/P15.pdf>.
- [2] Van Atta, L. C., "Electromagnetic Reflector," U.S. Patent No. 2,908,002, Oct. 6, 1959.
- [3] Chung, S-J., Chen, S-M., Lee, Y-C., "A Novel Bi-Directional Amplifier with Applications in Active Van Atta Retrodirective Arrays," *IEEE Trans. Microwave Theory and Techniques*, **51**, No. 2, Feb. 2003, p. 542.
- [4] Guo, Y. C., Shi, X. W., Chen, L., "Retrodirective Array Technology," *Prog. In Electromagnetics Research B (PIER B)*, **5**, pp. 153-167 (2008).
- [5] Goshi, D. S., Leong, K. M. K. H., and Itoh, T., "Recent Advances in Retrodirective System Technology," *IEEE Radio and Wireless Symposium*, pp. 459-462, 2006.
- [6] Chen, L., Wang, X.-H., Shi, X.-W., Zhang, T.-L., Ting, J.-Z., "Design of a Broadband Frequency Offset Van Atta Array," *Prog. In Electromagnetics Research Letters*, **13**, pp. 161-171 (2010).

- [7] Hsieh, S-N., and Chu, T-H., "Linear Retro-Directive Antenna Array Using 90° Hybrids," *IEEE Trans. Antennas and Propagation*, **56**, No. 6, June 2008.
- [8] Yao, H-Y., and Wang, C-F., "Investigation of Electromagnetics Properties of Two Types of Passive Retrodirective Antenna Arrays," *IEEE Antennas & Propagation Society International Symposium 2008 (AP-S 2008)*. DOI: 10.1109/APS.2008.4619052.
- [9] Cheng, H. R., Chen, X. Q., Chen, L., and Shi, X. W., "Design of a Fractal Dual-Polarized Aperture Coupled Microstrip Antenna," *Progress in Electromagnetics Research Letters*, **9**, pp. 175-181 (2009).
- [10] Ren, Y-J., and Chang, K., "A New Millimeter-Wave Broadband Retrodirective Antenna Array," *Microwave Symposium, 2007. IEEE/MTT-S International*. DOI: 10.1109/MWSYM.2007.380038.
- [11] Sun, J. S., Goshi, D. S., Itoh, T., "Optimization and Modeling of Sparse Conformal Retrodirective Array," *IEEE Trans. Antennas and Propagation*, **58**, No. 3, March 2010.
- [12] Fusco, V. F., and Buchanan, N., "Retrodirective Array Performance in the Presence of Near Field Obstructions," *IEEE Trans. Antennas and Propagation*, **58**, No. 3, March 2010.

3.0 Conclusions and Design Recommendations

Upon consideration of Table 1-1 at the end of Section 1 of this report we have concluded the following:

- There have been significant and potentially useful antenna design methods and actual hardware developed over the past 15 years that will improve the performance of low-profile, compact indoor/set-top DTV antennas.
- In the area of electro-magnetic computational and design optimization methods Genetic Algorithms (GA) and the Central Force Optimizer (CFO) have proven themselves as powerful tools in the design of broadband, compact antennas.
- Using the above, we have included an example of an advanced antenna technology, specifically the Fragmented Antenna as part of this project. We submit that it would be nearly impossible for a human to replicate its design and performance.
- The Non-Foster active broadband matching technology and its required semiconductors have matured to the point where they could be incorporated into a commercial indoor/set-top design to provide a matched antenna where it is considered as being electrically small. In the example shown below it would be used to provide acceptable performance with the Fragmented dipole within the 54-88 MHz band. Other element geometries are also possible.
- Many of the other advancements listed in Table 1-1, specifically 2.4 through 2.6, require a CE-909-A type interface with the DTV receiver, and while potentially useful if and when manufacturers start adding this feature to their products they offer no practical improvement for the near term.
- The technologies designated as 2.7 through 2.10 while interesting are either too embryonic (2.7 & 2.8), too complicated and too large (2.10) or not well vetted (2.9) to be considered in the near term.

Considering the above it is recommended that the NAB give consideration to further developing a computer generated/optimized broadband dipole antenna element, such as a Fragmented Planar Dipole with/without a Non-Foster Matching circuit in order to demonstrate that it is feasible to design a VHF/UHF antenna system that is both simple, have positive gain, be of reasonable size and weight and not require a CE-909-A interface with the DTV receiver.

As an example, a fragmented planar antenna was optimized for 54-698 MHz to cover all three DTV television bands. The antenna has dimension of 13" x 13" across the VHF and UHF bands, a block diagram of the proposed antenna system is shown in Figure 1. The computed directivity, after optimization, along the horizon is good at all DTV frequencies as shown in Figure 2. The antenna shows a good match at UHF frequencies, but as shown in Figures 4 and 5 some matching, using a simple L-C passive network of SMT components and Non-Foster Matching circuitry at the feed-point would be necessary for good performance in the high and low VHF bands respectively.

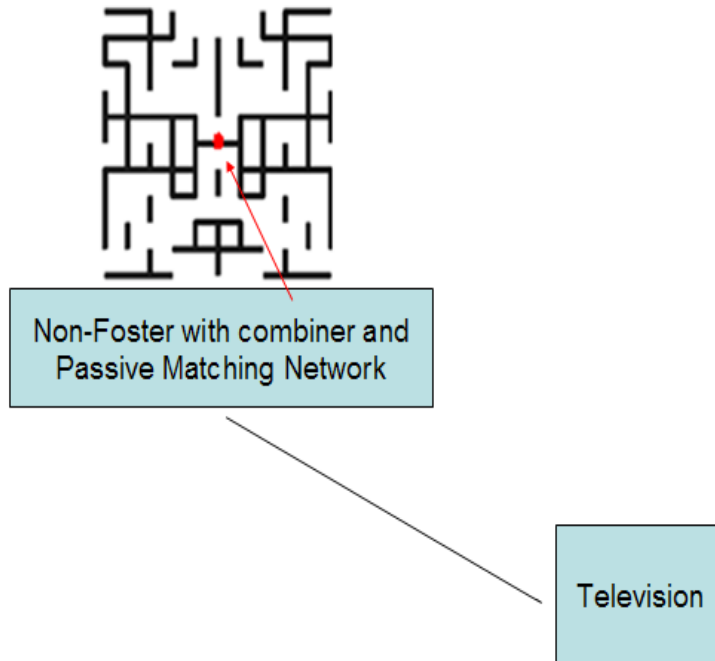


Figure 1. Fragmented Antenna Example, 13"x13"

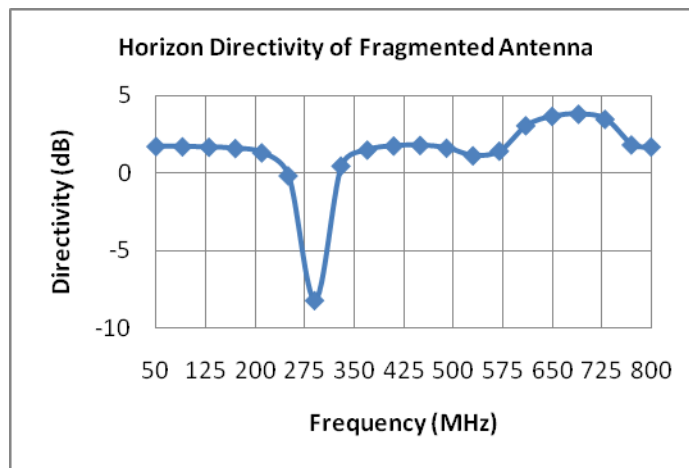


Figure 2. Directivity Along Horizon for Fragmented Antenna

The pattern of the antenna as currently designed is a “figure eight” dipole pattern at all frequencies, as shown in Figure 3. Figure 6 indicates that without any matching, a very low VSWR across the UHF 470-698MHz band.

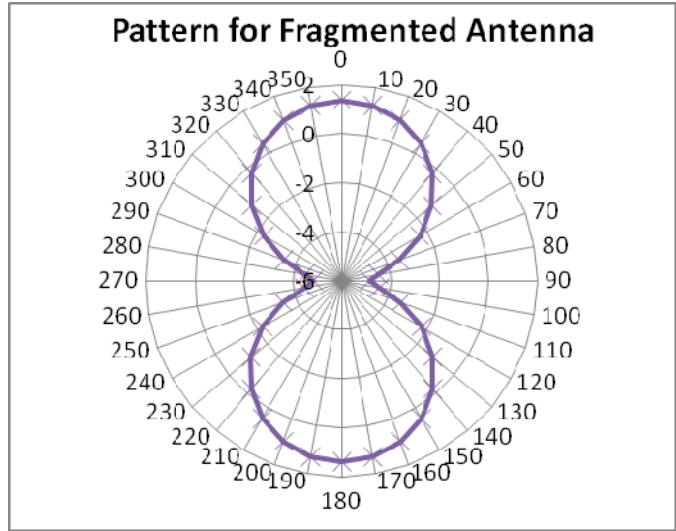


Figure 3. Azimuthal Pattern of Fragmented Antenna

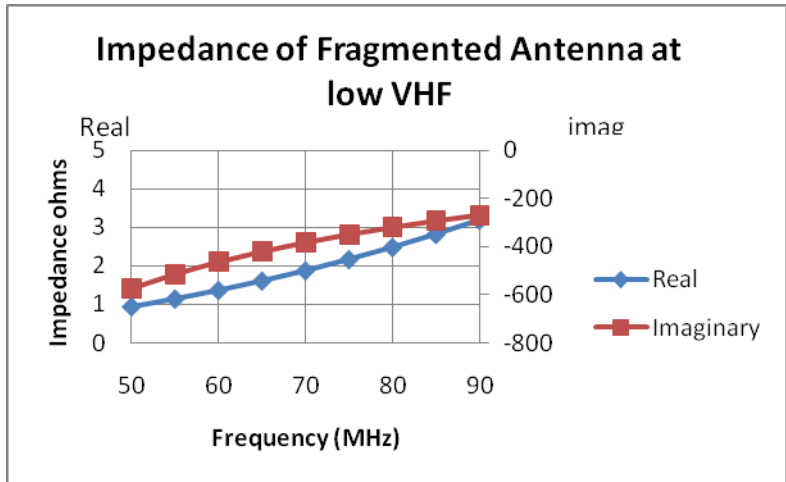


Figure 4. Impedance of Fragmented Antenna at low VHF

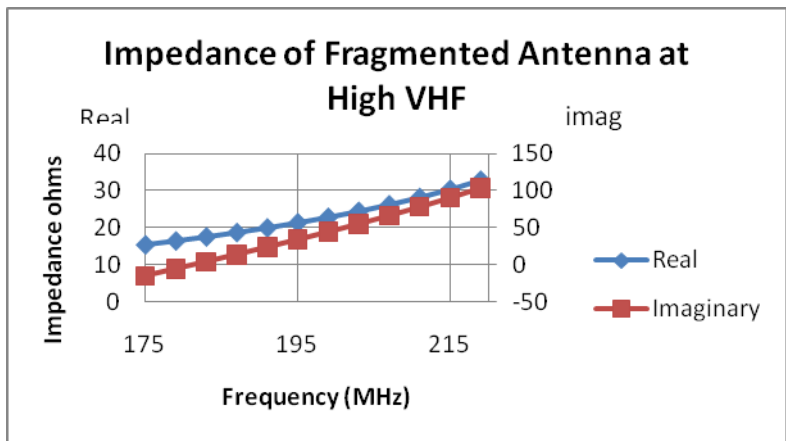


Figure 5. Impedance of Fragmented Antenna at high VHF

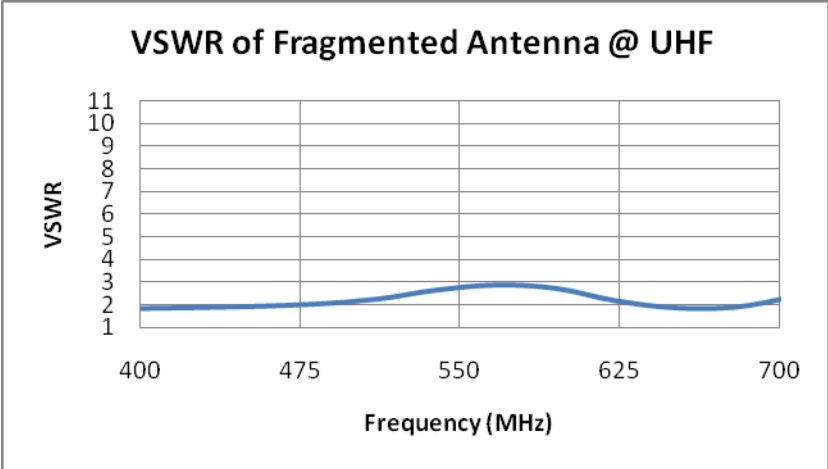


Figure 6. VSWR of Fragmented Antenna at UHF